学位論文

# Theoretical study on phases and phase transitions of ferromagnetic spin-1 bosons in optical lattices (光格子中の強磁性スピン1ボソンの相と相転移についての理論的研究)

平成28年12月博士(理学)申請

東京大学大学院理学系研究科
物理学専攻

曽弘博

**Abstract**

Since the experimental realization of Bose-Einstein condensation in 1995, the field of ultracold atoms has expanded rapidly, and has become an important arena for exploring diverse quantum many-body physics, as highlighted by the experimental observation of quantum phase transitions in the system of bosons in a periodic potential, which is described by the Bose-Hubbard model.

Recently, ultracold atoms with spin degrees of freedom are actively studied because the coupling between the internal spin degrees of freedom and the spatial degrees of freedom can give rise to novel and interesting physics. A minimal model for studying such physics is the spin-1 Bose-Hubbard model, which describes spin-1 bosons in a periodic potential. The model has a spin-dependent interaction, which can be ferromagnetic or antiferromagnetic, and it is known that although the ferromagnetic model resembles the spinless counterpart, the antiferromagnetic model exhibits totally different features, which make the model much more intensively studied compared with the ferromagnetic one.

However, the presence of an external magnetic field can change the situation, because the positive quadratic Zeeman energy competes with the ferromagnetic interaction, which can give rise to rich phases. In this thesis, we explore the ground-state and nonzero-temperature phase diagrams of the spin-1 Bose-Hubbard model under an external magnetic field. To analyze the model, we use an approximation method called the decoupling approximation, or equivalently, the Gutzwiller variational ansatz.

It is shown that, in addition to the Mott insulator phase, the model possesses two superfluid phases. Moreover, for large values of a spin-dependent interaction, the phase transitions between the two superfluid phases can be discontinuous. Such discontinuous phase transitions are shown to survive at nonzero but sufficiently low temperature. The discontinuous phase transitions are in clear contrast to the mean-field theory of weakly interacting spin-1 bosons without a lattice, which predicts that the corresponding phase transition is continuous, signifying the importance of the effect of strong interactions on the interplay between the spatial and spinor degrees of freedom.

# Acknowledgment

First, I would like to express my sincere gratitude to Prof. Masahito Ueda, my supervisor, for his advice, fruitful discussions, and continuous encouragements during my Ph.D. program. I deeply appreciate productive discussions and comments from many researchers, especially Prof. Hosho Katsura, Prof. Shunsuke Furukawa, Dr. Ulrich Ebling, Mr. Yusuke Horinouchi, Mr. Shuhei Yoshida, and Mr. Sho Higashikawa. I would like to thank Prof. Yusuke Kato, Prof. Naoki Kawashima, Prof. Seiji Miyashita, Prof. Masaki Oshikawa, and Prof. Yoshio Torii for refereeing my thesis and for valuable discussions.

I would like to express my deep gratitude to those who supported me in various ways; my friends, my family, and, last but not least, my fiancée, Ms. Mei Kobayashi.

Finally, I acknowledge financial supports from the Leading Graduates Schools Program "Advanced Leading Graduate Course for Photon Science" and the JSPS Research Fellowships for Young Scientists DC2 (Grant No. 16J07430).

# Contents

# Chapter 1

# Introduction

## 1.1 Background

### 1.1.1 Ultracold atoms in optical lattices

It was about 70 years after the theoretical prediction by Einstein [1, 2] that Bose-Einstein condensation was experimentally realized by several groups in 1995 [3, 4], which brought them the Nobel prize in physics 2001 "for the achievement of Bose-Einstein condensation in dilute gases of alkali atoms, and for early fundamental studies of the properties of the condensates" [5]. Since then, the field of ultracold atoms expanded rapidly [6, 7], incorporating various ideas and techniques from such diverse fields of physics as AMO (atomic, molecular, and optical) physics and condensed matter physics, and has become a unique and important arena for exploring the physics of various quantum many-body systems [8, 9].

One of the main reasons that ultracold atomic systems enjoy such popularity is their high controllability; the interaction between atoms can be tuned with the technique of Feshbach resonances, and the geometry of the system can be tailored with various optical techniques.

In particular, by combining multiple laser beams, we can create diverse periodic potentials, called optical lattices, which allow us to explore the physics beyond weak interaction approximations [9, 10]. Unlike conventional solid-state systems, systems of ultracold atoms in optical lattices can be free of defects, thus opening up the possibility of studying the physics of strongly interacting quantum many-body systems with unprecedentedly high precision.

A seminal example of this fact is the observation of the quantum phase transition between the superfluid phase and the Mott insulator phase in the system of ultracold bosons in an optical lattice. Jaksch et al. [11] have shown in 1998 that ultracold bosons in an optical lattice can be described by the Bose-Hubbard model, which was originally introduced heuristically as a way to describe the ground state and low-energy excitations of repulsively interacting bosons in continuum space [12], and later, motivated by experiments on superfluid $^4$He in porous media, analyzed in the context of condensed matter physics [13]. The Hamiltonian of the model is composed of two parts that compete with each other; the kinetic energy part which makes each boson spread over the whole system, and the repulsive interaction part which tends to localize bosons. The competition between these two terms is predicted to give rise to the quantum phase transition between the superfluid phase, in which each particle spreads over the whole system and hence is highly mobile, and the Mott insulator phase, in which each particle is localized due to the on-site repulsive interaction. Using ultracold bosons and an optical lattice, this phase transition was experimentally demonstrated in 2002 [14].

### 1.1.2 Spinor bosons

In the early days of researches of ultracold atoms, their internal degrees of freedom are frozen due to magnetic traps used in experiments. However, by the implementation of optical traps, bosons with spin degrees of freedom, which are called spinor bosons, can now be studied experimentally [15, 16], and have attracted considerable interest because of the possibility they offer of simulating quantum magnetism and exploring the interplay between the spatial degrees of freedom and the spin degrees of freedom [17, 18] .

At first, studies on spinor bosons mainly dealt with a weak interaction regime [19, 20, 21, 22, 23, 24], where, at zero and low enough temperature, almost all the particles Bose-Einstein condensate. Such studies revealed diverse quantum phases arising from the presence of the spin degrees of freedom and a spin-dependent interaction.

More recently, as mentioned above, optical lattices allow us to explore the strongly interacting regime of cold atoms, including spinor bosons. A minimal model for studying such physics is the spin-1 Bose-Hubbard model [25] , which describes spin-1 bosons in an optical lattice. The model resembles the Bose-Hubbard model for bosons without spin mentioned earlier, which is called the scalar Bose-Hubbard model to distinguish it from the spinor counterpart. However, the model involves a spin-dependent interaction term, whose sign depends on the specific atom considered, and changes the qualitative features of the system drastically; for a negative sign, the interaction is ferromagnetic, which maximizes the magnitude of the spin at each site, and for a positive sign, the interaction is antiferromagnetic, which minimizes the magnitude of the spin. For the ferromagnetic interaction, the zero-temperature phase diagram of the model is known to be similar to that of the scalar model, in which the quantum phase transition is continuous. On the other hand, for the antiferromagnetic interaction, the phase diagram exhibits distinct properties; Mott lobes with odd particle-number filling shrink, and the superfluid Mott insulator phase transition is known to be discontinuous for even particle-number filling. With such differences, the antiferromagnetic model is much more intensively studied compared with the ferromagnetic counterpart [25, 26, 27, 28, 29].

However, the situation is expected to change in the presence of an external magnetic field, where the competition between the positive quadratic Zeeman effect and the ferromagnetic interaction gives rise to rich phases; the ferromagnetic interaction favors states with larger spin, while the positive quadratic Zeeman energy penalizes such states. In systems without a lattice, this competition is known to yield two superfluid phases and the continuous phase transition between them [21].

To the best knowledge of the author, the ground-state phase diagram of the ferromagnetic spin-1 Bose-Hubbard model in the presence of an external magnetic field remains largely unexplored. Although there is a study on the unit-filling Mott insulator phase [30], the interplay between the spatial and spin degrees of freedom has yet to be fully explored.

## 1.2 Our study

In this thesis, we study the ground-state and nonzero temperature phase diagrams of the spin-1 ferromagnetic Bose-Hubbard model under an external magnetic field, using the Gutzwiller variational ansatz, or equivalently, the decoupling approximation. We consider the positive quadratic Zeeman energy, which competes with the ferromagnetic interaction.

For the ground-state case, we show that the competition between these two terms gives rise to discontinuous phase transitions between two superfluid phases. In the presence of the

positive quadratic Zeeman energy, there arise two superfluid phases; the polar superfluid phase, in which only the Zeeman sublevel $\sigma = 0$ particles are superfluid and the system possesses no magnetization, and the broken-axisymmetry phase, in which all the three components are superfluid, and the system exhibits nonzero transverse magnetization. Moreover, it was found that for large spin-dependent interaction, which corresponds to the spin-1 hyperfine manifold of $^7$Li, the phase transitions between the broken-axisymmetry phase and the other phases are discontinuous for some part of the phase boundary, which is in clear contrast to the case without an external magnetic field. Discontinuous phase transitions also occur when the quadratic Zeeman energy is varied, contrary to the mean-field theory of weakly interacting spin-1 bosons, in which the corresponding phase transition is continuous, implying the importance of the effect of strong interaction on the interplay between the spatial and spin degrees of freedom.

For the nonzero temperature case, two superfluid phases are also observed. The discontinuous phase transition is shown to survive for sufficiently low temperature, but the region of discontinuous phase transitions shrinks with the increase of the temperature, and for higher temperature, the phase transitions become continuous.

## 1.3 Outline of the thesis

The present thesis is organized as follows.

- Chapter 2 reviews some basic results on ultracold bosons with the spin degrees of freedom. We briefly discuss some single-particle properties, i.e., hyperfine spins and the Zeeman effect, after which the derivation of the Hamiltonian for interacting spin-1 bosons is discussed in detail. Then, we apply the mean-field theory, which assumes the interaction is weak, to the derived Hamiltonian, and discuss the obtained phase diagram.

- Chapter 3 is also a review chapter, which deals with optical lattices and ultracold bosons in them. We first describe the way to construct periodic potentials using multiple laser beams, and then we discuss the Bose-Hubbard models which describes bosons in optical lattices, for both the spinless and spinful cases. In each case, after derivation of the model, we discuss the ground-state phases of the system, focusing on the quantum phase transition between the superfluid phase and the Mott insulator phase. In particular, we emphasize the effect of the spin degrees of freedom, which alter qualitative features of the phase transition drastically.

- Chapter 4 describes the model we study, i.e., the spin-1 Bose-Hubbard model with an external magnetic field, and the method used to analyze it. After defining the model, we describe an approximation method called the Gutzwiller variational ansatz, which is known to be able to capture the qualitative features of the quantum phase transitions in the Bose-Hubbard models. Although the method, being a variational method, is conceptually transparent, in actual calculations we use a method called the decoupling approximation, which is shown to be equivalent to the Gutzwiller variational ansatz. Some details of numerical implementations are also discussed.

- Chapter 5 shows the results of this study, where both the zero-temperature and the nonzero-temperature phase diagrams are shown. It will be shown there that the competition between the ferromagnetic interaction and the quadratic Zeeman energy gives rise to two distinct superfluid phases, and moreover, the phase transition is discontinuous at

some part of the phase boundary, in clear contrast to the corresponding phase transition in the system without a lattice.

- Chapter 6 summarizes the thesis, and discuss outlook.

## 1.4 Notes on the notations

Throughout this thesis, we use the following notations.

**The size of a finite set**
For an arbitrary finite set $S$, we denote the number of its elements by $|S|$.

**Complex conjugate**
For an arbitrary complex number $z$, we denote its complex conjugate by $z^*$.

**Operators**
In principle, we do not use the symbol hat ( $\hat{}$ ) to indicate operators.

**Hermitian conjugate**
For an arbitrary linear operator $A$ on a Hilbert space, we denote its Hermitian conjugate by $A^\dagger$.

**State vector**
In principle, **we do not use the "bra-ket" notation.** Thus, instead of $|\psi\rangle \in \mathcal{H}$, we write $\psi \in \mathcal{H}$, where $\mathcal{H}$ is a Hilbert space.

**Inner product**
For an arbitrary Hilbert space $\mathcal{H}$ and $\psi, \phi \in \mathcal{H}$, we denote their inner product by $\langle \psi, \phi \rangle$. We define the inner product to be linear with respect to the second variable and antilinear with respect to the first variable.

**Others**
Important results are enclosed by boxes, and derivations are shown in between $(\cdot.\cdot)$ and ■. Lemmas used in these derivations are derived in between $(\cdot.\cdot)$ and □.

# Chapter 2

# Ultracold spinor bosons

In this chapter, we review some basic results about ground-state properties of spin-1 bosons. Note that we do not consider optical lattices here.

- Section 2.1 discusses the properties of (alkali) atoms, where we describe the origin of the hyperfine spin, and derive the expression for the linear and quadratic Zeeman energies, which will be used in later sections.
- Section 2.2 is devoted to the derivation of the Hamiltonian of interacting spin-1 bosons. In particular, we derive the spinor interaction by imposing the assumptions of the rotational symmetry and the contact interaction on the general form of interaction Hamiltonians.
- The mean-field theory for weakly interacting spin-1 bosons is discussed in section 2.3, where the ground-state phase diagrams and the properties of various phases are given.

The aims of this chapter are

- to introduce the Hamiltonian for interacting spin-1 bosons, which will be used to derive the spin-1 Bose-Hubbard model in the next chapter, and
- to show the mean-field phase diagram of the ferromagnetic interaction case, in which the competition between the ferromagnetic interaction and the positive quadratic Zeeman energy gives rise to two superfluid phases and continuous phase transitions between them, which will be compared with the results shown in chapter 5.

## 2.1 Atomic properties

In this section, we consider one-particle properties of an alkali atom. We describe the hyperfine spin and the Zeeman effect, which are needed in writing down the one-particle Hamiltonian in the next section.

### 2.1.1 Hyperfine spin

The total spin of an atom, $\boldsymbol{F}$, is composed of the electronic spin $\boldsymbol{s}$, the electronic orbital angular momentum $\boldsymbol{l}$ , and the nuclear spin $\boldsymbol{I}$, and we write $\boldsymbol{F} = \boldsymbol{I} + \boldsymbol{J}$ and $\boldsymbol{J} = \boldsymbol{s} + \boldsymbol{l}$.

Due to the presence of the hyperfine interaction, whose Hamiltonian is given by

$$H_{\rm hf} := A\boldsymbol{I}\cdot\boldsymbol{J}, \tag{2.1}$$

where $A$ is a constant, which could be positive or negative depending on the atom, the atomic ground-state subspace split into manifolds of states with definite total spin $F$, and their energy, $E_{F,I,J}$, is given by

$$E_{F,I,J} := \frac{A}{2}\left[F(F+1) - I(I+1) - J(J+1)\right], \tag{2.2}$$

where $I$ and $J$ denote the spins of the nucleus and the electrons, respectively.
$(\because)$

Assuming that the nucleus and the electrons have definite angular momentum $I$ and $J$, the Hamiltonian can be rewritten as

$$\begin{aligned} H_{\rm hf} &= \frac{A}{2}\left[(\boldsymbol{I}+\boldsymbol{J})^2 - \boldsymbol{I}^2 - \boldsymbol{J}^2\right] && (2.3)\\ &= \frac{A}{2}\left[\boldsymbol{F}^2 - I(I+1) - J(J+1)\right]. && (2.4)\end{aligned}$$

Thus, the atomic ground states split into manifolds in which states have a definite total spin $F$ in each manifold, and their energy, $E_{F,I,J}$, is given by

$$E_{F,I,J} := \frac{A}{2}\left[F(F+1) - I(I+1) - J(J+1)\right]. \tag{2.5}$$

■

**The hyperfine energy splitting of alkali atoms**

For alkali atoms, which are widely utilized in the field of ultracold atomic physics, $J = 1/2$ holds, because all electrons except for one occupy the inner shell, and the remaining one occupies the outermost $s$ orbital. Thus, the atomic ground states split into two manifolds with $F = I \pm 1/2$. The hyperfine energy splitting $\Delta E_{\rm hf}$ of an alkali atom is defined by

$$\begin{aligned} \Delta E_{\rm hf} &:= E_{I+\frac{1}{2},I,\frac{1}{2}} - E_{I-\frac{1}{2},I,\frac{1}{2}} && (2.6)\\ &= A\left(I+\frac{1}{2}\right) && (2.7)\end{aligned}$$

In table 2.1, we list these quantities for several alkali atoms. It can be seen that for atoms listed in the table, we have positive $\Delta E_{\rm hf}$ and consequently positive $A$. Thus, for these atoms, the hyperfine states with $F = I - \frac{1}{2}$ lies lower in energy than those with $F = I + \frac{1}{2}$.

### 2.1.2 The Zeeman effect

**The Hamiltonian and its energy eigenvalues**

In the presence of an external magnetic field, atomic levels further split into levels with different energies. The Hamiltonian which describes such system is given by

$$H_{\rm spin} = A\boldsymbol{I}\cdot\boldsymbol{J} + CJ^{(3)} + DI^{(3)}, \tag{2.8}$$

| Atom | $s$ | $l$ | $J$ | $I$ | $F$ | $\Delta E_{\rm hf}/(h\cdot\mathrm{GHz})$ | $\mu/\mu_N$ |
|---|---|---|---|---|---|---|---|
| $^{1}$H | 1/2 | 0 | 1/2 | 1/2 | 0, 1 | 1.42 | 2.793 |
| $^{6}$Li | 1/2 | 0 | 1/2 | 1 | 1/2, 3/2 | 0.228 | 0.822 |
| $^{7}$Li | 1/2 | 0 | 1/2 | 3/2 | 1, 2 | 0.804 | 3.256 |
| $^{23}$Na | 1/2 | 0 | 1/2 | 3/2 | 1, 2 | 1.772 | 2.218 |
| $^{85}$Rb | 1/2 | 0 | 1/2 | 5/2 | 2, 3 | 3.036 | 1.353 |
| $^{87}$Rb | 1/2 | 0 | 1/2 | 3/2 | 1, 2 | 6.835 | 2.751 |

Table 2.1: Angular momenta and other physical quantities for alkali atoms used in cold atom experiments. $s$: the electronic spin, $l$: the electronic orbital angular momentum, $J$: the total electronic angular momentum, $I$: the nuclear spin, $F$: the total angular momentum of the atom, $\Delta E_{\rm hf}$: the hyperfine splitting of the atomic ground state, and $\mu$: the nuclear magnetic moment in units of the nuclear magneton $\mu_N$. Values are taken from table 1 of [17], and tables 3.1 and 3.2 of [6].

where $C$ and $D$ are constants proportional to the external magnetic field $B$, and we take the axis of the external magnetic field to be the third direction. **In this section, we limit ourselves to the case of $J = 1/2$, i.e., the case of alkali atoms, and $I = 3/2$.** Then, the atomic ground states now split into states with energy

$$E_2 := \frac{3}{4}A + \frac{1}{2}C + \frac{3}{2}D, \tag{2.9}$$

$$E_{1,\pm} := -\frac{A}{4} + D \pm \sqrt{\frac{3}{4}A^2 + \frac{1}{4}(A + C - D)^2}, \tag{2.10}$$

$$E_{0,\pm} := -\frac{A}{4} \pm \sqrt{A^2 + \frac{1}{4}(C - D)^2}, \tag{2.11}$$

$$E_{-1,\pm} := -\frac{A}{4} - D \pm \sqrt{\frac{3}{4}A^2 + \frac{1}{4}(A - C + D)^2}, \tag{2.12}$$

$$E_{-2} := \frac{3}{4}A - \frac{1}{2}C - \frac{3}{2}D. \tag{2.13}$$

The first subscript of each $E$ refers to the value of $m_I + m_J$ for the corresponding eigenstate, where $m_I$ and $m_J$ are magnetic quantum numbers for the nucleus spin and the electronic angular momentum.
(∵)

The Hamiltonian can be rewritten as

$$H_{\rm spin} = A\left[I^{(3)}J^{(3)} + \frac{1}{2}\left(I^+J^- + I^-J^+\right)\right] + CJ^{(3)} + DI^{(3)}, \tag{2.14}$$

where $I^\pm := I^{(1)} \pm iI^{(2)}$ and $J^\pm := J^{(1)} \pm iJ^{(2)}$ are ladder operators.

Because the Hamiltonian conserves the value of $m_I + m_J$, we can consider subspaces with different values of $m_I + m_J$ separately. Hereafter in this derivation, the state with the magnetic quantum numbers $m_I$ and $m_J$ is denoted by $\phi_{m_I,m_J}$.

The cases with $m_I + m_J = \pm 2$ are trivial and we get

$$H_{\rm spin}\phi_{\pm\frac{3}{2},\pm\frac{1}{2}} = E_{\pm2}\phi_{\pm\frac{3}{2},\pm\frac{1}{2}}, \quad E_{\pm2} = \frac{3}{4}A \pm \frac{1}{2}C \pm \frac{3}{2}D. \tag{2.15}$$

For $m_I + m_J = 1$, we have

$$H_{\text{spin}}\phi_{\frac{3}{2},-\frac{1}{2}} = \left(-\frac{3}{4}A - \frac{1}{2}C + \frac{3}{2}D\right)\phi_{\frac{3}{2},-\frac{1}{2}} + \frac{\sqrt{3}}{2}A\phi_{\frac{1}{2},\frac{1}{2}}, \tag{2.16}$$

$$H_{\text{spin}}\phi_{\frac{1}{2},\frac{1}{2}} = \left(\frac{1}{4}A + \frac{1}{2}C + \frac{1}{2}D\right)\phi_{\frac{1}{2},\frac{1}{2}} + \frac{\sqrt{3}}{2}A\phi_{\frac{3}{2},-\frac{1}{2}}. \tag{2.17}$$

Thus, $H_{\text{spin}}$ in this subspace can be expressed as

$$\begin{pmatrix} -\frac{3}{4}A - \frac{1}{2}C + \frac{3}{2}D & \frac{\sqrt{3}}{2}A \\ \frac{\sqrt{3}}{2}A & \frac{1}{4}A + \frac{1}{2}C + \frac{1}{2}D \end{pmatrix}, \tag{2.18}$$

where the basis are placed in the order of $\phi_{\frac{3}{2},-\frac{1}{2}}$, $\phi_{\frac{1}{2},\frac{1}{2}}$. Thus, we obtain its eigenvalues

$$E_{1,\pm} := -\frac{A}{4} + D \pm \sqrt{\frac{3}{4}A^2 + \frac{1}{4}(A + C - D)^2}. \tag{2.19}$$

The result for $m_I + m_J = -1$ can be obtained by reversing the signs of $C$ and $D$ in the result for $m_I + m_J = 1$.

For $m_I + m_J = 0$, we have

$$H_{\text{spin}}\phi_{\frac{1}{2},-\frac{1}{2}} = \left(-\frac{1}{4}A - \frac{1}{2}C + \frac{1}{2}D\right)\phi_{\frac{1}{2},-\frac{1}{2}} + A\phi_{-\frac{1}{2},\frac{1}{2}}, \tag{2.20}$$

$$H_{\text{spin}}\phi_{-\frac{1}{2},\frac{1}{2}} = \left(-\frac{1}{4}A + \frac{1}{2}C - \frac{1}{2}D\right)\phi_{-\frac{1}{2},\frac{1}{2}} + A\phi_{\frac{1}{2},-\frac{1}{2}} \tag{2.21}$$

Thus, $H_{\text{spin}}$ in this subspace can be expressed as

$$\begin{pmatrix} -\frac{1}{4}A - \frac{1}{2}C + \frac{1}{2}D & A \\ A & -\frac{1}{4}A + \frac{1}{2}C - \frac{1}{2}D \end{pmatrix}, \tag{2.22}$$

where basis are placed in the order of $\phi_{\frac{1}{2},-\frac{1}{2}}$, $\phi_{-\frac{1}{2},\frac{1}{2}}$. Its eigenvalues are

$$E_{0,\pm} := -\frac{A}{4} \pm \sqrt{A^2 + \frac{1}{4}(C - D)^2}. \tag{2.23}$$

■

**Approximation: neglecting the $D$ term**

Physically, the constants $C$ and $D$ are given by

$$C = g\mu_B B, \quad D = -\frac{\mu}{I}B, \tag{2.24}$$

where $g$ is the electronic spin $g$ factor ($g \simeq 2.002$), $\mu_B$ is the Bohr magneton, and $\mu$ is the nuclear magnetic momentum [1].

It can be shown that the constant $D$ is much smaller than $A$ and $C$, and can be neglected for magnetic fields used in experiments.
(∵)

[1] This usage is limited to the present chapter. Later, we use the letter $\mu$ to denote the chemical potential.

First, let us consider $|D/C|$. Because the Landé $g$ factor and $I$ are of the order of 1, and the nuclear magnetic momentum $\mu$ is of the order of the nuclear magneton $\mu_N$ (table 2.1), we have

$$\left|\frac{D}{C}\right| \sim \frac{\mu_N}{\mu_B} \tag{2.25}$$

From their definitions, we have $\mu_B = \frac{e\hbar}{2m_e}$ and $\mu_N = \frac{e\hbar}{2m_p}$, where $e$ is the absolute value of the charge of the electron, $\hbar$ is the Dirac constant, $m_e$ is the electron mass, and $m_p$ is the proton mass. Thus, we have

$$\left|\frac{D}{C}\right| \sim \frac{\mu_N}{\mu_B} = \frac{m_e}{m_p} \sim 10^{-3} \tag{2.26}$$

To compare $D$ with $A$, we use the fact that $\Delta E_{\rm hf} = 2A$ (see (2.7)), which gives

$$\left|\frac{D}{A}\right| \sim \frac{\mu_N B}{\Delta E_{\rm hf}}. \tag{2.27}$$

Because $\mu_N \sim 5 \times 10^{-27}\mathrm{J\ T^{-1}}$ and $\Delta E_{\rm hf}$ is of the order of $6 \times 10^{-25}\mathrm{J}$ (see table 2.1), we have

$$\left|\frac{D}{A}\right| \sim 10^{-2}\mathrm{T}^{-1}|B|, \tag{2.28}$$

which shows that $|D|$ is much smaller than $A$ for magnetic fields usually used in ultracold atomic experiments, where $B$ is much smaller than 1T.

■

Based on this argument, we can approximate the atomic energy eigenvalues by

$$E_2 \simeq A\left(\frac{3}{4} + \frac{b}{2}\right) =: \tilde{E}_2, \tag{2.29}$$

$$E_{1,\pm} \simeq A\left(-\frac{1}{4} \pm \sqrt{\frac{3}{4} + \frac{1}{4}(1+b)^2}\right) =: \tilde{E}_{1,\pm}, \tag{2.30}$$

$$E_{0,\pm} \simeq A\left(-\frac{1}{4} \pm \sqrt{1 + \frac{b^2}{4}}\right) =: \tilde{E_{0,\pm}}, \tag{2.31}$$

$$E_{-1,\pm} \simeq A\left(-\frac{1}{4} \pm \sqrt{\frac{3}{4} + \frac{1}{4}(1-b)^2}\right) =: \tilde{E}_{-1,\pm}, \tag{2.32}$$

$$E_{-2} \simeq A\left(\frac{3}{4} - \frac{b}{2}\right) =: \tilde{E}_{-2}, \tag{2.33}$$

where the effective magnetic field $b$ is defined by

$$b := \frac{C}{A} = \frac{2g\mu_B B}{\Delta E_{\rm hf}} \tag{2.34}$$

and **we assume** $A > 0$, which is the case for atoms listed in table 2.1.

Figure 2.1 shows the plot of these energy eigenvalues as functions of $b$ after the approximation.

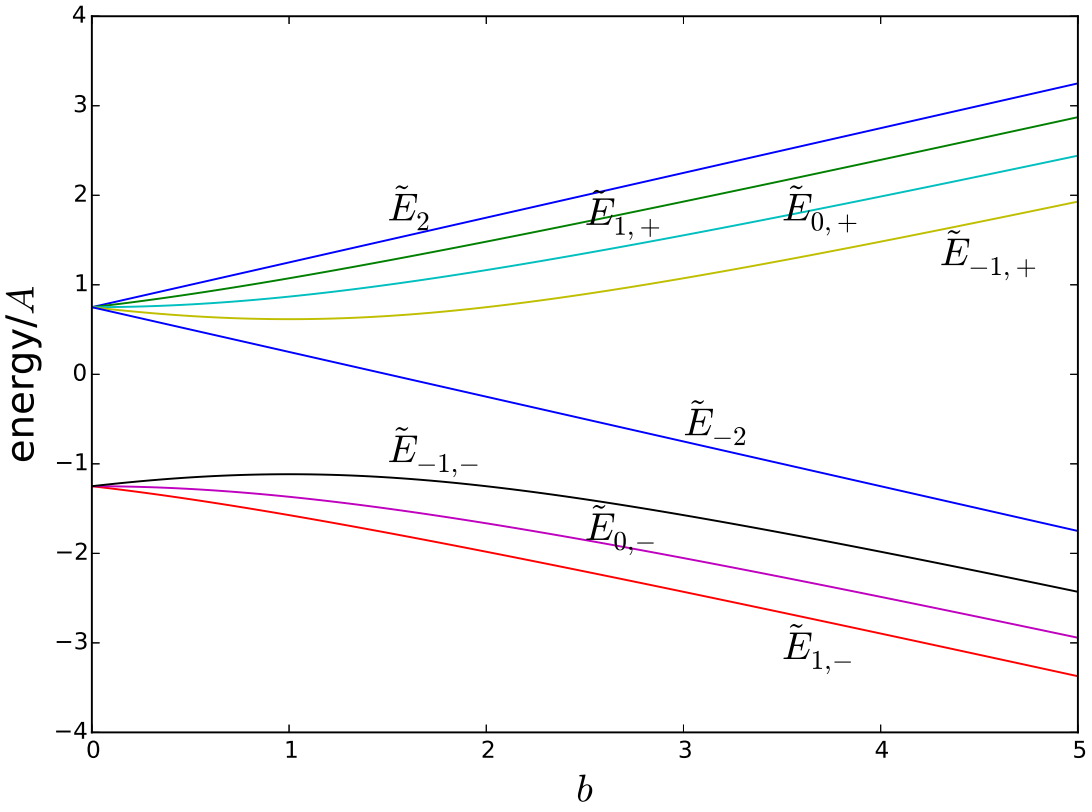


Figure 2.1: Approximate energy eigenvalues of the atomic Hamiltonian for $I = \frac{3}{2}$, $J = \frac{1}{2}$ after neglecting $D$, displayed as functions of the effective magnetic field $b$. Note that $A > 0$ is assumed, and the energies are measured in units of $A$.

### The linear and quadratic Zeeman energies

Usually, experiments on ultracold alkali atoms are carried out in relatively low magnetic field where $b \ll 1$ holds. Thus, we can expand energy eigenvalues in terms of $b$ and keep only a few low order terms. Concretely, we have, for low-lying three states,

$$\tilde{E}_{1,-} = A\left(-\frac{5}{4} - \frac{1}{4}b - \frac{3}{32}b^2\right) + \mathcal{O}(b^3) \tag{2.35}$$

$$\tilde{E}_{0,-} = A\left(-\frac{5}{4} - \frac{1}{8}b^2\right) + \mathcal{O}(b^3) \tag{2.36}$$

$$\tilde{E}_{1,-} = A\left(-\frac{5}{4} + \frac{1}{4}b - \frac{3}{32}b^2\right) + \mathcal{O}(b^3). \tag{2.37}$$

In the following sections, only the energy differences matter, and thus we can consider energy eigenvalues after subtracting $\tilde{E}_{0,-}$:

$$\tilde{E}_{1,-} - \tilde{E}_{0,-} = A\left(-\frac{1}{4}b + \frac{1}{32}b^2\right) + \mathcal{O}(b^3) = -p + q + \mathcal{O}(b^3), \tag{2.38}$$

$$\tilde{E}_{1,-} - \tilde{E}_{0,-} = A\left(\frac{1}{4}b + \frac{1}{32}b^2\right) + \mathcal{O}(b^3) = p + q + \mathcal{O}(b^3), \tag{2.39}$$

where we have defined

$$p := \frac{1}{4}Ab = \frac{1}{4}g\mu_B B, \tag{2.40}$$

$$q := \frac{1}{32}b^2 A = \frac{1}{16}\frac{(g\mu_B B)^2}{\Delta E_{\rm hf}}, \tag{2.41}$$

and call $p$ the linear Zeeman energy and $q$ the quadratic Zeeman energy.

### 2.1.3 Spin-1 bosons

In the next and later sections, we focus on the three low-lying states with energy $\tilde{E}_{1,-}, \tilde{E}_0$ and $\tilde{E}_{-1,0}$, and regard them as the internal degrees of freedom of a spin-1 bosonic atom [2].

## 2.2 Hamiltonian for spin-1 bosons

Based on the results in the previous section and symmetry discussion, we derive the Hamiltonian for interacting spin-1 bosons [19, 20]. In 2.2.1, we show the single-particle Hamiltonian, and 2.2.2 is devoted to the derivation of the interaction Hamiltonian. The final result is summarized in 2.2.3.

### 2.2.1 Single-particle Hamiltonian

According to the result of the previous section, the single-particle Hamiltonian $H_{\rm sp}$ is given by

$$H_{\rm sp} := \int_V d\boldsymbol{r} \sum_{\sigma\in\mathcal{S}} \hat{\psi}^\dagger(\boldsymbol{r},\sigma)\left[-\frac{\hbar^2}{2M}\nabla^2 + U(\boldsymbol{r}) - p\sigma + q\sigma^2\right]\hat{\psi}(\boldsymbol{r},\sigma), \tag{2.42}$$

where

- $V \subset \mathbb{R}^3$ denotes the region in which particles reside, $\boldsymbol{r} \in V$ represents the position [3], $\sigma \in \mathcal{S} := \{1, 0, -1\}$ represents the spin index,
- $\hat{\psi}(\boldsymbol{r},\sigma)$ is the field operator with position $\boldsymbol{r}$ and spin index $\sigma$,
- $M$ is the mass of the atom,
- $U$ is the external potential,
- $p$ and $q$ are the linear and quadratic Zeeman energies defined in (2.40) and (2.41), where we have subtracted the energy of the $\sigma = 0$ level.

[2] In the presence of an external magnetic field, the total spin $F$ is not a good quantum number, i.e., $H_{\rm spin}$ and $\boldsymbol{F}$ are not simultaneously diagonalizable. However, for a weak magnetic field, $F$ can be an approximate good quantum number, and we regard atoms in these three levels as $F = 1$ spinor atoms.

[3] Henceforth, the ranges of integrals are understood to be $V$ (or direct products of $V$) unless otherwise stated.

### 2.2.2 Interaction Hamiltonian

Here we show that the interaction Hamiltonian can be obtained by imposing the following two conditions on the general form of the interaction Hamiltonians:

- The interaction Hamiltonian commutes with the total spin operators, i.e., the interaction is invariant under global spin rotations.
- The interaction occurs only between two atoms at the same position, i.e., the interaction is a contact interaction.

Before showing the result, we first define several operators.

The particle-number density operator is defined by

$$\hat{n}(\boldsymbol{r}) := \sum_{\sigma \in \mathcal{S}} \hat{\psi}^\dagger(\boldsymbol{r}, \sigma)\hat{\psi}(\boldsymbol{r}, \sigma). \tag{2.43}$$

The spin density operators $\hat{F}^{(\alpha)}(\boldsymbol{r})$, where $\boldsymbol{r} \in V$ denotes the position and $\alpha \in \{1, 2, 3\}$ denotes the direction, are defined by

$$\hat{F}^{(\alpha)}(\boldsymbol{r}) := \sum_{\sigma,\tau \in \mathcal{S}} S^{(\alpha)}_{\sigma,\tau}\hat{\psi}^\dagger(\boldsymbol{r}, \sigma)\hat{\psi}(\boldsymbol{r}, \tau), \tag{2.44}$$

and spin-1 matrices $S^{(\alpha)}$ ($\alpha \in \{1, 2, 3\}$) are defined by

$$S^{(1)} := \frac{1}{\sqrt{2}} \begin{pmatrix} 0 & 1 & 0 \\ 1 & 0 & 1 \\ 0 & 1 & 0 \end{pmatrix}, \quad S^{(2)} := \frac{i}{\sqrt{2}} \begin{pmatrix} 0 & -1 & 0 \\ 1 & 0 & -1 \\ 0 & 1 & 0 \end{pmatrix}, \quad S^{(3)} := \begin{pmatrix} 1 & 0 & 0 \\ 0 & 0 & 0 \\ 0 & 0 & -1 \end{pmatrix}, \tag{2.45}$$

where it is understood that matrix indices are in the order of $1, 0, -1$ [a], and $\alpha = 3$ corresponds to the direction of the quantization axis.
The total spin operator $\hat{F}^{(\alpha)}_{\text{tot}}$is defined by

$$\hat{F}^{(\alpha)}_{\text{tot}} := \int d\boldsymbol{r}\hat{F}^{(\alpha)}(\boldsymbol{r}). \tag{2.46}$$

[a]For example, $S^{(3)}_{\sigma,\tau}$ can be written as $S^{(3)}_{\sigma,\tau} = \sigma\delta_{\sigma,\tau}$.

Under these definitions, the interaction Hamiltonian is given by

$$H_{\text{int}} = \frac{1}{2}\int d\boldsymbol{r}\left[c_0 : \hat{n}(\boldsymbol{r})\hat{n}(\boldsymbol{r}) : \ + c_1 : \hat{\boldsymbol{F}}(\boldsymbol{r})\cdot\hat{\boldsymbol{F}}(\boldsymbol{r}) :\right], \tag{2.47}$$

$$c_0 := \frac{g_0 + 2g_2}{3}, \quad c_1 := \frac{g_2 - g_0}{3}, \tag{2.48}$$

where $:\cdot:$ denotes the normal ordering of creation and annihilation operators,

$$g_F := \frac{4\pi\hbar^2}{M}a_F, \tag{2.49}$$

$M$ is the mass of the atom, and $a_F$ is the $s$-wave scattering length of the total spin-$F$ channel.

The derivation is given below, which proceeds step by step. It assumes spin-1 bosons, but the argument in step 1 and step 2 applies to general spinor bosons.

**Step 1: Rewriting the general interaction Hamiltonian**

First, we present the general form of the two-body interaction Hamiltonians.

In general, the two-body interaction Hamiltonian can be written as

$$H_{\text{int}} = \frac{1}{2}\sum_{\sigma_1,\sigma_2,\tau_1,\tau_2\in\mathcal{S}}\int d\boldsymbol{r}_1 d\boldsymbol{r}_2 V_{\sigma_1,\sigma_2,\tau_1,\tau_2}(\boldsymbol{r}_1,\boldsymbol{r}_2)\hat{\psi}^\dagger(\boldsymbol{r}_1,\sigma_1)\hat{\psi}^\dagger(\boldsymbol{r}_2,\sigma_2)\hat{\psi}(\boldsymbol{r}_1,\tau_1)\hat{\psi}(\boldsymbol{r}_2,\tau_2), \tag{2.50}$$

where $V$ is a function, which can be assumed to satisfy

$$V_{\sigma_1,\sigma_2,\tau_1,\tau_2}(\boldsymbol{r}_1,\boldsymbol{r}_2) = V_{\sigma_2,\sigma_1,\tau_2,\tau_1}(\boldsymbol{r}_2,\boldsymbol{r}_1) \ \ (\forall\ \boldsymbol{r}_1,\boldsymbol{r}_2\in V,\ \forall\ \sigma_1,\sigma_2,\tau_1,\tau_2\in\mathcal{S}) \tag{2.51}$$

without loss of generality.

To make the calculation easy, we rewrite the general interaction Hamiltonian in terms of the composite spin of two spins.

Let $F \in \{0,1,2\}$, $M \in \{-2,-1,0,1,2\}$ be quantum numbers representing the magnitude and the third component of the composite spin of two spins with magnitude 1, respectively. Here we denote the Clebsch-Gordan coefficients by $\langle F, M|\sigma_1, \sigma_2\rangle$, where $\sigma_1, \sigma_2 \in \mathcal{S}$. If we define

$$A_{F,M}(\boldsymbol{r}_1, \boldsymbol{r}_2) := \sum_{\sigma_1,\sigma_2\in\mathcal{S}} \langle F, M|\sigma_1, \sigma_2\rangle \hat{\psi}(\boldsymbol{r}_1, \sigma_1)\hat{\psi}(\boldsymbol{r}_2, \sigma_2), \tag{2.52}$$

$$U_{F,M,F',M'}(\boldsymbol{r}_1, \boldsymbol{r}_2) := \sum_{\sigma_1,\sigma_2,\tau_1,\tau_2\in\mathcal{S}} V_{\sigma_1,\sigma_2,\tau_1,\tau_2}(\boldsymbol{r}_1, \boldsymbol{r}_2)\langle F, M|\sigma_1, \sigma_2\rangle\langle\tau_1, \tau_2|F', M'\rangle, \tag{2.53}$$

then we can rewrite the general interaction Hamiltonian as

$$H_{\rm int} = \frac{1}{2}\int d\boldsymbol{r}_1 d\boldsymbol{r}_2 \sum_{F,F'=0}^{2}\sum_{M,M'=-2}^{2} U_{F,M,F',M'}(\boldsymbol{r}_1, \boldsymbol{r}_2)A^{\dagger}_{F,M}(\boldsymbol{r}_1, \boldsymbol{r}_2)A_{F',M'}(\boldsymbol{r}_1, \boldsymbol{r}_2). \tag{2.54}$$

In addition,

$$A_{F,M}(\boldsymbol{r}_2, \boldsymbol{r}_1) = (-1)^F A_{F,M}(\boldsymbol{r}_1, \boldsymbol{r}_2), \tag{2.55}$$

$$U_{F,M,F',M'}(\boldsymbol{r}_2, \boldsymbol{r}_1) = (-1)^{F+F'} U_{F,M,F',M'}(\boldsymbol{r}_1, \boldsymbol{r}_2) \tag{2.56}$$

hold, and in particular, for odd $F$, we have $A_{F,M}(\boldsymbol{r}, \boldsymbol{r}) = 0$.

The meaning of $A_{F,M}(\boldsymbol{r}_1, \boldsymbol{r}_2)$ will be shown in the next box.
(∵)

From the completeness of the CG coefficients

$$\delta_{\sigma_1,\sigma_1'}\delta_{\sigma_2,\sigma_2'} = \sum_{F=0}^{2}\sum_{M=-2}^{2}\langle\sigma_1', \sigma_2'|F, M\rangle\langle F, M|\sigma_1, \sigma_2\rangle, \tag{2.57}$$

we have

$$\begin{aligned}
& H_{\rm int} \\
= & \frac{1}{2}\sum_{\sigma_1,\sigma_2,\tau_1,\tau_2\in\mathcal{S}}\int d\boldsymbol{r}_1 d\boldsymbol{r}_2 V_{\sigma_1,\sigma_2,\tau_1,\tau_2}(\boldsymbol{r}_1, \boldsymbol{r}_2)\hat{\psi}^{\dagger}(\boldsymbol{r}_1, \sigma_1)\hat{\psi}^{\dagger}(\boldsymbol{r}_2, \sigma_2)\hat{\psi}(\boldsymbol{r}_1, \tau_1)\hat{\psi}(\boldsymbol{r}_2, \tau_2) \qquad (2.58)\\
= & \frac{1}{2}\int d\boldsymbol{r}_1 d\boldsymbol{r}_2 \sum_{\substack{\sigma_1,\sigma_2,\\ \tau_1,\tau_2\in\mathcal{S}}}\sum_{\substack{\sigma_1',\sigma_2',\\ \tau_1',\tau_2'\in\mathcal{S}}}\sum_{F,F'=0}^{2}\sum_{M,M'=-2}^{2} V_{\sigma_1,\sigma_2,\tau_1,\tau_2}(\boldsymbol{r}_1, \boldsymbol{r}_2) \\
& \times\langle F, M|\sigma_1, \sigma_2\rangle\langle\sigma_1', \sigma_2'|F, M\rangle\hat{\psi}^{\dagger}(\boldsymbol{r}_1, \sigma_1')\hat{\psi}^{\dagger}(\boldsymbol{r}_2, \sigma_2') \\
& \times\langle F', M'|\tau_1', \tau_2'\rangle\langle\tau_1, \tau_2|F', M'\rangle\hat{\psi}(\boldsymbol{r}_1, \tau_1')\hat{\psi}(\boldsymbol{r}_2, \tau_2') \qquad (2.59)\\
= & \frac{1}{2}\int d\boldsymbol{r}_1 d\boldsymbol{r}_2 \sum_{F,F'=0}^{2}\sum_{M,M'=-2}^{2}\left[\sum_{\substack{\sigma_1,\sigma_2,\\ \tau_1,\tau_2\in\mathcal{S}}} V_{\sigma_1,\sigma_2,\tau_1,\tau_2}(\boldsymbol{r}_1, \boldsymbol{r}_2)\langle F, M|\sigma_1, \sigma_2\rangle\langle\tau_1, \tau_2|F', M'\rangle\right] \\
& \times\sum_{\sigma_1',\sigma_2'\in\mathcal{S}}\langle\sigma_1', \sigma_2'|F, M\rangle\hat{\psi}^{\dagger}(\boldsymbol{r}_1, \sigma_1')\hat{\psi}^{\dagger}(\boldsymbol{r}_2, \sigma_2')
\end{aligned}$$

$$\times \sum_{\tau_1',\tau_2' \in \mathcal{S}} \langle F', M' | \tau_1', \tau_2' \rangle \hat{\psi}(\boldsymbol{r}_1, \tau_1') \hat{\psi}(\boldsymbol{r}_2, \tau_2') \tag{2.60}$$

$$= \frac{1}{2} \int d\boldsymbol{r}_1 d\boldsymbol{r}_2 \sum_{F,F'=0}^{2} \sum_{M,M'=-2}^{2} U_{F,M,F',M'}(\boldsymbol{r}_1, \boldsymbol{r}_2) A^{\dagger}_{F,M}(\boldsymbol{r}_1, \boldsymbol{r}_2) A_{F',M'}(\boldsymbol{r}_1, \boldsymbol{r}_2). \tag{2.61}$$

Next, we show the latter part. By noting the property

$$\langle F, M | \sigma_2, \sigma_1 \rangle = (-1)^F \langle F, M | \sigma_1, \sigma_2 \rangle, \tag{2.62}$$

we have

$$\begin{aligned} A_{F,M}(\boldsymbol{r}_2, \boldsymbol{r}_1) &= \sum_{\sigma_1,\sigma_2 \in \mathcal{S}} \langle F, M | \sigma_2, \sigma_1 \rangle \hat{\psi}(\boldsymbol{r}_2, \sigma_2) \hat{\psi}(\boldsymbol{r}_1, \sigma_1) && (2.63) \\ &= (-1)^F \sum_{\sigma_1,\sigma_2 \in \mathcal{S}} \langle F, M | \sigma_1, \sigma_2 \rangle \hat{\psi}(\boldsymbol{r}_1, \sigma_1) \hat{\psi}(\boldsymbol{r}_2, \sigma_2) && (2.64) \\ &= (-1)^F A_{F,M}(\boldsymbol{r}_1, \boldsymbol{r}_2). && (2.65) \end{aligned}$$

For $U$, the definition

$$U_{F,M,F',M'}(\boldsymbol{r}_2, \boldsymbol{r}_1) = \sum_{\sigma_1,\sigma_2,\tau_1,\tau_2 \in \mathcal{S}} V_{\sigma_2,\sigma_1,\tau_2,\tau_1}(\boldsymbol{r}_2, \boldsymbol{r}_1) \langle F, M | \sigma_2, \sigma_1 \rangle \langle \tau_2, \tau_1 | F', M' \rangle \tag{2.66}$$

and the properties

$$\begin{aligned} V_{\sigma_2,\sigma_1,\tau_2,\tau_1}(\boldsymbol{r}_2, \boldsymbol{r}_1) &= V_{\sigma_1,\sigma_2,\tau_1,\tau_2}(\boldsymbol{r}_1, \boldsymbol{r}_2), && (2.67) \\ \langle F, M | \sigma_2, \sigma_1 \rangle &= (-1)^F \langle F, M | \sigma_1, \sigma_2 \rangle, && (2.68) \\ \langle \tau_2, \tau_1 | F', M' \rangle &= (-1)^{F'} \langle \tau_1, \tau_2 | F', M' \rangle && (2.69) \end{aligned}$$

yield

$$U_{F,M,F',M'}(\boldsymbol{r}_2, \boldsymbol{r}_1) = (-1)^{F+F'} U_{F,M,F',M'}(\boldsymbol{r}_1, \boldsymbol{r}_2). \tag{2.70}$$

■

$A^{\dagger}_{F,M}(\boldsymbol{r}_1, \boldsymbol{r}_2)$ can be regarded as an operator which creates a pair of two particles, one at $\boldsymbol{r}_1$ and the other at $\boldsymbol{r}_2$, with total spin $(F, M)$. This can be seen from the following results, which will be used later:

Let $\Phi_{\text{vac}}$ be the vacuum state. Then, it follows that

$$\begin{aligned} \hat{n}(\boldsymbol{r}) A^{\dagger}_{F,M}(\boldsymbol{r}_1, \boldsymbol{r}_2) \Phi_{\text{vac}} &= \left[ \delta(\boldsymbol{r} - \boldsymbol{r}_1) + \delta(\boldsymbol{r} - \boldsymbol{r}_2) \right] A^{\dagger}_{F,M}(\boldsymbol{r}_1, \boldsymbol{r}_2) \Phi_{\text{vac}}, && (2.71) \\ \hat{F}^{(3)}_{\text{tot}} A^{\dagger}_{F,M}(\boldsymbol{r}_1, \boldsymbol{r}_2) \Phi_{\text{vac}} &= M A^{\dagger}_{F,M}(\boldsymbol{r}_1, \boldsymbol{r}_2) \Phi_{\text{vac}}, && (2.72) \\ \hat{F}^{\pm}_{\text{tot}} A^{\dagger}_{F,M}(\boldsymbol{r}_1, \boldsymbol{r}_2) \Phi_{\text{vac}} &= \sqrt{(F \mp M)(F \pm M + 1)} A^{\dagger}_{F,M\pm1}(\boldsymbol{r}_1, \boldsymbol{r}_2) \Phi_{\text{vac}}, && (2.73) \\ \hat{\boldsymbol{F}}^2_{\text{tot}} A^{\dagger}_{F,M}(\boldsymbol{r}_1, \boldsymbol{r}_2) \Phi_{\text{vac}} &= F(F+1) A^{\dagger}_{F,M}(\boldsymbol{r}_1, \boldsymbol{r}_2) \Phi_{\text{vac}}. && (2.74) \end{aligned}$$

(∵)

**Particle number density**

From the definition of $A^\dagger_{F,M}(\boldsymbol{r}_1,\boldsymbol{r}_2)$, we have

$$\begin{aligned}
&\hat{n}(\boldsymbol{r})A^\dagger_{F,M}(\boldsymbol{r}_1,\boldsymbol{r}_2)\Phi_{\rm vac}\\
=&\sum_{\sigma,\sigma_1,\sigma_2\in\mathcal{S}}\langle\sigma_1,\sigma_2|F,M\rangle\hat{\psi}^\dagger(\boldsymbol{r},\sigma)\hat{\psi}(\boldsymbol{r},\sigma)\hat{\psi}^\dagger(\boldsymbol{r}_1,\sigma_1)\hat{\psi}^\dagger(\boldsymbol{r}_2,\sigma_2)\Phi_{\rm vac} &(2.75)\\
=&\sum_{\sigma,\sigma_1,\sigma_2\in\mathcal{S}}\langle\sigma_1,\sigma_2|F,M\rangle\hat{\psi}^\dagger(\boldsymbol{r},\sigma)\\
&\times\Big([\hat{\psi}(\boldsymbol{r},\sigma),\hat{\psi}^\dagger(\boldsymbol{r}_1,\sigma_1)]\hat{\psi}^\dagger(\boldsymbol{r}_2,\sigma_2)+\hat{\psi}^\dagger(\boldsymbol{r}_1,\sigma_1)[\hat{\psi}(\boldsymbol{r},\sigma),\hat{\psi}^\dagger(\boldsymbol{r}_2,\sigma_2)]\Big)\Phi_{\rm vac} &(2.76)\\
=&\sum_{\sigma,\sigma_1,\sigma_2\in\mathcal{S}}\langle\sigma_1,\sigma_2|F,M\rangle\hat{\psi}^\dagger(\boldsymbol{r},\sigma)\\
&\times\Big(\delta_{\sigma,\sigma_1}\delta(\boldsymbol{r}-\boldsymbol{r}_1)\hat{\psi}^\dagger(\boldsymbol{r}_2,\sigma_2)+\delta_{\sigma,\sigma_2}\delta(\boldsymbol{r}-\boldsymbol{r}_2)\hat{\psi}^\dagger(\boldsymbol{r}_1,\sigma_1)\Big)\Phi_{\rm vac} &(2.77)\\
=&[\delta(\boldsymbol{r}-\boldsymbol{r}_1)+\delta(\boldsymbol{r}-\boldsymbol{r}_2)]\sum_{\sigma_1,\sigma_2\in\mathcal{S}}\langle\sigma_1,\sigma_2|F,M\rangle\hat{\psi}^\dagger(\boldsymbol{r}_1,\sigma_1)\hat{\psi}^\dagger(\boldsymbol{r}_2,\sigma_2)\Phi_{\rm vac} &(2.78)\\
=&[\delta(\boldsymbol{r}-\boldsymbol{r}_1)+\delta(\boldsymbol{r}-\boldsymbol{r}_2)]A^\dagger_{F,M}(\boldsymbol{r}_1,\boldsymbol{r}_2)\Phi_{\rm vac}. &(2.79)
\end{aligned}$$

**The $\alpha=3$ component of the total spin**

From the definitions, we have

$$\begin{aligned}
&\hat{F}^{(\alpha)}_{\rm tot}A^\dagger_{F,M}(\boldsymbol{r}_1,\boldsymbol{r}_2)\Phi_{\rm vac}\\
=&\int d\boldsymbol{r}\sum_{\sigma,\tau,\sigma_1,\sigma_2\in\mathcal{S}}S^{(\alpha)}_{\sigma,\tau}\langle\sigma_1,\sigma_2|F,M\rangle\hat{\psi}^\dagger(\boldsymbol{r},\sigma)\hat{\psi}(\boldsymbol{r},\tau)\hat{\psi}^\dagger(\boldsymbol{r}_1,\sigma_1)\hat{\psi}^\dagger(\boldsymbol{r}_2,\sigma_2)\Phi_{\rm vac}. &(2.80)
\end{aligned}$$

Because

$$\begin{aligned}
&\hat{\psi}(\boldsymbol{r},\tau)\hat{\psi}^\dagger(\boldsymbol{r}_1,\sigma_1)\hat{\psi}^\dagger(\boldsymbol{r}_2,\sigma_2)\Phi_{\rm vac}\\
=&[\hat{\psi}(\boldsymbol{r},\tau),\hat{\psi}^\dagger(\boldsymbol{r}_1,\sigma_1)\hat{\psi}^\dagger(\boldsymbol{r}_2,\sigma_2)]\Phi_{\rm vac} &(2.81)\\
=&\Big([\hat{\psi}(\boldsymbol{r},\tau),\hat{\psi}^\dagger(\boldsymbol{r}_1,\sigma_1)]\hat{\psi}^\dagger(\boldsymbol{r}_2,\sigma_2)+\hat{\psi}^\dagger(\boldsymbol{r}_1,\sigma_1)[\hat{\psi}(\boldsymbol{r},\tau),\hat{\psi}^\dagger(\boldsymbol{r}_2,\sigma_2)]\Big)\Phi_{\rm vac} &(2.82)\\
=&(\delta(\boldsymbol{r}-\boldsymbol{r}_1)\delta_{\tau,\sigma_1}\hat{\psi}^\dagger(\boldsymbol{r}_2,\sigma_2)+\delta(\boldsymbol{r}-\boldsymbol{r}_2)\delta_{\tau,\sigma_2}\hat{\psi}^\dagger(\boldsymbol{r}_1,\sigma_1))\Phi_{\rm vac}, &(2.83)
\end{aligned}$$

it follows that

$$\begin{aligned}
&\hat{F}^{(\alpha)}_{\rm tot}A^\dagger_{F,M}(\boldsymbol{r}_1,\boldsymbol{r}_2)\Phi_{\rm vac}\\
=&\int d\boldsymbol{r}\sum_{\sigma,\tau,\sigma_1,\sigma_2\in\mathcal{S}}S^{(\alpha)}_{\sigma,\tau}\langle\sigma_1,\sigma_2|F,M\rangle\hat{\psi}^\dagger(\boldsymbol{r},\sigma)\\
&\times(\delta(\boldsymbol{r}-\boldsymbol{r}_1)\delta_{\tau,\sigma_1}\hat{\psi}^\dagger(\boldsymbol{r}_2,\sigma_2)+\delta(\boldsymbol{r}-\boldsymbol{r}_2)\delta_{\tau,\sigma_2}\hat{\psi}^\dagger(\boldsymbol{r}_1,\sigma_1))\Phi_{\rm vac} &(2.84)\\
=&\sum_{\sigma_1,\sigma_2\in\mathcal{S}}\langle\sigma_1,\sigma_2|F,M\rangle\\
&\times\sum_{\sigma\in\mathcal{S}}\Big(S^{(\alpha)}_{\sigma,\sigma_1}\hat{\psi}^\dagger(\boldsymbol{r}_1,\sigma)\hat{\psi}^\dagger(\boldsymbol{r}_2,\sigma_2)+S^{(\alpha)}_{\sigma,\sigma_2}\hat{\psi}^\dagger(\boldsymbol{r}_2,\sigma)\hat{\psi}^\dagger(\boldsymbol{r}_1,\sigma_1)\Big)\Phi_{\rm vac} &(2.85)\\
=&\sum_{\sigma_1,\sigma_2\in\mathcal{S}}\sum_{\sigma\in\mathcal{S}}\big[\langle\sigma,\sigma_2|F,M\rangle S^{(\alpha)}_{\sigma_1,\sigma}+\langle\sigma_1,\sigma|F,M\rangle S^{(\alpha)}_{\sigma_2,\sigma}\big]\\
&\times\hat{\psi}^\dagger(\boldsymbol{r}_1,\sigma_1)\hat{\psi}^\dagger(\boldsymbol{r}_2,\sigma_2)\Phi_{\rm vac}. &(2.86)
\end{aligned}$$

From the relation

$$M\langle\sigma_1,\sigma_2|F,M\rangle=\sum_{\sigma\in\mathcal{S}}\left[\langle\sigma,\sigma_2|F,M\rangle S^{(3)}_{\sigma_1,\sigma}+\langle\sigma_1,\sigma|F,M\rangle S^{(3)}_{\sigma_2,\sigma}\right], \tag{2.87}$$

which will be shown later, we obtain

$$\begin{aligned}\hat{F}^{(3)}_{\rm tot}A^{\dagger}_{F,M}(\boldsymbol{r}_1,\boldsymbol{r}_2)\Phi_{\rm vac} &= M\sum_{\sigma_1,\sigma_2\in\mathcal{S}}\langle\sigma_1,\sigma_2|F,M\rangle\hat{\psi}^{\dagger}(\boldsymbol{r}_1,\sigma_1)\hat{\psi}^{\dagger}(\boldsymbol{r}_2,\sigma_2)\Phi_{\rm vac} &(2.88)\\ &= MA^{\dagger}_{F,M}(\boldsymbol{r}_1,\boldsymbol{r}_2)\Phi_{\rm vac} &(2.89)\end{aligned}$$

**Ladder operators**

It follows from (2.86) that

$$\begin{aligned}&\hat{F}^{\pm}_{\rm tot}A^{\dagger}_{F,M}(\boldsymbol{r}_1,\boldsymbol{r}_2)\Phi_{\rm vac}\\ =&\sum_{\sigma_1,\sigma_2\in\mathcal{S}}\sum_{\sigma\in\mathcal{S}}\left[\langle\sigma,\sigma_2|F,M\rangle S^{\pm}_{\sigma_1,\sigma}+\langle\sigma_1,\sigma|F,M\rangle S^{\pm}_{\sigma_2,\sigma}\right]\\ &\times\hat{\psi}^{\dagger}(\boldsymbol{r}_1,\sigma_1)\hat{\psi}^{\dagger}(\boldsymbol{r}_2,\sigma_2)\Phi_{\rm vac}. &(2.90)\end{aligned}$$

From the relation

$$\sqrt{(F\mp M)(F\pm M+1)}\langle\sigma_1,\sigma_2|F,M\pm1\rangle=\sum_{\sigma\in\mathcal{S}}\left[\langle\sigma,\sigma_2|F,M\rangle S^{\pm}_{\sigma_1,\sigma}+\langle\sigma_1,\sigma|F,M\rangle S^{\pm}_{\sigma_2,\sigma}\right], \tag{2.91}$$

which also will be shown later, we arrive at

$$\begin{aligned}&\hat{F}^{\pm}_{\rm tot}A^{\dagger}_{F,M}(\boldsymbol{r}_1,\boldsymbol{r}_2)\Phi_{\rm vac}\\ =&\sqrt{(F\mp M)(F\pm M+1)}\sum_{\sigma_1,\sigma_2\in\mathcal{S}}\langle\sigma_1,\sigma_2|F,M\pm1\rangle\hat{\psi}^{\dagger}(\boldsymbol{r}_1,\sigma_1)\hat{\psi}^{\dagger}(\boldsymbol{r}_2,\sigma_2)\Phi_{\rm vac} &(2.92)\\ =&\sqrt{(F\mp M)(F\pm M+1)}A^{\dagger}_{F,M\pm1}(\boldsymbol{r}_1,\boldsymbol{r}_2)\Phi_{\rm vac}. &(2.93)\end{aligned}$$

**The magnitude of the total spin**

From the equalities

$$\hat{F}^{(1)}_{\rm tot}=\frac{\hat{F}^{+}_{\rm tot}+\hat{F}^{-}_{\rm tot}}{2},\quad \hat{F}^{(2)}_{\rm tot}=\frac{\hat{F}^{+}_{\rm tot}-\hat{F}^{-}_{\rm tot}}{2i}, \tag{2.94}$$

it follows that

$$\hat{\boldsymbol{F}}^{2}_{\rm tot}=\sum_{\alpha=1}^{3}\left(\hat{F}^{(\alpha)}_{\rm tot}\right)^2=\frac{1}{2}\left(\hat{F}^{+}_{\rm tot}\hat{F}^{-}_{\rm tot}+\hat{F}^{-}_{\rm tot}\hat{F}^{+}_{\rm tot}\right)+\left(\hat{F^{(3)}}_{\rm tot}\right)^2, \tag{2.95}$$

which, combined with (2.72) and (2.73) yields

$$\begin{aligned}&\hat{\boldsymbol{F}}^{2}_{\rm tot}A^{\dagger}_{F,M}(\boldsymbol{r}_1,\boldsymbol{r}_2)\Phi_{\rm vac}\\ =&\frac{1}{2}\Big[\sqrt{(F+M)(F-M+1)}\sqrt{(F-M+1)(F+M)}+\\ &\sqrt{(F-M)(F+M+1)}\sqrt{(F+M+1)(F-M)}+2M^2\Big]\\ &\times A^{\dagger}_{F,M}(\boldsymbol{r}_1,\boldsymbol{r}_2)\Phi_{\rm vac} &(2.96)\\ =&F(F+1)A^{\dagger}_{F,M}(\boldsymbol{r}_1,\boldsymbol{r}_2)\Phi_{\rm vac}. &(2.97)\end{aligned}$$

■

Here we show equalities (2.87) and (2.91) used in the previous derivation:

$$
\begin{aligned}
& M\langle\sigma_1,\sigma_2|F,M\rangle \\
= & \sum_{\sigma\in\mathcal{S}}\left[\langle\sigma,\sigma_2|F,M\rangle S^{(3)}_{\sigma_1,\sigma}+\langle\sigma_1,\sigma|F,M\rangle S^{(3)}_{\sigma_2,\sigma}\right], \qquad (2.98)\\
& \sqrt{(F\mp M)(F\pm M+1)}\langle\sigma_1,\sigma_2|F,M\pm 1\rangle \\
= & \sum_{\sigma\in\mathcal{S}}\left[\langle\sigma,\sigma_2|F,M\rangle S^{\pm}_{\sigma_1,\sigma}+\langle\sigma_1,\sigma|F,M\rangle S^{\pm}_{\sigma_2,\sigma}\right]. \qquad (2.99)
\end{aligned}
$$

(∵)

We start from an equality for two-spins

$$|F,M\rangle=\sum_{\tau_1,\tau_2\in\mathcal{S}}\langle\tau_1,\tau_2|F,M\rangle|\tau_1,\tau_2\rangle, \qquad (2.100)$$

where $\tau_1,\tau_2$ refer to each spin, while $F$ and $M$ refer to the composite spin, and $\langle\tau_1,\tau_2|F,M\rangle$ means CG coefficients.

By operating $F^{(\alpha)}\otimes I$ and $I\otimes F^{(\alpha)}$ on this equation, and then taking the inner product with $|\sigma_1,\sigma_2\rangle$, we obtain

$$
\begin{aligned}
\langle\sigma_1,\sigma_2|F^{(\alpha)}\otimes I|F,M\rangle &= \sum_{\tau_1\in\mathcal{S}}\langle\tau_1,\sigma_2|F,M\rangle\langle\sigma_1|F^{\alpha}|\tau_1\rangle \qquad (2.101)\\
&= \sum_{\sigma\in\mathcal{S}}\langle\sigma,\sigma_2|F,M\rangle S^{(\alpha)}_{\sigma_1,\sigma} \qquad (2.102)\\
\langle\sigma_1,\sigma_2|I\otimes F^{(\alpha)}|F,M\rangle &= \sum_{\tau_2\in\mathcal{S}}\langle\sigma_1,\tau_2|F,M\rangle\langle\sigma_2|F^{\alpha}|\tau_2\rangle \qquad (2.103)\\
&= \sum_{\sigma\in\mathcal{S}}\langle\sigma_1,\sigma|F,M\rangle S^{(\alpha)}_{\sigma_2,\sigma}. \qquad (2.104)
\end{aligned}
$$

Summing up these equations yields

$$
\begin{aligned}
& \langle\sigma_1,\sigma_2|F^{(\alpha)}\otimes I+I\otimes F^{(\alpha)}|F,M\rangle \\
= & \sum_{\sigma\in\mathcal{S}}\left[\langle\sigma,\sigma_2|F,M\rangle S^{(\alpha)}_{\sigma_1,\sigma}+\langle\sigma_1,\sigma|F,M\rangle S^{(\alpha)}_{\sigma_2,\sigma}\right]. \qquad (2.105)
\end{aligned}
$$

The equality (2.87) can be obtained by setting $\alpha=3$, and the equality (2.91) can be obtained by taking [(2.105) with $\alpha=1$] $\pm i$ [(2.105) with $\alpha=2$].

■

For later convenience, we calculate matrix elements of $H_{\rm int}$:

$$
\begin{aligned}
& \left\langle A^{\dagger}_{F,M}(\boldsymbol{r}_1,\boldsymbol{r}_2)\Phi_{\rm vac}, H_{\rm int}A^{\dagger}_{F',M'}(\boldsymbol{r}'_1,\boldsymbol{r}'_2)\Phi_{\rm vac}\right\rangle \\
= & U_{F,M,F',M'}(\boldsymbol{r}_1,\boldsymbol{r}_2)\left[\delta(\boldsymbol{r}_1-\boldsymbol{r}'_1)\delta(\boldsymbol{r}_2-\boldsymbol{r}'_2)+(-1)^{F'}\delta(\boldsymbol{r}_1-\boldsymbol{r}'_2)\delta(\boldsymbol{r}_2-\boldsymbol{r}'_1)\right]. \qquad (2.106)
\end{aligned}
$$

(∵)

First, we show that

$$\begin{aligned} & A_{\tilde{F},\tilde{M}}(\boldsymbol{q}_1,\boldsymbol{q}_2)A^{\dagger}_{F,M}(\boldsymbol{r}_1,\boldsymbol{r}_2)\Phi_{\rm vac} \\ = \; & \left[(-1)^F\delta(\boldsymbol{q}_1-\boldsymbol{r}_2)\delta(\boldsymbol{q}_2-\boldsymbol{r}_1)+\delta(\boldsymbol{q}_1-\boldsymbol{r}_1)\delta(\boldsymbol{q}_2-\boldsymbol{r}_2)\right] \\ & \times\delta_{F,\tilde{F}}\delta_{M,\tilde{M}}\Phi_{\rm vac} \end{aligned} \tag{2.107}$$

holds.
(∵)

From the definition of the operator $A_{F,M}(\boldsymbol{r}_1,\boldsymbol{r}_2)$, we have

$$\begin{aligned} & A_{\tilde{F},\tilde{M}}(\boldsymbol{q}_1,\boldsymbol{q}_2)A^{\dagger}_{F,M}(\boldsymbol{r}_1,\boldsymbol{r}_2)\Phi_{\rm vac} \\ = \; & \sum_{\substack{\sigma_1,\sigma_2 \\ \sigma_1',\sigma_2'\in\mathcal{S}}} \langle\tilde{F},\tilde{M}|\sigma_1,\sigma_2\rangle\langle\sigma_1',\sigma_2'|F,M\rangle \\ & \times\hat{\psi}(\boldsymbol{q}_1,\sigma_1)\hat{\psi}(\boldsymbol{q}_2,\sigma_2)\hat{\psi}^{\dagger}(\boldsymbol{r}_1,\sigma_1')\hat{\psi}^{\dagger}(\boldsymbol{r}_2,\sigma_2')\Phi_{\rm vac}. \end{aligned} \tag{2.108}$$

Because

$$\begin{aligned} & \hat{\psi}(\boldsymbol{q}_1,\sigma_1)\hat{\psi}(\boldsymbol{q}_2,\sigma_2)\hat{\psi}^{\dagger}(\boldsymbol{r}_1,\sigma_1')\hat{\psi}^{\dagger}(\boldsymbol{r}_2,\sigma_2')\Phi_{\rm vac} \\ = \; & \left[\delta(\boldsymbol{q}_2-\boldsymbol{r}_1)\delta(\boldsymbol{q}_1-\boldsymbol{r}_2)\delta_{\sigma_2,\sigma_1'}\delta_{\sigma_1,\sigma_2'}\right. \\ & \left.+\,\delta(\boldsymbol{q}_1-\boldsymbol{r}_1)\delta(\boldsymbol{q}_2-\boldsymbol{r}_2)\delta_{\sigma_1,\sigma_1'}\delta_{\sigma_2,\sigma_2'}\right]\Phi_{\rm vac}, \end{aligned} \tag{2.109}$$

it follows that

$$\begin{aligned} & A_{\tilde{F},\tilde{M}}(\boldsymbol{q}_1,\boldsymbol{q}_2)A^{\dagger}_{F,M}(\boldsymbol{r}_1,\boldsymbol{r}_2)\Phi_{\rm vac} \\ = \; & \sum_{\sigma_1,\sigma_2\in\mathcal{S}}\Big[\delta(\boldsymbol{q}_2-\boldsymbol{r}_1)\delta(\boldsymbol{q}_1-\boldsymbol{r}_2)\langle\tilde{F},\tilde{M}|\sigma_1,\sigma_2\rangle\langle\sigma_2,\sigma_1|F,M\rangle \\ & +\delta(\boldsymbol{q}_1-\boldsymbol{r}_1)\delta(\boldsymbol{q}_2-\boldsymbol{r}_2)\langle\tilde{F},\tilde{M}|\sigma_1,\sigma_2\rangle\langle\sigma_1,\sigma_2|F,M\rangle\Big]\Phi_{\rm vac} \end{aligned} \tag{2.110}$$

$$\begin{aligned} = \; & \sum_{\sigma_1,\sigma_2\in\mathcal{S}}\Big[(-1)^F\delta(\boldsymbol{q}_2-\boldsymbol{r}_1)\delta(\boldsymbol{q}_1-\boldsymbol{r}_2)\langle\tilde{F},\tilde{M}|\sigma_1,\sigma_2\rangle\langle\sigma_1,\sigma_2|F,M\rangle \\ & +\delta(\boldsymbol{q}_1-\boldsymbol{r}_1)\delta(\boldsymbol{q}_2-\boldsymbol{r}_2)\langle\tilde{F},\tilde{M}|\sigma_1,\sigma_2\rangle\langle\sigma_1,\sigma_2|F,M\rangle\Big]\Phi_{\rm vac} \end{aligned} \tag{2.111}$$

$$\begin{aligned} = \; & \left[(-1)^F\delta(\boldsymbol{q}_1-\boldsymbol{r}_2)\delta(\boldsymbol{q}_2-\boldsymbol{r}_1)+\delta(\boldsymbol{q}_1-\boldsymbol{r}_1)\delta(\boldsymbol{q}_2-\boldsymbol{r}_2)\right] \\ & \times\delta_{F,\tilde{F}}\delta_{M,\tilde{M}}\Phi_{\rm vac}. \end{aligned} \tag{2.112}$$

□

From (2.54), we have

$$
\begin{aligned}
& \left\langle A^{\dagger}_{F,M}(\boldsymbol{r}_1,\boldsymbol{r}_2)\Phi_{\rm vac}, H_{\rm int}A^{\dagger}_{F',M'}(\boldsymbol{r}'_1,\boldsymbol{r}'_2)\Phi_{\rm vac}\right\rangle \\
= \;& \frac{1}{2}\int d\boldsymbol{q}_1 d\boldsymbol{q}_2 \sum_{\tilde{F},\tilde{M},\tilde{F}',\tilde{M}'} U_{\tilde{F},\tilde{M},\tilde{F}',\tilde{M}'}(\boldsymbol{q}_1,\boldsymbol{q}_2) \\
& \times \Big\langle A_{\tilde{F},\tilde{M}}(\boldsymbol{q}_1,\boldsymbol{q}_2)A^{\dagger}_{F,M}(\boldsymbol{r}_1,\boldsymbol{r}_2)\Phi_{\rm vac}, \\
& A_{\tilde{F}',\tilde{M}'}(\boldsymbol{q}_1,\boldsymbol{q}_2)A^{\dagger}_{F',M'}(\boldsymbol{r}'_1,\boldsymbol{r}'_2)\Phi_{\rm vac}\Big\rangle \qquad (2.113) \\
= \;& \frac{1}{2}\int d\boldsymbol{q}_1 d\boldsymbol{q}_2 \sum_{\tilde{F},\tilde{M},\tilde{F}',\tilde{M}'} U_{\tilde{F},\tilde{M},\tilde{F}',\tilde{M}'}(\boldsymbol{q}_1,\boldsymbol{q}_2)\delta_{\tilde{F},F}\delta_{\tilde{M},M}\delta_{\tilde{F}',F'}\delta_{\tilde{M}',M'} \\
& \times \left[(-1)^F\delta(\boldsymbol{q}_1-\boldsymbol{r}_2)\delta(\boldsymbol{q}_2-\boldsymbol{r}_1)+\delta(\boldsymbol{q}_1-\boldsymbol{r}_1)\delta(\boldsymbol{q}_2-\boldsymbol{r}_2)\right] \\
& \times \Big[(-1)^{F'}\delta(\boldsymbol{q}_1-\boldsymbol{r}'_2)\delta(\boldsymbol{q}_2-\boldsymbol{r}'_1)+\delta(\boldsymbol{q}_1-\boldsymbol{r}'_1)\delta(\boldsymbol{q}_2-\boldsymbol{r}'_2)\Big] \qquad (2.114) \\
= \;& \frac{1}{2}\int d\boldsymbol{q}_1 d\boldsymbol{q}_2 U_{F,M,F',M'}(\boldsymbol{q}_1,\boldsymbol{q}_2) \\
& \times \Big[(-1)^{F+F'}\delta(\boldsymbol{q}_1-\boldsymbol{r}_2)\delta(\boldsymbol{q}_2-\boldsymbol{r}_1)\delta(\boldsymbol{q}_1-\boldsymbol{r}'_2)\delta(\boldsymbol{q}_2-\boldsymbol{r}'_1) \\
& +(-1)^{F}\delta(\boldsymbol{q}_1-\boldsymbol{r}_2)\delta(\boldsymbol{q}_2-\boldsymbol{r}_1)\delta(\boldsymbol{q}_1-\boldsymbol{r}'_1)\delta(\boldsymbol{q}_2-\boldsymbol{r}'_2) \\
& +(-1)^{F'}\delta(\boldsymbol{q}_1-\boldsymbol{r}'_2)\delta(\boldsymbol{q}_2-\boldsymbol{r}'_1)\delta(\boldsymbol{q}_1-\boldsymbol{r}_1)\delta(\boldsymbol{q}_2-\boldsymbol{r}_2) \\
& \delta(\boldsymbol{q}_1-\boldsymbol{r}_1)\delta(\boldsymbol{q}_2-\boldsymbol{r}_2)\delta(\boldsymbol{q}_1-\boldsymbol{r}'_1)\delta(\boldsymbol{q}_2-\boldsymbol{r}'_2)] \qquad (2.115) \\
= \;& \frac{1}{2}(-1)^{F+F'}U_{F,M,F',M'}(\boldsymbol{r}_2,\boldsymbol{r}_1)\delta(\boldsymbol{r}_2-\boldsymbol{r}'_2)\delta(\boldsymbol{r}_1-\boldsymbol{r}'_1) \\
& +\frac{1}{2}(-1)^{F}U_{F,M,F',M'}(\boldsymbol{r}_2,\boldsymbol{r}_1)\delta(\boldsymbol{r}_2-\boldsymbol{r}'_1)\delta(\boldsymbol{r}_1-\boldsymbol{r}'_2) \\
& +\frac{1}{2}(-1)^{F'}U_{F,M,F',M'}(\boldsymbol{r}_1,\boldsymbol{r}_2)\delta(\boldsymbol{r}_1-\boldsymbol{r}'_2)\delta(\boldsymbol{r}_2-\boldsymbol{r}'_1) \\
& +\frac{1}{2}U_{F,M,F',M'}(\boldsymbol{r}_1,\boldsymbol{r}_2)\delta(\boldsymbol{r}_1-\boldsymbol{r}'_1)\delta(\boldsymbol{r}_2-\boldsymbol{r}'_2) \qquad (2.116) \\
= \;& U_{F,M,F',M'}(\boldsymbol{r}_1,\boldsymbol{r}_2)\delta(\boldsymbol{r}_1-\boldsymbol{r}'_1)\delta(\boldsymbol{r}_2-\boldsymbol{r}'_2) \\
& +(-1)^{F'}U_{F,M,F',M'}(\boldsymbol{r}_1,\boldsymbol{r}_2)\delta(\boldsymbol{r}_1-\boldsymbol{r}'_2)\delta(\boldsymbol{r}_2-\boldsymbol{r}'_1) \qquad (2.117) \\
= \;& U_{F,M,F',M'}(\boldsymbol{r}_1,\boldsymbol{r}_2) \\
& \times \Big[\delta(\boldsymbol{r}_1-\boldsymbol{r}'_1)\delta(\boldsymbol{r}_2-\boldsymbol{r}'_2)+(-1)^{F'}\delta(\boldsymbol{r}_1-\boldsymbol{r}'_2)\delta(\boldsymbol{r}_2-\boldsymbol{r}'_1)\Big], \qquad (2.118)
\end{aligned}
$$

where, in going from (2.116) to (2.117), we used (2.56).

■

**Step 2: Imposing the two conditions on the interaction Hamiltonian**

Having finished the preparation, we move on to imposing the two conditions stated at the beginning of this subsection on the interaction Hamiltonian.

We assume

$$[H_{\rm int}, \hat{F}^{(1)}_{\rm tot}] = [H_{\rm int}, \hat{F}^{(2)}_{\rm tot}] = [H_{\rm int}, \hat{F}^{(3)}_{\rm tot}] = 0 \tag{2.119}$$

holds. Then, $U_{F,M,F',M'}(\boldsymbol{r}_1, \boldsymbol{r}_2)$ can be expressed as

$$U_{F,M,F',M'}(\boldsymbol{r}_1, \boldsymbol{r}_2) = \delta_{F,F'}\delta_{M,M'}U_F(\boldsymbol{r}_1, \boldsymbol{r}_2) \tag{2.120}$$

by a function $U_F$.
Thus, we have

$$H_{\rm int} = \frac{1}{2}\int d\boldsymbol{r}_1 d\boldsymbol{r}_2 \sum_{F=0}^{2} U_F(\boldsymbol{r}_1, \boldsymbol{r}_2) \sum_{M=-F}^{F} A^\dagger_{F,M}(\boldsymbol{r}_1, \boldsymbol{r}_2) A_{F,M}(\boldsymbol{r}_1, \boldsymbol{r}_2). \tag{2.121}$$

$(\because)$

**$U$ is diagonal with respect to $M$.**

Because $H_{\rm int}$ and $\hat{F}^{(3)}_{\rm tot}$ commute with each other, we have

$$\begin{aligned} & \left\langle A^\dagger_{F,M}(\boldsymbol{r}_1, \boldsymbol{r}_2)\Phi_{\rm vac}, \hat{F}^{(3)}_{\rm tot} H_{\rm int} A^\dagger_{F',M'}(\boldsymbol{r}'_1, \boldsymbol{r}'_2)\Phi_{\rm vac} \right\rangle \\ = & \left\langle A^\dagger_{F,M}(\boldsymbol{r}_1, \boldsymbol{r}_2)\Phi_{\rm vac}, H_{\rm int}\hat{F}^{(3)}_{\rm tot} A^\dagger_{F',M'}(\boldsymbol{r}'_1, \boldsymbol{r}'_2)\Phi_{\rm vac} \right\rangle . \end{aligned} \tag{2.122}$$

Combining this equation with (2.72) and (2.106), we obtain

$$\begin{aligned} 0 &= (M - M') \left\langle A^\dagger_{F,M}(\boldsymbol{r}_1, \boldsymbol{r}_2)\Phi_{\rm vac}, H_{\rm int} A^\dagger_{F',M'}(\boldsymbol{r}'_1, \boldsymbol{r}'_2)\Phi_{\rm vac} \right\rangle & (2.123) \\ &= (M - M')U_{F,M,F',M'}(\boldsymbol{r}_1, \boldsymbol{r}_2) \\ &\quad \times \left[\delta(\boldsymbol{r}_1 - \boldsymbol{r}'_1)\delta(\boldsymbol{r}_2 - \boldsymbol{r}'_2) + (-1)^{F'}\delta(\boldsymbol{r}_1 - \boldsymbol{r}'_2)\delta(\boldsymbol{r}_2 - \boldsymbol{r}'_1)\right] . & (2.124) \end{aligned}$$

Assuming $M \neq M'$ yields

$$0 = U_{F,M,F',M'}(\boldsymbol{r}_1, \boldsymbol{r}_2) \left[\delta(\boldsymbol{r}_1 - \boldsymbol{r}'_1)\delta(\boldsymbol{r}_2 - \boldsymbol{r}'_2) + (-1)^{F'}\delta(\boldsymbol{r}_1 - \boldsymbol{r}'_2)\delta(\boldsymbol{r}_2 - \boldsymbol{r}'_1)\right] . \tag{2.125}$$

When $\boldsymbol{r}_1 \neq \boldsymbol{r}_2$, $U_{F,M,F',M'}(\boldsymbol{r}_1, \boldsymbol{r}_2)$ must be zero, which can be shown by integrating $\boldsymbol{r}'_1$over a small neighborhood of $\boldsymbol{r}_1$, and $\boldsymbol{r}'_2$ over a small neighborhood of $\boldsymbol{r}_2$.

When $\boldsymbol{r}_1 = \boldsymbol{r}_2 =: \boldsymbol{r}$, we have

$$0 = U_{F,M,F',M'}(\boldsymbol{r}, \boldsymbol{r}) \left[1 + (-1)^{F'}\right] \delta(\boldsymbol{r} - \boldsymbol{r}'_1)\delta(\boldsymbol{r} - \boldsymbol{r}'_2). \tag{2.126}$$

Thus, for even $F'$, $U_{F,M,F',M'}(\boldsymbol{r}, \boldsymbol{r})$ must be zero. For odd $F'$, because $A_{F',M'}(\boldsymbol{r}, \boldsymbol{r}) = 0$, it can be seen from (2.54) that $U_{F,M,F',M'}(\boldsymbol{r}, \boldsymbol{r})$ can be set to be zero without changing $H_{\rm int}$.

**$U$ is diagonal with respect to $F$**

Because $H_{\rm int}$ commutes with $\hat{\boldsymbol{F}}^2_{\rm tot}$, it follows that

$$\begin{aligned} & \left\langle A^\dagger_{F,M}(\boldsymbol{r}_1, \boldsymbol{r}_2)\Phi_{\rm vac}, \hat{\boldsymbol{F}}^2_{\rm tot} H_{\rm int} A^\dagger_{F',M}(\boldsymbol{r}'_1, \boldsymbol{r}'_2)\Phi_{\rm vac} \right\rangle \\ = & \left\langle A^\dagger_{F,M}(\boldsymbol{r}_1, \boldsymbol{r}_2)\Phi_{\rm vac}, H_{\rm int}\hat{\boldsymbol{F}}^2_{\rm tot} A^\dagger_{F',M}(\boldsymbol{r}'_1, \boldsymbol{r}'_2)\Phi_{\rm vac} \right\rangle . \end{aligned} \tag{2.127}$$

Combining this relation with (2.74) and (2.106), we obtain

$$0 = [F(F+1) - F'(F'+1)] \left\langle A^\dagger_{F,M}(\boldsymbol{r}_1, \boldsymbol{r}_2)\Phi_{\rm vac}, H_{\rm int} A^\dagger_{F',M}(\boldsymbol{r}'_1, \boldsymbol{r}'_2)\Phi_{\rm vac} \right\rangle . \quad (2.128)$$

When $F \neq F'$, we have

$$0 = \left\langle A^\dagger_{F,M}(\boldsymbol{r}_1, \boldsymbol{r}_2)\Phi_{\rm vac}, H_{\rm int} A^\dagger_{F',M}(\boldsymbol{r}'_1, \boldsymbol{r}'_2)\Phi_{\rm vac} \right\rangle \quad (2.129)$$

$$= U_{F,M,F',M}(\boldsymbol{r}_1, \boldsymbol{r}_2) \times \left[ \delta(\boldsymbol{r}_1 - \boldsymbol{r}'_1)\delta(\boldsymbol{r}_2 - \boldsymbol{r}'_2) + (-1)^{F'} \delta(\boldsymbol{r}_1 - \boldsymbol{r}'_2)\delta(\boldsymbol{r}_2 - \boldsymbol{r}'_1) \right] . \quad (2.130)$$

The same discussion as that in the previous paragraph yields $U_{F,M,F',M}(\boldsymbol{r}_1, \boldsymbol{r}_2) = 0$ when $F \neq F'$.

**$U$ does not depend on $M$**

From the results we have shown, $U$ can be rewritten as

$$U_{F,M,F',M'}(\boldsymbol{r}_1, \boldsymbol{r}_2) = \delta_{F,F'}\delta_{M,M'} U_{F,M}(\boldsymbol{r}_1, \boldsymbol{r}_2) \quad (2.131)$$

with a function $U_{F,M}$. Because $H_{\rm int}$ and $\hat{F}^\pm_{\rm tot}$ commute, it follows that

$$\left\langle A^\dagger_{F,M}(\boldsymbol{r}_1, \boldsymbol{r}_2)\Phi_{\rm vac}, H_{\rm int} \hat{F}^\pm_{\rm tot} A^\dagger_{F,M\mp1}(\boldsymbol{r}'_1, \boldsymbol{r}'_2)\Phi_{\rm vac} \right\rangle$$

$$= \left\langle \hat{F}^\mp_{\rm tot} A^\dagger_{F,M}(\boldsymbol{r}_1, \boldsymbol{r}_2)\Phi_{\rm vac}, H_{\rm int} A^\dagger_{F,M\mp1}(\boldsymbol{r}'_1, \boldsymbol{r}'_2)\Phi_{\rm vac} \right\rangle . \quad (2.132)$$

It follows from (2.73) that

$$\text{(LHS)} = \sqrt{(F \pm M)(F \mp M + 1)} \times \left\langle A^\dagger_{F,M}(\boldsymbol{r}_1, \boldsymbol{r}_2)\Phi_{\rm vac}, H_{\rm int} A^\dagger_{F,M}(\boldsymbol{r}'_1, \boldsymbol{r}'_2)\Phi_{\rm vac} \right\rangle , \quad (2.133)$$

$$\text{(RHS)} = \sqrt{(F \pm M)(F \mp M + 1)} \times \left\langle A^\dagger_{F,M\mp1}(\boldsymbol{r}_1, \boldsymbol{r}_2)\Phi_{\rm vac}, H_{\rm int} A^\dagger_{F,M\mp1}(\boldsymbol{r}'_1, \boldsymbol{r}'_2)\Phi_{\rm vac} \right\rangle . \quad (2.134)$$

Thus, we can see that

$$\left\langle A^\dagger_{F,M}(\boldsymbol{r}_1, \boldsymbol{r}_2)\Phi_{\rm vac}, H_{\rm int} A^\dagger_{F,M}(\boldsymbol{r}'_1, \boldsymbol{r}'_2)\Phi_{\rm vac} \right\rangle \quad (2.135)$$

does not depend on $M$, and hence, from (2.106),

$$U_{F,M}(\boldsymbol{r}_1, \boldsymbol{r}_2) \left[ \delta(\boldsymbol{r}_1 - \boldsymbol{r}'_1)\delta(\boldsymbol{r}_2 - \boldsymbol{r}'_2) + (-1)^F \delta(\boldsymbol{r}_1 - \boldsymbol{r}'_2)\delta(\boldsymbol{r}_2 - \boldsymbol{r}'_1) \right] \quad (2.136)$$

also does not depend on $M$. Thus, $U_{F,M}(\boldsymbol{r}_1, \boldsymbol{r}_2)$ does not depend on $M$. (When $F$ is odd and $\boldsymbol{r}_1 = \boldsymbol{r}_2$, $U_{F,M}(\boldsymbol{r}_1, \boldsymbol{r}_2)$ can be set to be zero. )

■

Further, we assume that the system is dilute, so that the interaction can be approximated by a contact interaction:

By imposing $U_F(\boldsymbol{r}_1, \boldsymbol{r}_2) = g_F \delta(\boldsymbol{r}_1 - \boldsymbol{r}_2)$, we obtain

$$H_{\text{int}} = \frac{1}{2} \int d\boldsymbol{r} \sum_{F=0,2} g_F \sum_{M=-F}^{F} A_{F,M}^\dagger(\boldsymbol{r}) A_{F,M}(\boldsymbol{r}), \tag{2.137}$$

$$A_{F,M}(\boldsymbol{r}) := A_{F,M}(\boldsymbol{r}, \boldsymbol{r}). \tag{2.138}$$

Note that the summation over $F$ is restricted to even numbers.
Physically,

$$g_F = \frac{4\pi\hbar^2}{M} a_F, \tag{2.139}$$

where $M$ is the mass of the atom, and $a_F$ is the $s$-wave scattering length of the total spin-$F$ channel.

$(\because)$

By plugging the expression for $U_F$ into (2.121), we obtain

$$H_{\text{int}} = \frac{1}{2} \int d\boldsymbol{r} \sum_{F=0}^{2} g_F \sum_{M=-F}^{F} A_{F,M}^\dagger(\boldsymbol{r}, \boldsymbol{r}) A_{F,M}(\boldsymbol{r}, \boldsymbol{r}). \tag{2.140}$$

When $F$ is odd, $A_{F,M}(\boldsymbol{r}, \boldsymbol{r}) = 0$, and hence the summation is restricted to even $F$.

■

**Step 3: rewriting the obtained interaction Hamiltonian**

Here, we rewrite the obtained interaction Hamiltonian (2.137) using more intuitively understandable operators.

We start by deriving two equalities:

Let :: be the normal ordering. Then,

$$\begin{aligned}
& : \hat{n}(\boldsymbol{r}_1) \hat{n}(\boldsymbol{r}_2) : \\
:= & \sum_{\sigma_1, \sigma_2 \in \mathcal{S}} \hat{\psi}^\dagger(\boldsymbol{r}_1, \sigma_1) \hat{\psi}^\dagger(\boldsymbol{r}_2, \sigma_2) \hat{\psi}(\boldsymbol{r}_1, \sigma_1) \hat{\psi}(\boldsymbol{r}_2, \sigma_2) && (2.141) \\
= & \sum_{F=0}^{2} \sum_{M=-F}^{F} A_{F,M}^\dagger(\boldsymbol{r}_1, \boldsymbol{r}_2) A_{F,M}(\boldsymbol{r}_1, \boldsymbol{r}_2) && (2.142) \\
& : \hat{\boldsymbol{F}}(\boldsymbol{r}_1) \cdot \hat{\boldsymbol{F}}(\boldsymbol{r}_2) : \\
:= & \sum_{\sigma_1, \sigma_2, \tau_1, \tau_2 \in \mathcal{S}} \sum_{\alpha=1}^{3} S^{(\alpha)}_{\sigma_1, \tau_1} S^{(\alpha)}_{\sigma_2, \tau_2} \hat{\psi}^\dagger(\boldsymbol{r}_1, \sigma_1) \hat{\psi}^\dagger(\boldsymbol{r}_2, \sigma_2) \hat{\psi}(\boldsymbol{r}_1, \tau_1) \hat{\psi}(\boldsymbol{r}_2, \tau_2) && (2.143) \\
= & \sum_{F=0}^{2} \left[ \frac{1}{2} F(F+1) - 2 \right] \sum_{M=-F}^{F} A_{F,M}^\dagger(\boldsymbol{r}_1, \boldsymbol{r}_2) A_{F,M}(\boldsymbol{r}_1, \boldsymbol{r}_2). && (2.144)
\end{aligned}$$

(∵)

In $\mathbb{C}^3 \otimes \mathbb{C}^3$, the Hilbert space of two spin-1 spins,

$$1 = \sum_{F=0}^{2} \sum_{M=-F}^{F} |F, M\rangle\langle F, M| \tag{2.145}$$

holds, where the left hand side denotes the identity operator in $\mathbb{C}^3 \otimes \mathbb{C}^3$.

First, let us think about the paricle number. By multiplying $\hat{\psi}^\dagger(\boldsymbol{r}_1, \sigma_1)\hat{\psi}^\dagger(\boldsymbol{r}_2, \sigma_2)\langle\sigma_1, \sigma_2|$ from the left, multiplying $|\sigma_1', \sigma_2'\rangle\hat{\psi}(\boldsymbol{r}_1, \sigma_1')\hat{\psi}(\boldsymbol{r}_2, \sigma_2')$ from the right, and taking the summation over $\sigma_1, \sigma_2, \sigma_1', \sigma_2'$, we get

$$\text{(LHS)} = \sum_{\sigma_1, \sigma_2 \in \mathcal{S}} \hat{\psi}^\dagger(\boldsymbol{r}_1, \sigma_1)\hat{\psi}^\dagger(\boldsymbol{r}_2, \sigma_2)\hat{\psi}(\boldsymbol{r}_1, \sigma_1)\hat{\psi}(\boldsymbol{r}_2, \sigma_2), \tag{2.146}$$

$$\text{(RHS)} = \sum_{F=0}^{2} \sum_{M=-F}^{F} A_{F,M}^\dagger(\boldsymbol{r}_1, \boldsymbol{r}_2) A_{F,M}(\boldsymbol{r}_1, \boldsymbol{r}_2). \tag{2.147}$$

Next, we consider the spin. Let $\hat{\boldsymbol{f}}$ be the spin operators in $\mathbb{C}^3$, and define the spin operators in $\mathbb{C}^3 \otimes \mathbb{C}^3$ by $\hat{\boldsymbol{f}}_1 := \hat{\boldsymbol{f}} \otimes I$, $\hat{\boldsymbol{f}}_2 := I \otimes \hat{\boldsymbol{f}}$, and $\hat{\boldsymbol{f}}_{\text{tot}} := \hat{\boldsymbol{f}}_1 + \hat{\boldsymbol{f}}_2$. Then,

$$\hat{\boldsymbol{f}}_1 \cdot \hat{\boldsymbol{f}}_2 = \frac{1}{2}\left[(\hat{\boldsymbol{f}}_1 + \hat{\boldsymbol{f}}_2)^2 - \hat{\boldsymbol{f}}_1^2 - \hat{\boldsymbol{f}}_2^2\right] = \frac{1}{2}\hat{\boldsymbol{f}}_{\text{tot}}^2 - 2. \tag{2.148}$$

From this relation and (2.145), we obtain

$$\hat{\boldsymbol{f}}_1 \cdot \hat{\boldsymbol{f}}_2 = \sum_{F=0}^{2} \left[\frac{1}{2}F(F+1) - 2\right] \sum_{M=-F}^{F} |F, M\rangle\langle F, M|. \tag{2.149}$$

By multiplying $\hat{\psi}^\dagger(\boldsymbol{r}_1, \sigma_1)\hat{\psi}^\dagger(\boldsymbol{r}_2, \sigma_2)\langle\sigma_1, \sigma_2|$ from the left, multiplying $|\tau_1, \tau_2\rangle\hat{\psi}(\boldsymbol{r}_1, \tau_1)\hat{\psi}(\boldsymbol{r}_2, \tau_2)$ from the right, and taking the summation over $\sigma_1, \sigma_2, \tau_1, \tau_2$, we get

$$\begin{aligned}\text{(LHS)} &= \sum_{\alpha=1}^{3} \sum_{\sigma_1, \sigma_2, \tau_1, \tau_2 \in \mathcal{S}} S^{(\alpha)}_{\sigma_1, \tau_1} S^{(\alpha)}_{\sigma_2, \tau_2} \\ &\quad \times \hat{\psi}^\dagger(\boldsymbol{r}_1, \sigma_1)\hat{\psi}^\dagger(\boldsymbol{r}_2, \sigma_2)\hat{\psi}(\boldsymbol{r}_1, \tau_1)\hat{\psi}(\boldsymbol{r}_2, \tau_2), \qquad (2.150) \\ \text{(RHS)} &= \sum_{F=0}^{2} \left[\frac{1}{2}F(F+1) - 2\right] \sum_{M=-F}^{F} A_{F,M}^\dagger(\boldsymbol{r}_1, \boldsymbol{r}_2) A_{F,M}(\boldsymbol{r}_1, \boldsymbol{r}_2). \qquad (2.151)\end{aligned}$$

■

The interaction Hamiltonian (2.137) can be rewritten as

$$H_{\text{int}} = \frac{1}{2}\int d\boldsymbol{r} \left[c_0 : \hat{n}(\boldsymbol{r})\hat{n}(\boldsymbol{r}) : \; + c_1 : \hat{\boldsymbol{F}}(\boldsymbol{r}) \cdot \hat{\boldsymbol{F}}(\boldsymbol{r}) :\right], \tag{2.152}$$

where

$$c_0 := \frac{g_0 + 2g_2}{3}, \quad c_1 := \frac{g_2 - g_0}{3}. \tag{2.153}$$

(∵)

Equation (2.137) means

$$H_{\rm int} = \frac{1}{2}\int d\boldsymbol{r}\left[g_0 A^\dagger_{0,0}(\boldsymbol{r})A_{0,0}(\boldsymbol{r}) + g_2\sum_{M=-2}^{2} A^\dagger_{2,M}(\boldsymbol{r})A_{2,M}(\boldsymbol{r})\right]. \tag{2.154}$$

If follows from equations (2.142) and (2.144) that

$$:\hat{n}(\boldsymbol{r})\hat{n}(\boldsymbol{r}): \;=\; A^\dagger_{0,0}(\boldsymbol{r})A_{0,0}(\boldsymbol{r}) + \sum_{M=-2}^{2} A^\dagger_{2,M}(\boldsymbol{r})A_{2,M}(\boldsymbol{r}) \tag{2.155}$$

$$:\hat{\boldsymbol{F}}(\boldsymbol{r})\cdot\hat{\boldsymbol{F}}(\boldsymbol{r}): \;=\; -2A^\dagger_{0,0}(\boldsymbol{r})A_{0,0}(\boldsymbol{r}) + \sum_{M=-2}^{2} A^\dagger_{2,M}(\boldsymbol{r})A_{2,M}(\boldsymbol{r}). \tag{2.156}$$

By comparing these three equations, we obtain

$$\begin{aligned}&\frac{g_0+2g_2}{3}:\hat{n}(\boldsymbol{r})\hat{n}(\boldsymbol{r}): \;+\frac{g_2-g_0}{3}:\hat{\boldsymbol{F}}(\boldsymbol{r})\cdot\hat{\boldsymbol{F}}(\boldsymbol{r}):\\ =\;& g_0 A^\dagger_{0,0}(\boldsymbol{r})A_{0,0}(\boldsymbol{r}) + g_2\sum_{M=-2}^{2} A^\dagger_{2,M}(\boldsymbol{r})A_{2,M}(\boldsymbol{r}),\end{aligned} \tag{2.157}$$

which yields

$$H_{\rm int} = \frac{1}{2}\int d\boldsymbol{r}\left[\frac{g_0+2g_2}{3}:\hat{n}(\boldsymbol{r})\hat{n}(\boldsymbol{r}): \;+\frac{g_2-g_0}{3}:\hat{\boldsymbol{F}}(\boldsymbol{r})\cdot\hat{\boldsymbol{F}}(\boldsymbol{r}):\right]. \tag{2.158}$$

■

### 2.2.3 The full Hamiltonian

The full Hamiltonian for spin-1 bosons is given by

$$\begin{aligned}H \;=\;& \int d\boldsymbol{r}\sum_{\sigma\in\mathcal{S}}\hat{\psi}^\dagger(\boldsymbol{r},\sigma)\left[-\frac{\hbar^2}{2M}\nabla^2 + U(\boldsymbol{r}) - p\sigma + q\sigma^2\right]\hat{\psi}(\boldsymbol{r},\sigma)\\ &+\frac{1}{2}\int d\boldsymbol{r}\left[c_0:\hat{n}(\boldsymbol{r})\hat{n}(\boldsymbol{r}): \;+c_1:\hat{\boldsymbol{F}}(\boldsymbol{r})\cdot\hat{\boldsymbol{F}}(\boldsymbol{r}):\right],\end{aligned} \tag{2.159}$$

where

- the normal ordering is defined by

$$\begin{aligned}&:\hat{n}(\boldsymbol{r})\hat{n}(\boldsymbol{r}):\\ :=\;&\sum_{\sigma_1,\sigma_2\in\mathcal{S}}\hat{\psi}^\dagger(\boldsymbol{r},\sigma_1)\hat{\psi}^\dagger(\boldsymbol{r},\sigma_2)\hat{\psi}(\boldsymbol{r},\sigma_1)\hat{\psi}(\boldsymbol{r},\sigma_2),\end{aligned} \tag{2.160}$$

$$\begin{aligned}&:\hat{\boldsymbol{F}}(\boldsymbol{r})\cdot\hat{\boldsymbol{F}}(\boldsymbol{r}):\\ :=\;&\sum_{\sigma_1,\sigma_2,\tau_1,\tau_2\in\mathcal{S}}\sum_{\alpha=1}^{3} S^{(\alpha)}_{\sigma_1,\tau_1}S^{(\alpha)}_{\sigma_2,\tau_2}\hat{\psi}^\dagger(\boldsymbol{r},\sigma_1)\hat{\psi}^\dagger(\boldsymbol{r},\sigma_2)\hat{\psi}(\boldsymbol{r},\tau_1)\hat{\psi}(\boldsymbol{r},\tau_2),\end{aligned} \tag{2.161}$$

| Atom | $a_0/a_B$ | $a_2/a_B$ | $c_1/c_0$ |
|---|---|---|---|
| $^7$Li | 39.1 | 4.9 | $\sim -0.7$ |
| $^{23}$Na | $50.0 \pm 1.6$ | $55.0 \pm 1.7$ | $\sim 0.03$ |
| $^{87}$Rb | $101.8 \pm 0.2$ | $100.4 \pm 0.1$ | $\sim -0.005$ |

Table 2.2: The scattering lengths and the ratio of coefficients of the spin-dependent and the spin-independent interaction for various spin-1 atoms (i.e., $F = 1$ is assumed ). Scattering lengths are shown in units of the Bohr radius $a_B \simeq 0.529 \times 10^{-10}$m. The values of scattering lengths are taken from table II of [18] ($^{23}$Na, $^{87}$Rb) and [31] ($^7$Li), and the ratio is calculated by $c_1/c_0 = (g_2 - g_0)/(g_0 + 2g_2) = (a_2 - a_0)/(a_0 + 2a_2)$.

- spin matrices $S^{(\alpha)}$ are defined in (2.45), and
- the coefficients of the interaction part are defined by

$$c_0 := \frac{g_0 + 2g_2}{3}, \quad c_1 := \frac{g_2 - g_0}{3} \tag{2.162}$$

and

$$g_F := \frac{4\pi\hbar^2}{M} a_F, \tag{2.163}$$

with $a_F$ being the $s$-wave scattering length of the total spin $F$ channel.

Hereafter, we assume $a_F > 0$, which ensures $c_0 > 0$, i.e., the spin-independent interaction is repulsive. On the other hand, the sign of $c_1$ can be positive or negative, depending on the atom. In table 2.2, we list the scattering lengths of a few spin-1 alkali atoms [4].

- When $c_1 > 0$, it is energetically favorable to minimize the spin, and we call the interaction antiferromagnetic. For $^{23}$Na ($F = 1$), its spin-dependent interaction is antiferromagnetic.
- when $c_1 < 0$, it is energetically favorable to maximize the spin, and we call the interaction ferromagnetic. For $^{87}$Rb ($F = 1$)and $^7$Li ($F = 1$), their spin-dependent interaction is ferromagnetic.

As we will see later, the sign of the spin-dependent interaction greatly affects the physics of the system.

## 2.3 The mean-field phase diagrams for weakly interacting spin-1 bosons

In this section, we give the ground-state phase diagrams of spin-1 bosons by assuming the following two conditions:

- the interaction between bosons is weak enough so that each ground state can be written as the product of an identical one-particle state, and
- the trapping potential is negligible so that the ground states are uniform in space.

[4] Spin-1 Bose-Einstein condensation has been experimentally realized for $^{23}$Na ($F = 1$) [15] and $^{87}$Rb ($F = 1$) [16], and recently experimental efforts to realize that of $^7$Li are underway [31].

Based on these conditions, we restrict our variational states to be the products of an identical one-particle state, and then minimize the expectation value of the Hamiltonian with respect to this one-particle state.

### 2.3.1 The variational state and the expectation value of the Hamiltonian

In the mean-field theory for weakly interacting spin-1 bosons, it is assumed that the ground state can be written as

$$\Psi_\phi := \frac{1}{\sqrt{N!}} \left(A_\phi^\dagger\right)^N \Phi_{\text{vac}} \tag{2.164}$$

$$A_\phi^\dagger := \int d\boldsymbol{r} \sum_{\sigma\in\mathcal{S}} \phi(\boldsymbol{r},\sigma)\hat{\psi}^\dagger(\boldsymbol{r},\sigma), \tag{2.165}$$

where

- $N \in \mathbb{N}$ represents the number of particles, and
- $\phi \in L^2(V,\mathbb{C}^3)$ is a one-particle wave function (or a condensate wave function), which is normalized : $\int d\boldsymbol{r} \sum_{\sigma\in\mathcal{S}} |\phi(\boldsymbol{r},\sigma)|^2 = 1$.

The normalization $\langle\Psi_\phi,\Psi_\phi\rangle = 1$ is ensured by the equality $[A_\phi, A_\phi^\dagger] = 1$, which is in turn ensured by the normalization of the one-particle wave function $\phi$. The variational state means that all the $N$ particles are condensed into the same one-particle state represented by the wave function $\phi$.

Using this variational state, we calculate the expectation value of the Hamiltonian.

The expectation value of the full Hamiltonian (2.159) with respect to the variational state (2.164) is given by

$$\begin{aligned} E(\phi) \;:=\; & \int d\boldsymbol{r} \left\{ N \sum_{\sigma\in\mathcal{S}} \phi(\boldsymbol{r},\sigma) \left[ -\frac{\hbar^2}{2M}\nabla^2 + U(\boldsymbol{r}) - p\sigma + q\sigma^2 \right] \phi(\boldsymbol{r},\sigma) \right. \\ & \left. + \frac{c_0}{2} n(\boldsymbol{r})^2 + \frac{c_1}{2} |\boldsymbol{F}(\boldsymbol{r})|^2 \right\}, \end{aligned} \tag{2.166}$$

where

$$n(\boldsymbol{r}) := N \sum_{\sigma\in\mathcal{S}} |\phi(\boldsymbol{r},\sigma)|^2, \tag{2.167}$$

$$\boldsymbol{F}(\boldsymbol{r}) := (F^{(1)}(\boldsymbol{r}), F^{(2)}(\boldsymbol{r}), F^{(3)}(\boldsymbol{r})), \tag{2.168}$$

$$F^{(\alpha)}(\boldsymbol{r}) := N \sum_{\sigma,\tau\in\mathcal{S}} S^{(\alpha)}_{\sigma,\tau} \phi^*(\boldsymbol{r},\sigma)\phi(\boldsymbol{r},\tau), \tag{2.169}$$

and we assumed that $N \gg 1$ so that $1 - 1/N$ can be well approximated by 1.

(∵)

It can be easily shown by induction that, for an arbitrary integer $k$ such that $k \geq 1$,

$$\begin{aligned}
\left[\hat{\psi}(\boldsymbol{r},\sigma),(A_\phi^\dagger)^k\right] &= k\phi(\boldsymbol{r},\sigma)(A_\phi^\dagger)^{k-1}, && (2.170)\\
\left[\hat{\psi}(\boldsymbol{r}_1,\sigma_1)\hat{\psi}(\boldsymbol{r}_2,\sigma_2),(A_\phi^\dagger)^k\right] &= k\phi(\boldsymbol{r}_2,\sigma_2)\hat{\psi}(\boldsymbol{r}_1,\sigma_1)(A_\phi^\dagger)^{k-1} \\
&\quad +k\phi(\boldsymbol{r}_1,\sigma_1)(A_\phi^\dagger)^{k-1}\hat{\psi}(\boldsymbol{r}_2,\sigma_2) && (2.171)
\end{aligned}$$

hold. Thus, we have

$$\begin{aligned}
\hat{\psi}(\boldsymbol{r},\sigma)(A_\phi^\dagger)^k\Phi_{\rm vac} &= k\phi(\boldsymbol{r},\sigma)(A_\phi^\dagger)^{k-1}\Phi_{\rm vac}, && (2.172)\\
\hat{\psi}(\boldsymbol{r}_1,\sigma_1)\hat{\psi}(\boldsymbol{r}_2,\sigma_2)(A_\phi^\dagger)^k\Phi_{\rm vac} &= k(k-1)\phi(\boldsymbol{r}_1,\sigma_1)\phi(\boldsymbol{r}_2,\sigma_2) \\
&\quad \times(A_\phi^\dagger)^{k-2}\Phi_{\rm vac}. && (2.173)
\end{aligned}$$

Using these equalities, we obtain

$$\begin{aligned}
\left\langle \Psi_\phi,\hat{\psi}(\boldsymbol{r},\sigma)\Psi_\phi\right\rangle &= \left\langle \Psi_\phi,\hat{\psi}^\dagger(\boldsymbol{r},\sigma)\Psi_\phi\right\rangle = 0, && (2.174)\\
\left\langle \Psi_\phi,\hat{\psi}^\dagger(\boldsymbol{r}_1,\sigma_1)\hat{\psi}(\boldsymbol{r}_2,\sigma_2)\Psi_\phi\right\rangle &= N\phi^*(\boldsymbol{r}_1,\sigma_1)\phi(\boldsymbol{r}_2,\sigma_2), && (2.175)
\end{aligned}$$

$$\begin{aligned}
&\left\langle \Psi_\phi,\hat{\psi}^\dagger(\boldsymbol{r}_1,\sigma_1)\hat{\psi}^\dagger(\boldsymbol{r}_2,\sigma_2)\hat{\psi}(\boldsymbol{r}_3,\sigma_3)\hat{\psi}(\boldsymbol{r}_4,\sigma_4)\Psi_\phi\right\rangle \\
&= N(N-1)\phi^*(\boldsymbol{r}_1,\sigma_1)\phi^*(\boldsymbol{r}_2,\sigma_2)\phi(\boldsymbol{r}_3,\sigma_3)\phi(\boldsymbol{r}_4,\sigma_4). \qquad (2.176)
\end{aligned}$$

Thus, we obtain ($\langle\cdot\rangle$ is the abbreviation of $\langle\Psi_\phi,\cdot\Psi_\phi\rangle$)

$$\begin{aligned}
&\left\langle \int d\boldsymbol{r}\sum_{\sigma\in\mathcal{S}}\hat{\psi}^\dagger(\boldsymbol{r},\sigma)\left[-\frac{\hbar^2}{2M}\nabla^2+U(\boldsymbol{r})-p\sigma+q\sigma^2\right]\hat{\psi}(\boldsymbol{r},\sigma)\right\rangle \\
&= N\int d\boldsymbol{r}\sum_{\sigma\in\mathcal{S}}\phi^*(\boldsymbol{r},\sigma)\left[-\frac{\hbar^2}{2M}\nabla^2+U(\boldsymbol{r})-p\sigma+q\sigma^2\right]\phi(\boldsymbol{r},\sigma) \qquad (2.177)
\end{aligned}$$

and

$$\begin{aligned}
&\left\langle \frac{1}{2}\int d\boldsymbol{r}\left[c_0:\hat{n}(\boldsymbol{r})\hat{n}(\boldsymbol{r}):\ +c_1:\hat{\boldsymbol{F}}(\boldsymbol{r})\cdot\hat{\boldsymbol{F}}(\boldsymbol{r}):\right]\right\rangle \\
&= \int d\boldsymbol{r}\left[\frac{c_0}{2}\sum_{\sigma,\tau\in\mathcal{S}}\left\langle\hat{\psi}^\dagger(\boldsymbol{r},\sigma)\hat{\psi}^\dagger(\boldsymbol{r},\tau)\hat{\psi}(\boldsymbol{r},\sigma)\hat{\psi}(\boldsymbol{r},\tau)\right\rangle\right. \\
&\quad \left.+\frac{c_1}{2}\sum_{\substack{\sigma_1,\sigma_2,\\ \tau_1,\tau_2\in\mathcal{S}}}\sum_{\alpha=1}^{3}S^{(\alpha)}_{\sigma_1,\tau_1}S^{(\alpha)}_{\sigma_2,\tau_2}\left\langle\hat{\psi}^\dagger(\boldsymbol{r},\sigma_1)\hat{\psi}^\dagger(\boldsymbol{r},\sigma_2)\hat{\psi}(\boldsymbol{r},\tau_1)\hat{\psi}(\boldsymbol{r},\tau_2)\right\rangle\right] \qquad (2.178)\\
&= N(N-1)\int d\boldsymbol{r}\left[\frac{c_0}{2}\sum_{\sigma,\tau\in\mathcal{S}}\phi^*(\boldsymbol{r},\sigma)\phi^*(\boldsymbol{r},\tau)\phi(\boldsymbol{r},\sigma)\phi(\boldsymbol{r},\tau)\right. \\
&\quad \left.+\frac{c_1}{2}\sum_{\substack{\sigma_1,\sigma_2,\\ \tau_1,\tau_2\in\mathcal{S}}}\sum_{\alpha=1}^{3}S^{(\alpha)}_{\sigma_1,\tau_1}S^{(\alpha)}_{\sigma_2,\tau_2}\phi^*(\boldsymbol{r},\sigma_1)\phi^*(\boldsymbol{r},\sigma_2)\phi(\boldsymbol{r},\tau_1)\phi(\boldsymbol{r},\tau_2)\right] \qquad (2.179)
\end{aligned}$$

$$
\begin{aligned}
&= N(N-1)\int d\boldsymbol{r} \\
&\quad \left\{ \frac{c_0}{2}\left[\sum_{\sigma\in\mathcal{S}}|\phi(\boldsymbol{r},\sigma)|^2\right]^2 + \frac{c_1}{2}\sum_{\alpha=1}^{3}\left[\sum_{\sigma,\tau\in\mathcal{S}} S^{(\alpha)}_{\sigma,\tau}\phi^*(\boldsymbol{r},\sigma)\phi(\boldsymbol{r},\tau)\right]^2 \right\} \qquad (2.180)\\
&= \left(1-\frac{1}{N}\right)\int d\boldsymbol{r}\left[\frac{c_0}{2}n^2(\boldsymbol{r}) + \frac{c_1}{2}|\boldsymbol{F}(\boldsymbol{r})|^2\right]. \qquad (2.181)
\end{aligned}
$$

■

Further, we assume that the trapping potential is negligible and that the one-particle state is uniform in space.

Assume that the trapping potential $U$ is zero, and that $\phi(\boldsymbol{r},\sigma) = \frac{1}{\sqrt{|V|}}\chi(\sigma)$, where $|V|$ is the volume of the region $V$, and $\chi$ is a function of spin indices satisfying $\sum_{\sigma\in\mathcal{S}}|\chi(\sigma)|^2 = 1$. Then, the variational degree of freedom is $\chi$, and the energy functional to be minimized becomes

$$
\begin{aligned}
\varepsilon(\chi) &:= \frac{1}{N}E\left(\frac{1}{\sqrt{|V|}}\chi\right)\\
&= \sum_{\sigma\in\mathcal{S}}(-p\sigma+q\sigma^2)|\chi(\sigma)|^2 + \frac{c_0}{2}\rho + \frac{c_1}{2}\rho|\boldsymbol{f}|^2, \qquad (2.182)
\end{aligned}
$$

where

$$
\begin{aligned}
\rho &:= \frac{N}{|V|}, \qquad (2.183)\\
\boldsymbol{f} &:= (f^{(1)}, f^{(2)}, f^{(3)}), \qquad (2.184)\\
f^{(\alpha)} &:= \sum_{\sigma,\tau\in\mathcal{S}} S^{(\alpha)}_{\sigma,\tau}\chi^*(\sigma)\chi(\tau). \qquad (2.185)
\end{aligned}
$$

($\because$)

The result follows directly from the assumption $\phi(\boldsymbol{r},\sigma) = \frac{1}{\sqrt{|V|}}\chi(\sigma)$ and (2.166).

■

### 2.3.2 The phase diagrams

By a straightforward but lengthy calculation, the energy functional $\varepsilon$ (2.182) can be analytically minimized with respect to $\chi$ [17], and we can obtain the ground-state phase diagrams of the system, which are shown in figure 2.2 [21]. As was already pointed out, the sign of $c_1$ crucially affects the structure of the phase diagrams.

We first describe five phases and their properties which can be obtained from the minimization procedure, and then turn to the phase diagrams.

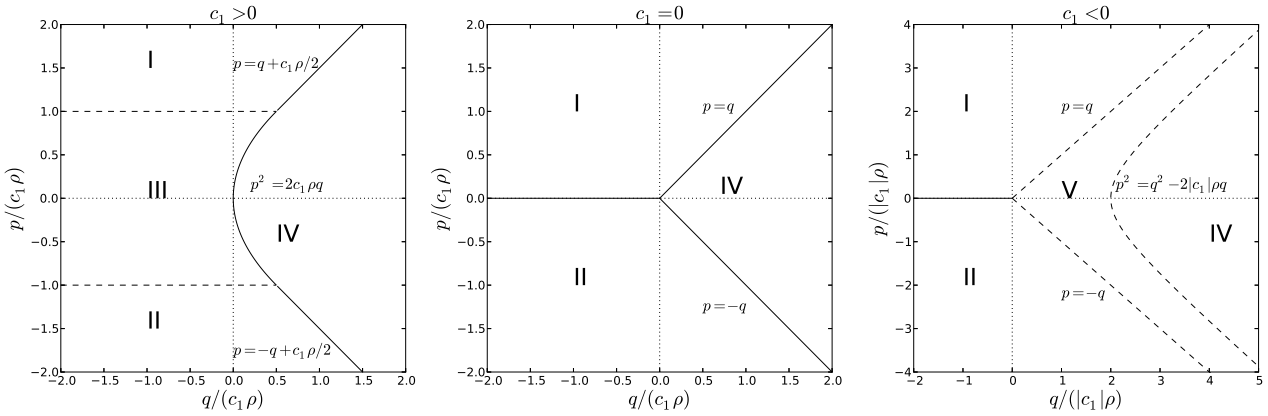


Figure 2.2: Ground-state phase diagram of uniform spin-1 bosons, within the mean-field theory for weakly interacting bosons. Solid curves indicate discontinuous phase transition boundaries, while dashed curves show continuous phase transition boundaries, where the continuity/discontinuity of a phase transition is judged by whether there is a jump of the spin expectation value $\boldsymbol{f}$.

### The property of each phase

Here, $\chi$ is denoted by a vector $(\chi(1), \chi(0), \chi(-1))$.

- The phase I and II are the ferromagnetic phases, in which all particles populate $\sigma = 1$ (phase I) or $\sigma = -1$ (phase II) states, and the system possesses the largest value of $\left|f^{(3)}\right|$.

$$\text{I}: \quad \chi = (e^{i\theta}, 0, 0) \ (\theta \in \mathbb{R}), \tag{2.186}$$
$$\boldsymbol{f} = (0, 0, 1), \tag{2.187}$$
$$\varepsilon = -p + q + \frac{1}{2}c_1\rho + \frac{1}{2}c_0\rho, \tag{2.188}$$
$$\text{II}: \quad \chi = (0, 0, e^{i\theta}) \ (\theta \in \mathbb{R}), \tag{2.189}$$
$$\boldsymbol{f} = (0, 0, -1), \tag{2.190}$$
$$\varepsilon = p + q + \frac{1}{2}c_1\rho + \frac{1}{2}c_0\rho. \tag{2.191}$$

  It is natural that phase I (phase II) appears when the linear Zeeman energy $p$ is large (negatively large) enough, as can be confirmed from figure 2.2.

- The phase III is the antiferromagnetic phase, in which all the particles populate the $\sigma = \pm 1$ states.

$$\text{III}: \quad \chi = \left(e^{i\theta_+}\sqrt{\frac{1 + p/(c_1\rho)}{2}}, 0, e^{i\theta_-}\sqrt{\frac{1 - p/(c_1\rho)}{2}}\right) \ (\theta_\pm \in \mathbb{R}), \tag{2.192}$$
$$\boldsymbol{f} = \left(0, 0, \frac{p}{c_1\rho}\right), \tag{2.193}$$
$$\varepsilon = q - \frac{p^2}{2c_1\rho} + \frac{1}{2}c_0\rho. \tag{2.194}$$

- The phase IV is the polar phase, in which all the particles populate the $\sigma = 0$ state. The state does not possess magnetization.

$$\text{IV}: \quad \chi = \left(0, e^{i\theta}, 0\right) \ (\theta \in \mathbb{R}), \tag{2.195}$$
$$\boldsymbol{f} = (0,0,0)\,, \tag{2.196}$$
$$\varepsilon = \frac{1}{2}c_0\rho. \tag{2.197}$$

  The polar phase appears when the positive quadratic Zeeman energy $q$, which penalizes particles in $\sigma = \pm 1$ levels, is strong enough.

- The phase V is the broken-axisymmetry phase, in which the magnetization tilts with respect to the axis of the external magnetic field, and the symmetry around the axis is spontaneously broken.

$$\begin{aligned}\text{V}: \quad \chi = \Bigg( & e^{i(\theta_0-\theta_3)}\frac{q+p}{2q}\sqrt{\frac{p^2-q^2+2|c_1|\rho q}{2|c_1|\rho q}}, \\ & e^{i\theta_0}\sqrt{\frac{(q^2-p^2)(p^2+q^2+2|c_1|\rho q)}{4|c_1|\rho q^3}}, \\ & e^{i(\theta_0+\theta_3)}\frac{q-p}{2q}\sqrt{\frac{p^2-q^2+2|c_1|\rho q}{2|c_1|\rho q}}\Bigg) \ (\theta_0,\theta_3 \in \mathbb{R}),\end{aligned} \tag{2.198}$$

$$\begin{aligned}\boldsymbol{f} = \Bigg( & \cos\theta_3\frac{\sqrt{(q^2-p^2)[(p^2+2|c_1|\rho q)^2-q^4]}}{2|c_1|\rho q^2} \\ & \sin\theta_3\frac{\sqrt{(q^2-p^2)[(p^2+2|c_1|\rho q)^2-q^4]}}{2|c_1|\rho q^2}, \\ & \frac{p(p^2-q^2+2|c_1|\rho q)}{2|c_1|\rho q^2}\Bigg),\end{aligned} \tag{2.199}$$

$$\varepsilon = \frac{(p^2-q^2+2q|c_1|\rho)^2}{8|c_1|\rho q^2} + \frac{1}{2}c_0\rho. \tag{2.200}$$

  The phase arises as a result of the competition between the ferromagnetic interaction, which energetically favors a larger spin state, and the positive quadratic Zeeman energy, which penalizes the $\sigma = \pm 1$ spins.

The properties of each phase are summarized in table 2.3.

**The phase diagram and phase transitions**

- **antiferromagnetic interaction**

  When $c_1 > 0$, the spin-dependent interaction favors the state with smaller $|\boldsymbol{f}|$. In the absence of an external magnetic field ($p = q = 0$), the ground state becomes $\chi = (0,1,0), \frac{1}{\sqrt{2}}(1,0,1)$, (which satisfy $|\boldsymbol{f}| = 0$) or any states represented by spin rotations of these states. (In fact, the latter can be obtained from the former by a spin rotation. )

| | Phase | order parameter $\chi$ | magnetization $\boldsymbol{f}$ | energy $\varepsilon - \frac{1}{2}c_0\rho$ |
|---|---|---|---|---|
| I | ferromagnetic | $(e^{i\theta}, 0, 0)$ | $(0, 0, 1)$ | $-p + q + \frac{1}{2}c_1\rho$ |
| II | ferromagnetic | $(0, 0, e^{i\theta})$ | $(0, 0, -1)$ | $p + q + \frac{1}{2}c_1\rho$ |
| III | antiferromagnetic | (2.192) | $\left(0, 0, \frac{p}{c_1\rho}\right)$ | $q - \frac{p^2}{2c_1\rho}$ |
| IV | polar | $\left(0, e^{i\theta}, 0\right)$ | $(0, 0, 0)$ | 0 |
| V | broken-axisymmetry | (2.198) | (2.199) | (2.200) |

Table 2.3: Five ground-state phases of spin-1 bosons and their properties. $\theta, \theta_\pm \in \mathbb{R}$. The roman numbers correspond to those shown in figure 2.2.

When $p = 0$ and $q < 0$, the state $\chi = \frac{1}{\sqrt{2}}(1, 0, 1)$ is favored, and when $|p|$ is increased, the state follows the change by changing the population in the $\sigma = \pm 1$ levels (the antiferromagnetic phase III) until it finally becomes ferromagnetic (the ferromagnetic phases I and II). This phase transition is continuous as can be seen from table 2.3.

When $p = 0$ and $q > 0$, the state $\chi = (0, 1, 0)$ is favored (the polar phase IV). By increasing $|p|$, the ground-state turns ferromagnetic at a threshold value (except for the case in which $q$ is small so that the ground-state first becomes antiferromagnetic and then ferromagnetic.). The phase transitions between the ferromagnetic phases and the polar phase, and the phase transitions between the antiferromagnetic phase and the polar phase are discontinuous.

- **ferromagnetic interaction**

  When $c_1 < 0$, the spin-dependent interaction favors the state with larger $|\boldsymbol{f}|$. In the absence of an external magnetic field ($p = q = 0$), the ground state becomes $\chi = (1, 0, 0)$, which satisfies $|\boldsymbol{f}| = 1$, or any states represented by spin rotations of this state.

  For a negative $q$, the quadratic Zeeman term is compatible with the ferromagnetic spin-dependent interaction, and the mean-field ground state becomes $\chi = (1, 0, 0)$ or $(0, 0, 1)$, depending on the sign of the linear Zeeman energy $p$.

  For a positive $q$, the quadratic Zeeman term penalizes the population in the $\sigma = \pm 1$ levels, and competes with the ferromagnetic spin-dependent interaction. This competition gives rise to the broken-axisymmetry phase V, in which the magnetization tilts with respect to the axis of the external magnetic field, and the rotational symmetry around the axis is explicitly broken. By increasing $q$, the transverse magnetization gradually shrink, and the ground state continuously changes to the polar phase. This phase transition has been experimentally observed [32, 33].

# Chapter 3

# Ultracold bosons in optical lattices

In this section, we review some basic results on bosons in optical lattices, i.e., periodic potentials created by laser beams. We consider both scalar and spinor bosons, emphasizing the phase transition between the superfluid phase and the Mott insulator phase.

- Section 3.1 discusses two topics:
  1. We describe the way to create periodic potentials with various geometries using laser beams, and some examples including square/triangular lattices are shown.
  2. To describe bosons in an optical lattice from the viewpoint of localized particles, we introduce the Wannier functions, which will be used to derive the Bose-Hubbard Hamiltonian.
- Section 3.2 deals with the scalar (i.e., spinless) Bose-Hubbard model, which describes spinless bosons in optical lattices. We derive the Bose-Hubbard Hamiltonian using the Wannier function introduced in the previous section, assuming deep lattice (i.e., the tight-binding approximation) and low temperature (i.e., only the lowest band is considered). After discussing two extreme cases, namely, the no-hopping (i.e. strong interaction) case and the non-interacting case, we turn to the fascinating topic of the quantum phase transition between the superfluid phase and the Mott-insulator phase, which we will analyze using a simple approximation.
- Section 3.3 deals with the spin-1 Bose-Hubbard model, which describes spin-1 bosons in optical lattices. After deriving the model, we examine its ground state properties in the no-hopping case. Then, we again discuss the properties of superfluid to Mott-insulator phase transitions in the model, emphasizing the distinction from the scalar case.

## 3.1 Optical lattices

### 3.1.1 Creating periodic potentials

First, we begin by discussing the single-particle problem with a uniform electric field. It is known [6] that a time-dependent, spatially uniform electric field $\boldsymbol{E}(t) = \boldsymbol{E}^{(-)}e^{-i\omega t} + \boldsymbol{E}^{(+)}e^{i\omega t}$

changes the ground-state energy [1] of an atom by

$$\Delta E = -\frac{1}{2}\alpha(\omega)\left\langle |\boldsymbol{E}(t)|^2 \right\rangle_t , \tag{3.4}$$

where

- $\alpha(\omega)$ is the polarizability of the atom [2] , and
- $\langle\cdot\rangle_t$ denotes the time average over a multiple of the oscillation period of the electric field.

Here we assume that the oscillating electric field is off-resonant, i.e., $\hbar\omega \neq E_n - E_m$, where $E_n$ and $E_m$ denote arbitrary energy eigenvalues of the atom.

When the spatial variation of an oscillating electric field is much larger than the spatial extent of the atom, we can assume that (3.4) holds locally, and view the energy shift as an external potential

$$U(\boldsymbol{r}) = -\frac{1}{2}\alpha(\omega)\left\langle |\boldsymbol{E}(\boldsymbol{r},t)|^2 \right\rangle_t . \tag{3.5}$$

We show that, based on (3.5), spatially periodic potentials can be created by superposing laser beams propagating in different directions. First, take

$$\boldsymbol{E}(\boldsymbol{r},t) = \sum_{j=1}^{n} \boldsymbol{E}_j \cos\left(\boldsymbol{k}_j\cdot\boldsymbol{r} - \omega t + \delta_j\right) \tag{3.6}$$

$$= \sum_{j=1}^{n} \frac{1}{2}\boldsymbol{E}_j \left[e^{i(\boldsymbol{k}_j\cdot\boldsymbol{r}-\omega t+\delta_j)} + e^{-i(\boldsymbol{k}_j\cdot\boldsymbol{r}-\omega t+\delta_j)}\right], \tag{3.7}$$

[1] Here, the "energy eigenvalue" under an oscillating perturbation is defined by considering time-average as follows: Let us expand the state $\psi$ by

$$\psi(t) = \sum_n c_n(t)\phi_n, \tag{3.1}$$

where $(\phi_n)_n$ are energy eigenstates of the unperturbed Hamiltonian, and we assume that $\psi(0) = \phi_0$. Note that, without the perturbation, $c_n$ evolves as $c_n(t) = e^{-iE_nt/h}$, where $E_n$ is the energy eigenvalue of the state $\phi_n$.

Define the phase $\theta_0(t)$ of the time-dependent coefficient $c_0(t)$ by

$$\theta_0(t) := \frac{1}{i}\log c_0(t), \tag{3.2}$$

where it is understood that $\theta_0$ is defined to be continuous with respect to time $t$. Then, $\tilde{E}_0$, the "energy eigenvalue" of $\phi_0$ under the oscillating perturbation is defined by

$$\tilde{E}_0 := -\hbar \lim_{l\to\infty, l\in\mathbb{N}} \frac{\theta_0(lT)}{lT}, \tag{3.3}$$

where $T$ is the period of the oscillating perturbation.

[2] Generally, the polarizability is a tensor, but here we assume it is rotationally symmetric so that it can be expressed by a scalar.

where each $\boldsymbol{E}_j \in \mathbb{R}^3$ is a real vector denoting the direction of the electric field, and each $\boldsymbol{k}_j \in \mathbb{R}^3$ is a real vector denoting the wave number of the mode. Then,

$$\begin{aligned}
&\left\langle |\boldsymbol{E}(\boldsymbol{r},t)|^2 \right\rangle_t \\
&= \frac{1}{4}\sum_{j,j'=1}^{n} \boldsymbol{E}_j \cdot \boldsymbol{E}_{j'} \left\langle \left[e^{i(\boldsymbol{k}_j\cdot\boldsymbol{r}-\omega t+\delta_j)} + e^{-i(\boldsymbol{k}_j\cdot\boldsymbol{r}-\omega t+\delta_j)}\right]\left[e^{i(\boldsymbol{k}_{j'}\cdot\boldsymbol{r}-\omega t+\delta_{j'})} + e^{-i(\boldsymbol{k}_{j'}\cdot\boldsymbol{r}-\omega t+\delta_{j'})}\right]\right\rangle_t \quad (3.8)\\
&= \frac{1}{4}\sum_{j,j'=1}^{n} \boldsymbol{E}_j \cdot \boldsymbol{E}_{j'} \left\{e^{i[(\boldsymbol{k}_j-\boldsymbol{k}_{j'})\cdot\boldsymbol{r}+\delta_j-\delta_{j'}]} + e^{-i[(\boldsymbol{k}_j-\boldsymbol{k}_{j'})\cdot\boldsymbol{r}+\delta_j-\delta_{j'}]}\right\} \quad (3.9)\\
&= \frac{1}{2}\sum_{j=1}^{n} |\boldsymbol{E}_j|^2 + \sum_{j<j'} \boldsymbol{E}_j \cdot \boldsymbol{E}_{j'} \cos[(\boldsymbol{k}_j-\boldsymbol{k}_{j'})\cdot\boldsymbol{r}+\delta_j-\delta_{j'}]. \quad (3.10)
\end{aligned}$$

By subtracting the first term in the right-hand side, which does not depend on the position, we obtain the potential [3]

$$U(\boldsymbol{r}) = -\frac{1}{2}\alpha(\omega)\sum_{j<j'} \boldsymbol{E}_j \cdot \boldsymbol{E}_{j'} \cos[(\boldsymbol{k}_j-\boldsymbol{k}_{j'})\cdot\boldsymbol{r}+\delta_j-\delta_{j'}]. \quad (3.11)$$

Thus, by choosing $n$, $\boldsymbol{E}_j$, $\boldsymbol{k}_j$ properly, we can realize various lattice geometries. A few examples are shown below.

**One-dimensional lattice**

To implement a one-dimensional lattice, we take $n = 2$, $\boldsymbol{k}_1 = \boldsymbol{k}, \boldsymbol{k}_2 = -\boldsymbol{k}$, $\boldsymbol{E}_1 = \boldsymbol{E}_2$, where $\boldsymbol{k} \in \mathbb{R}^3$, with $|\boldsymbol{E}_i| = 1$ [4], and for simplicity, $\delta_1 = \delta_2$. Then, by denoting $\boldsymbol{r}\cdot\boldsymbol{k}/|\boldsymbol{k}| = x$, we obtain a periodic potential

$$U(\boldsymbol{r}) = -\frac{1}{2}\alpha(\omega)\cos(2|\boldsymbol{k}|x) \quad (3.12)$$

whose period in space (or lattice spacing) is given by $\pi/|\boldsymbol{k}|$ i.e., the half of the wavelength of the laser light.

**Three-dimensional cubic lattice**

The two-dimensional case and the three-dimensional case are similar, so we treat the three-dimensional case here. The idea is to reproduce the one dimensional case in three directions. Here, we need $n = 6$ laser beams, and take

$$\boldsymbol{k}_1 = -\boldsymbol{k}_2 = k\boldsymbol{e}_1, \quad \boldsymbol{k}_3 = -\boldsymbol{k}_4 = k\boldsymbol{e}_2, \quad \boldsymbol{k}_5 = -\boldsymbol{k}_6 = k\boldsymbol{e}_3, \quad (3.13)$$

where $\boldsymbol{e}_i$ denotes the unit vector in the $i$ direction, and $k$ denotes the magnitude of the wavenumber. To avoid interference between beams of different axes, we take

$$\boldsymbol{E}_1 = \boldsymbol{E}_2 = \boldsymbol{e}_2, \quad \boldsymbol{E}_3 = \boldsymbol{E}_4 = \boldsymbol{e}_3, \quad \boldsymbol{E}_5 = \boldsymbol{E}_6 = \boldsymbol{e}_1. \quad (3.14)$$

For simplicity, we take all $\delta_i$ to be zero. Then, we obtain the three dimensional cubic potential

$$U(\boldsymbol{r}) = -\frac{1}{2}\alpha(\omega)\left[\cos(2kx_1) + \cos(2kx_2) + \cos(2kx_3)\right] \quad (3.15)$$

with lattice spacing $\pi/k$.

[3] This potential is different from the one in (3.4) by the constant $\frac{1}{4}\alpha(\omega)\sum_{j=1}^{n}|\boldsymbol{E}_j|^2$, but we slightly abuse notation.

[4] $\boldsymbol{E}_1$ and $\boldsymbol{E}_2$ can be chosen arbitrarily as long as $\boldsymbol{E}_1 \cdot \boldsymbol{E}_2 \neq 0$.

**Two-dimensional triangular lattice**

As a less trivial example, here we show how to construct a two dimensional triangular optical lattice [34]. Here, we use $n = 3$ beams, with

$$\boldsymbol{k}_1 = k(0,1,0), \quad \boldsymbol{k}_2 = k\left(-\frac{\sqrt{3}}{2}, -\frac{1}{2}, 0\right) \quad \boldsymbol{k}_3 = k\left(\frac{\sqrt{3}}{2}, -\frac{1}{2}, 0\right) \tag{3.16}$$

$$\boldsymbol{E}_1 = \boldsymbol{E}_2 = \boldsymbol{E}_3 = \boldsymbol{e}_3, \tag{3.17}$$

and we set $\delta_i = 0$ for simplicity. Then, the potential becomes

$$U(\boldsymbol{r}) = -\frac{1}{2}\alpha(\omega)\left\{\cos(\boldsymbol{b}_1 \cdot \boldsymbol{r}) + \cos(\boldsymbol{b}_2 \cdot \boldsymbol{r}) + \cos[(\boldsymbol{b}_1 + \boldsymbol{b}_2) \cdot \boldsymbol{r}]\right\}, \tag{3.18}$$

where

$$\boldsymbol{b}_1 := \boldsymbol{k}_2 - \boldsymbol{k}_3 = \sqrt{3}k(-1,0,0), \tag{3.19}$$

$$\boldsymbol{b}_2 := \boldsymbol{k}_3 - \boldsymbol{k}_1 = \sqrt{3}k\left(\frac{1}{2}, -\frac{\sqrt{3}}{2}, 0\right) \tag{3.20}$$

are reciprocal lattice vectors. The corresponding direct lattice vectors are given by

$$\boldsymbol{a}_1 := \frac{4\pi}{3k}\left(-\frac{\sqrt{3}}{2}, -\frac{1}{2}, 0\right), \tag{3.21}$$

$$\boldsymbol{a}_2 := \frac{4\pi}{3k}(0,-1,0) \tag{3.22}$$

which satisfy $\boldsymbol{a}_i \cdot \boldsymbol{b}_j = 2\pi\delta_{i,j}$, from which we can see that the potential forms a triangular lattice.

Figure 3.1 shows optical lattice potentials discussed above. For more complex optical lattices, see [35]

### 3.1.2 Bloch wave functions and Wannier functions

Here, we consider a one-particle problem under a periodic potential $U_L$. For simplicity, we consider a finite lattice, whose lattice points are collectively denoted by $\Lambda$, and integrals are understood to be over the whole lattice (not the whole space $\mathbb{R}^d$. ).

**Bloch wave function**

From Bloch's theorem in condensed matter physics, we can write down energy eigenstates in the form of

$$\phi_{b,\boldsymbol{k}}(\boldsymbol{r}) = e^{i\boldsymbol{k}\cdot\boldsymbol{r}} u_{b,\boldsymbol{k}}(\boldsymbol{r}), \tag{3.23}$$

where

- $\boldsymbol{k}$ is a crystal wave vector in the first Brillouin zone, which is determined from the direct lattice vectors,
- $b$ is a label specifying the band, and

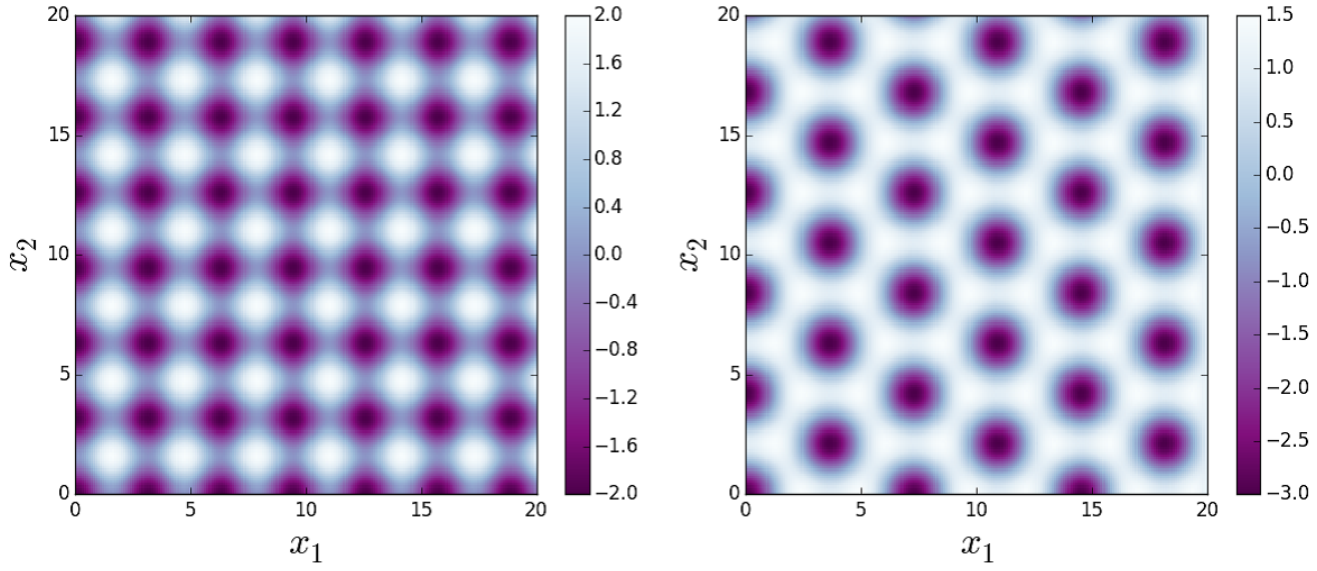


Figure 3.1: Examples of periodic potentials. Here we assume $\alpha$ is positive, and the color bars are in an arbitrary unit. Left: a square lattice, which can be obtained in a way similar to (3.15). Right: a triangular lattice represented by (3.18).

- $u$ is a function with the same periodicity as the periodic potential $U_L$.

We assume that the set of Bloch wave functions forms a complete orthonormal basis:

$$\int d\boldsymbol{r}\phi^*_{b,\boldsymbol{k}}(\boldsymbol{r})\phi_{b',\boldsymbol{k}'}(\boldsymbol{r}) = \delta_{b,b'}\delta_{\boldsymbol{k},\boldsymbol{k}'}, \tag{3.24}$$

$$\sum_{b,\boldsymbol{k}} \phi_{b,\boldsymbol{k}}(\boldsymbol{r})\phi^*_{b,\boldsymbol{k}}(\boldsymbol{r}') = \delta(\boldsymbol{r}-\boldsymbol{r}'). \tag{3.25}$$

### Wannier functions

Bloch wave functions represents a particle extending over the whole lattice. To describe the particle in terms of localized states, we can employ another basis set called the Wannier functions defined by

$$W_{b,x}(\boldsymbol{r}) := \frac{1}{\sqrt{|\Lambda|}} \sum_{\boldsymbol{k}} e^{-i\boldsymbol{k}\cdot\boldsymbol{r}_x}\phi_{b,\boldsymbol{k}}(\boldsymbol{r}), \tag{3.26}$$

where the summation is over the first Brillouin zone, and $x \in \Lambda$ [5].

It follows from the properties of the Bloch wave function (3.24) and (3.25) that the set of all the Wannier functions constitutes a complete orthonormal basis:

$$\int d\boldsymbol{r}W^*_{b,x}(\boldsymbol{r})W_{b',x'}(\boldsymbol{r}) = \delta_{b,b'}\delta_{x,x'}, \tag{3.27}$$

$$\sum_{b,x} W_{b,x}(\boldsymbol{r})W^*_{b,x}(\boldsymbol{r}') = \delta(\boldsymbol{r}-\boldsymbol{r}'). \tag{3.28}$$

[5] Concretely, $x \in \mathbb{N}^d$, and, if we denote the $i$-th component of $x$ by $x^i$, then $\boldsymbol{r}_x$ can be expressed as $\boldsymbol{r}_x = \sum_{j=1}^d x^j \boldsymbol{a}_j$, where $\boldsymbol{a}_j$ denotes primitive vectors of the lattice.

Note that, because $W_{b,x}(\boldsymbol{r}+\boldsymbol{r}_x)$ does not depend on $x$ [6] , the Wannier functions can be expressed as

$$W_{b,x}(\boldsymbol{r}) = W_b(\boldsymbol{r}-\boldsymbol{r}_x), \tag{3.29}$$

$$W_b(\boldsymbol{r}) := \frac{1}{\sqrt{|\Lambda|}}\sum_{\boldsymbol{k}} \phi_{b,\boldsymbol{k}}(\boldsymbol{r}). \tag{3.30}$$

## 3.2 Scalar Bose-Hubbard model

### 3.2.1 Derivation

In this subsection, we derive the Bose-Hubbard model. Our starting point is the Hamiltonian for scalar bosons interacting through a contact interaction

$$\begin{aligned} H &= \int d\boldsymbol{r}\hat{\psi}^\dagger(\boldsymbol{r})\left[-\frac{\hbar^2}{2M}\nabla^2 + U_T(\boldsymbol{r}) + U_L(\boldsymbol{r})\right]\hat{\psi}(\boldsymbol{r}) \\ &\quad + \frac{g}{2}\int d\boldsymbol{r}\hat{\psi}^\dagger(\boldsymbol{r})\hat{\psi}^\dagger(\boldsymbol{r})\hat{\psi}(\boldsymbol{r})\hat{\psi}(\boldsymbol{r}), \end{aligned} \tag{3.31}$$

where $U_L$ represents the optical lattice potential, and $U_T$ represents a trapping potential.

To derive the Bose-Hubbard Hamiltonian, we first define the boson creation/annihilation operators from the Wannier functions;

$$a_{b,x} := \int d\boldsymbol{r} W^*_{b,x}(\boldsymbol{r})\hat{\psi}(\boldsymbol{r}), \tag{3.32}$$

$$a^\dagger_{b,x} := \int d\boldsymbol{r} W_{b,x}(\boldsymbol{r})\hat{\psi}^\dagger(\boldsymbol{r}), \tag{3.33}$$

which, from the orthonormality (3.27), satisfy the bosonic canonical commutation relations

$$[a_{b,x}, a_{b',x'}] = [a^\dagger_{b,x}, a^\dagger_{b',x'}] = 0, \quad [a_{b,x}, a^\dagger_{b',x'}] = \delta_{b,b'}\delta_{x,x'}. \tag{3.34}$$

Then, we can rewrite the Hamiltonian (3.31) as

$$\begin{aligned} H &= \sum_{b_1,x_1,b_2,x_2}\left(-t^{b_1,b_2}_{x_1,x_2} + U^{b_1,b_2}_{x_1,x_2}\right)a^\dagger_{b_1,x_1}a_{b_2,x_2} \\ &\quad + \frac{1}{2}\sum_{b_1,x_1,b_2,x_2,b_3,x_3,b_4,x_4} U^{b_1,b_2,b_3,b_4}_{x_1,x_2,x_3,x_4}a^\dagger_{b_1,x_1}a^\dagger_{b_2,x_2}a_{b_3,x_3}a_{b_4,x_4}, \end{aligned} \tag{3.35}$$

where

$$t^{b_1,b_2}_{x_1,x_2} := -\int d\boldsymbol{r} W^*_{b_1}(\boldsymbol{r}-\boldsymbol{r}_{x_1})\left[-\frac{\hbar^2}{2M}\nabla^2 + U_L(\boldsymbol{r})\right]W_{b_2}(\boldsymbol{r}-\boldsymbol{r}_{x_2}), \tag{3.36}$$

$$U^{b_1,b_2}_{x_1,x_2} := \int d\boldsymbol{r} W^*_{b_1}(\boldsymbol{r}-\boldsymbol{r}_{x_1})U_T(\boldsymbol{r})W_{b_2}(\boldsymbol{r}-\boldsymbol{r}_{x_2}), \tag{3.37}$$

$$U^{b_1,b_2,b_3,b_4}_{x_1,x_2,x_3,x_4} := g\int d\boldsymbol{r} W^*_{b_1}(\boldsymbol{r}-\boldsymbol{r}_{x_1})W^*_{b_2}(\boldsymbol{r}-\boldsymbol{r}_{x_2})W_{b_3}(\boldsymbol{r}-\boldsymbol{r}_{x_3})W_{b_4}(\boldsymbol{r}-\boldsymbol{r}_{x_4}). \tag{3.38}$$

[6] This property can be seen from the definition (3.26), the form of the Bloch wave function, and the fact that $u_{b,\boldsymbol{k}}$ possesses the same periodicity as the lattice.

$(\because)$

From the completeness relation (3.28),

$$\hat{\psi}(\boldsymbol{r}) = \sum_{b,x} W_{b,x}(\boldsymbol{r}) a_{b,x}, \tag{3.39}$$

$$\hat{\psi}^\dagger(\boldsymbol{r}) = \sum_{b,x} W^*_{b,x}(\boldsymbol{r}) a^\dagger_{b,x} \tag{3.40}$$

holds. Substituting these relations into (3.31) yields

$$\begin{aligned} H &= \sum_{b_1,x_1,b_2,x_2} \left\{ \int d\boldsymbol{r} W^*_{b_1,x_1}(\boldsymbol{r}) \left[ -\frac{\hbar^2}{2M}\nabla^2 + U_L(\boldsymbol{r}) \right] W_{b_2,x_2}(\boldsymbol{r}) \right\} a^\dagger_{b_1,x_1} a_{b_2,x_2} \\ &+ \sum_{b_1,x_1,b_2,x_2} \left[ \int d\boldsymbol{r} W^*_{b_1,x_1}(\boldsymbol{r}) U_T(\boldsymbol{r}) W_{b_2,x_2}(\boldsymbol{r}) \right] a^\dagger_{b_1,x_1} a_{b_2,x_2} \\ &+ \frac{g}{2} \sum_{b_1,x_1,b_2,x_2,b_3,x_3,b_4,x_4} \left[ \int d\boldsymbol{r} W^*_{b_1,x_1}(\boldsymbol{r}) W^*_{b_2,x_2}(\boldsymbol{r}) W_{b_3,x_3}(\boldsymbol{r}) W_{b_4,x_4}(\boldsymbol{r}) \right] \\ &\times a^\dagger_{b_1,x_1} a^\dagger_{b_2,x_2} a_{b_3,x_3} a_{b_4,x_4} \end{aligned} \tag{3.41}$$

Then, by using (3.29) and (3.30), and defining symbols as above, we obtain the result.

■

Various models can be obtained by imposing different approximations on the Hamiltonian [36]. Here we consider the simplest case:

We impose the following three assumptions:

- All bands except for the lowest one, which we label as $b = 0$, can be neglected.
- The lattice potential is so deep that the Wannier functions are strongly localized at each site (i.e., the tight-binding approximation).
- The trapping potential $U$ changes much slowly in space compared with the lattice potential $U_L$.

Then, the Hamiltonian (3.35) can be approximated by the Bose-Hubbard Hamiltonian

$$H_{\rm BH} = -\sum_{\substack{x,y \\ \text{neighboring}}} t_{x,y} a_x^\dagger a_y + \sum_x V_x a_x^\dagger a_x + \frac{U_0}{2} \sum_x \hat{n}_x(\hat{n}_x - 1), \tag{3.42}$$

where

$$\begin{aligned}
a_x &:= a_{0,x} = \int d\boldsymbol{r} W_{0,x}^*(\boldsymbol{r}) \hat{\psi}(\boldsymbol{r}), && (3.43)\\
t_{x,y} &:= -\int d\boldsymbol{r} W_0^*(\boldsymbol{r} - \boldsymbol{r}_x) \left[ -\frac{\hbar^2}{2M} \nabla^2 + U_L(\boldsymbol{r}) \right] W_0(\boldsymbol{r} - \boldsymbol{r}_y), && (3.44)\\
V_x &:= U_T(\boldsymbol{r}_x), && (3.45)\\
U_0 &:= g \int d\boldsymbol{r} |W_0(\boldsymbol{r})|^4, && (3.46)\\
\hat{n}_x &:= a_x^\dagger a_x, && (3.47)
\end{aligned}$$

and the first summation is restricted to neighboring sites $x$ and $y$.

($\because$)

From the first assumption, we neglect all the terms with $b \neq 0$, and the Hamiltonian can be approximated by

$$\sum_{x,y} \left( -t_{x,y} + U_{x,y} \right) a_x^\dagger a_y + \frac{1}{2} \sum_{x_1,x_2,x_3,x_4} U_{x_1,x_2,x_3,x_4} a_{x_1}^\dagger a_{x_2}^\dagger a_{x_3} a_{x_4}, \tag{3.48}$$

where

$$\begin{aligned}
a_x &:= a_{0,x}, && (3.49)\\
t_{x,y} &:= t_{x,y}^{0,0} \\
&= -\int d\boldsymbol{r} W_0^*(\boldsymbol{r} - \boldsymbol{r}_x) \left[ -\frac{\hbar^2}{2M} \nabla^2 + U_L(\boldsymbol{r}) \right] W_0(\boldsymbol{r} - \boldsymbol{r}_y), && (3.50)\\
U_{x,y} &:= U_{x,y}^{0,0} = \int d\boldsymbol{r} W_0^*(\boldsymbol{r} - \boldsymbol{r}_x) U_T(\boldsymbol{r}) W_0(\boldsymbol{r} - \boldsymbol{r}_y), && (3.51)\\
U_{x_1,x_2,x_3,x_4} &:= U_{x_1,x_2,x_3,x_4}^{0,0,0,0} \\
&= g \int d\boldsymbol{r} W_0^*(\boldsymbol{r} - \boldsymbol{r}_{x_1}) W_0^*(\boldsymbol{r} - \boldsymbol{r}_{x_2}) \\
&\quad \times W_0(\boldsymbol{r} - \boldsymbol{r}_{x_3}) W_0(\boldsymbol{r} - \boldsymbol{r}_{x_4}). && (3.52)
\end{aligned}$$

From the second assumption, $t_{x,y}$, $U_{x,y}$, and $U_{x_1,x_2,x_3,x_4}$ rapidly decay as separations between different variables ($x$ and $y$) become larger. Thus, we neglect

- $U_{x,y}$ if $x \neq y$,
- $U_{x_1,x_2,x_3,x_4}$ unless $x_1 = x_2 = x_3 = x_4$, and
- $t_{x,y}$ unless $x$ and $y$ represent a pair of neighboring sites [7] .

We define

$$U_0 := U_{x,x,x,x} = g \int d\boldsymbol{r} |W_0(\boldsymbol{r})|^4. \tag{3.53}$$

Further, from the slow variation assumptions on $U_T$, we approximate the integral (3.52) by $U_T(\boldsymbol{r}_x)$. Then, we arrive at

$$- \sum_{\substack{x,y \\ \text{neighboring}}} t_{x,y} a_x^\dagger a_y + \sum_x U_T(\boldsymbol{r}_x) a_x^\dagger a_x + \frac{U_0}{2} \sum_x a_x^\dagger a_x^\dagger a_x a_x. \tag{3.54}$$

■

### 3.2.2 Ground-state properties for two limits

Hereafter, we assume $U_0 \geq 0$, and $t_{x,y} \geq 0$.

#### Non-interacting case ($U_0 = 0$)

In the non-interacting, i.e., $U_0 = 0$ case, it is easy to show that the Hamiltonian can be diagonalized as follows:

[7] Because of the discrete translational invariance, the terms with $x = y$ gives Const. $\times$ (Total particle number), which does not affect the physics of the system.

Let $K$ be an appropriate finite set, $(\phi_k)_{k\in K}$ be a complete orthonormal basis of $L^2(\Lambda)$, and $(\varepsilon_k)_{k\in K}$ be a family of real numbers which satisfy

$$-\sum_{y\in\Lambda} t_{x,y}\phi_k(y) + V_x\phi_k(x) = \varepsilon_k\phi_k(x) \quad (\forall x \in \Lambda,\ k \in K). \tag{3.55}$$

(Because the equation has the form of the eigenvalue problem of a Hermitian matrix, such $(\phi_k)_{k\in K}$ and $(\varepsilon_k)_{k\in K}$ exist. ). Let us define

$$\tilde{a}_k := \sum_{x\in\Lambda} \phi_k(x)^* a_x. \tag{3.56}$$

Then, the Hamiltonian can be diagonalized as

$$H_{\mathrm{BH}} = \sum_{k\in K} \varepsilon_k \tilde{a}_k^\dagger \tilde{a}_k, \tag{3.57}$$

and a ground state, whose total particle number is $N \in \mathbb{N}$, can be expressed as

$$\Phi_{\mathrm{GS}} = \frac{1}{\sqrt{N!}} \left(\tilde{a}_0^\dagger\right)^N \Phi_{\mathrm{vac}}, \tag{3.58}$$

where $\Phi_{\mathrm{vac}}$ denotes the vacuum state.

In particular, if we take $V = 0$ and consider the $d$-dimensional hypercubic lattice, we can easily obtain the following results for the ground state.

The ground state for the $d$-dimensional hypercubic lattice

Let $N$ be the total particle number. We also assume the hopping amplitude $t_{x,y}$ for two neighboring sites does not depend on $x, y$ and can be written as $t_{x,y} = t > 0$. Let $L$ be the linear length (measured by the lattice spacing) of the lattice.

- The ground state is unique, and can be expressed as

$$\Phi_{\mathrm{GS}} = \frac{1}{\sqrt{N!}} \left(\tilde{a}_0^\dagger\right)^N \Phi_{\mathrm{vac}}, \quad \tilde{a}_0 = \frac{1}{L^{d/2}} \sum_{x \in \Lambda} a_x. \tag{3.59}$$

  The ground energy is $-2tdN$, and the energy difference between the ground state and the first excited state is $2t(1 - \cos(2\pi/L))$. .

- For the ground state, $\mathrm{Prob}_x(n|\Phi_{\mathrm{GS}})$, the probability distribution of the number of particle $n$ at site $x \in \Lambda$, is a binomial distribution

$$\mathrm{Prob}_x(n|\Phi_{\mathrm{GS}}) = \frac{N!}{n!(N-n)!} \left(\frac{1}{L^d}\right)^n \left(1 - \frac{1}{L^d}\right)^{N-n}, \tag{3.60}$$

  which, in the thermodynamic limit, can be approximated by a Poisson distribution

$$\mathrm{Prob}_x(n|\Phi_{\mathrm{GS}}) = e^{-\overline{n}} \frac{\overline{n}^n}{n!}, \tag{3.61}$$

  where $\overline{n} = N/L^d$.

- The one-body correlation function satisfies

$$\langle \Phi_{\mathrm{GS}}, a_x^\dagger a_y \Phi_{\mathrm{GS}} \rangle = \overline{n}. \tag{3.62}$$

From these results, we can see

- there is no energy gap in the thermodynamic limit,
- the particle number at each site has a large fluctuation, and
- the state possesses the off-diagonal long range order (ODLRO) because $\langle \Phi_{\mathrm{GS}}, a_x^\dagger a_y \Phi_{\mathrm{GS}} \rangle$ does not decay even if $x$ and $y$ are largely separated from each other.

**No-hopping case($t = 0$)**

In the no-hopping case, Fock states become energy eigenstates, where Fock states are defined by

$$\mathcal{I}_N := \left\{ \boldsymbol{n} = (n_x)_{x \in \Lambda} \;\middle|\; \forall x \in \Lambda \ (n_x \geq 0), \ \sum_{x \in \Lambda} n_x = N \right\}, \tag{3.63}$$

$$\Phi_{\boldsymbol{n}} := \prod_{x \in \Lambda} \frac{1}{\sqrt{n_x!}} \left(a_x^\dagger\right)^{n_x} \Phi_{\mathrm{vac}} \quad (\boldsymbol{n} \in \mathcal{I}_N). \tag{3.64}$$

Assume $t_{x,y} = 0$.

- $\Phi_{\boldsymbol{n}}$ ($\boldsymbol{n} \in \mathcal{I}_N$) are eigenstates of $H_{\rm BH}$, and

$$H_{\rm BH}\Phi_{\boldsymbol{n}} = E_{\boldsymbol{n}}\Phi_{\boldsymbol{n}}, \quad E_{\boldsymbol{n}} = \sum_{x\in\Lambda}\left[V_x n_x + \frac{U_0}{2}n_x(n_x-1)\right]. \tag{3.65}$$

- For $\Phi_{\boldsymbol{n}}$, $\mathrm{Prob}_x(n|\Phi_{\boldsymbol{n}})$ ($n \in \mathbb{N}$) becomes a Kronecker delta:

$$\mathrm{Prob}_x(n|\Phi_{\boldsymbol{n}}) = \delta_{n_x,n} \tag{3.66}$$

- The one-body correlation function satisfies

$$\langle \Phi_{\boldsymbol{n}}, a_x^\dagger a_y \Phi_{\boldsymbol{n}}\rangle = \delta_{x,y} n_x. \tag{3.67}$$

For the simples case with $V = 0$, the uniqueness of the ground state depends on whether $N/|\Lambda|$ is an integer or not.

Assume $t_{x,y} = 0$, $V_x = 0$ ($\forall x, y \in \Lambda$) and that the particle number $N$ satisfies

$$N = n_{\rm c}|\Lambda| + n_{\rm r} \ (n_{\rm c} \in \mathbb{Z}_+, 0 \le n_{\rm r} < |\Lambda|). \tag{3.68}$$

**•ground state**

Let us take a configuration $\boldsymbol{n}$ that satisfies

$$n_x = n_{\rm c} \ (\forall x \in \Lambda) \text{ if } n_r = 0, \tag{3.69}$$
$$n_x = n_{\rm c} \text{ or } n_{\rm c}+1 \ (\forall x \in \Lambda) \text{ if } n_r \neq 0. \tag{3.70}$$

Then, the corresponding $\Phi_{\boldsymbol{n}}$ is a ground state of $H_{\rm BH}$. We call the former case the commensurate filling case, and the latter the incommensurate filling case. The ground state is unique for the commensurate filling case, while ground states are degenerate for the incommensurate filling case.

**• ground-state energy**

The ground energy $E_{\rm GS}$ can be expressed as

$$E_{\rm GS} = \frac{U_0}{2}n_{\rm c}\left[|\Lambda|(n_{\rm c}-1) + 2n_{\rm r}\right]. \tag{3.71}$$

**• energy gap**

The energy difference between the ground state and the first excited state is $U_0$.

Thus, for the commensurate filling case,

- the energy gap exists in the thermodynamic limit,
- the particle number at each site is fixed, and
- the state possesses no ODLRO.

For incommensurate case, it can be shown that linear combinations of the degenerate ground states can possess ODLRO.

### 3.2.3 Superfluid to Mott-Insulator transition

Hereafter, we assume that $t_{x,y}$ does not depend on $x, y$ as long as they are neighboring sites, and write $t_{x,y} = t$

We have seen in the previous subsection that the ground state of the non-interacting case and that of the no-hopping case with commensurate filling exhibit completely different properties; each particle spreads over the whole system in the former state, while each particle is completely localized in the latter state.

When we have the Bose-Hubbard Hamiltonian with both terms being non-zero, there is a competition between these two terms; it is energetically favorable to delocalize particles for the hopping term, while it is energetically favorable to localize particles for the interaction term [8]. This competition gives rise to a fascinating phenomenon; the quantum phase transition between the superfluid phase and the Mott-insulator phase. The former phase is defined by non-zero ODLRO, and it is known to have no energy gap, while the latter phase does not exhibit ODLRO, and has a non-zero energy gap.

Let us first analyze the system using a simple approximation of the Gutzwiller variational ansatz [37, 38]. To make the discussion simple, we consider the grand canonical ensemble at zero temperature specified by the grand Hamiltonian $\hat{K}_{\mathrm{BH}} = H_{\mathrm{BH}} - \mu\hat{N}$, where $\mu$ is the chemical potential, and $\hat{N}$ is the total particle-number operator. We assume that the trapping potential $U_T$ is zero. We calculate its approximate ground state using a variational method, with the variational states being the product of identical local states:

[8] We assume $t > 0$ and $U_0 > 0$.

Gutzwiller variational ansatz for the ground state

To approximate the ground state, we use the following variational wave function $\Psi_{c,\Lambda}$

$$\Psi_{c,\Lambda} = \bigotimes_{x\in\Lambda} \sum_{n=0}^{n_{\max}} c(n)\Phi_{n_x}^{(x)}, \tag{3.72}$$

where

- the states
$$\Phi_{n_x}^{(x)} := \frac{1}{\sqrt{n_x!}} \left(a_x^\dagger\right)^{n_x} \Phi_{\text{vac}}^{(x)} \tag{3.73}$$
are local Fock states, and $\Phi_{\text{vac}}^{(x)}$ stands for the vacuum state of the Hilbert space of a single site $x$.
- Although the particle number can be infinite in principle, for simplicity we assume that the particle number at each site is not larger than a given value $n_{\max}$.
- The function $c$ satisfies the normalization condition $\sum_{n=0}^{n_{\max}} |c(n)|^2 = 1$.

Here, the function $c$ is the variational degree of freedom, and we search for such $c$ that minimizes the expectation value of $\hat{K}_{\text{BH}}$

$$\left\langle \Psi_{c,\Lambda},\ \hat{K}_{\text{BH}}\Psi_{c,\Lambda} \right\rangle. \tag{3.74}$$

The rationale behind this approximation is that, in both the non-interacting and no-hopping limits, the corresponding ground states can be written in the form of (3.72), and hence it is natural to assume that states in this form can interpolate these two limits, and can capture the quantum phase transition well.

It is straightforward to show

$$\begin{aligned}\frac{1}{|\Lambda|}\left\langle \Psi_{c,\Lambda},\ \hat{K}_{\text{BH}}\Psi_{c,\Lambda} \right\rangle &= -zt \left| \sum_{n=0}^{n_{\max}-1} \sqrt{n+1}\, c(n)^* c(n+1) \right|^2 \\ &\quad + \sum_{n=0}^{n_{\max}} \left[ \frac{U_0}{2} n(n-1) - \mu n \right] |c(n)|^2, \end{aligned} \tag{3.75}$$

where $z$ is the number of the nearest neighbor sites of a site, and we assume that this number does not depend on the chosen specific site.

First, consider the $t = 0$ case. It is easy to see the minimum is attained by

$$c(n) = \delta_{n,n_c}, \tag{3.76}$$

where $n_c \in \mathbb{N}$ is an integer satisfying [9]

$$U_0(n_c - 1) < \mu < U_0 n_c. \tag{3.77}$$

This is nothing but the exact ground state for commensurate filling, and has no ODLRO, i.e., the state is a Mott insulator.

[9] We assume $\mu/U_0 \notin \mathbb{Z}$ for simplicity.

Next, we examine the stability of this state against a small fluctuation in the particle-number density, when $t$ is non-zero. Assume that $c$ takes the form of

$$c(n_c \pm 1) = \varepsilon_{\pm 1}, \quad c(n_c) = \sqrt{1 - \varepsilon_1^2 - \varepsilon_{-1}^2}, \quad c(n) = 0 \text{ (otherwise)}, \tag{3.78}$$

where $\varepsilon_{\pm 1} > 0$ are assumed to be small. Then, the expectation value of the grand Hamiltonian becomes

$$\begin{aligned} \frac{1}{|\Lambda|} \left\langle \Psi_{c,\Lambda},\ \hat{K}_{\mathrm{BH}} \Psi_{c,\Lambda} \right\rangle \ &= \ [-U_0(n_1 - 1) + \mu - ztn_c]\, \varepsilon_{-1}^2 + [U_0 n_c - \mu - zt(n_c + 1)]\, \varepsilon_1^2 \\ &\quad -2zt\sqrt{n_c(n_c+1)}\varepsilon_{-1}\varepsilon_1 \\ &\quad +\text{const.} + (\text{higher order terms of } \varepsilon_1 \text{ and } \varepsilon_{-1})\,. \end{aligned} \tag{3.79}$$

Thus, the Mott-insulator state is stable against small fluctuations in the particle-number density if and only if the quadratic form

$$[-U_0(n_1 - 1) + \mu - ztn_c]\, \varepsilon_{-1}^2 + [U_0 n_c - \mu - zt(n_c + 1)]\, \varepsilon_1^2 - 2zt\sqrt{n_c(n_c+1)}\varepsilon_{-1}\varepsilon_1 \tag{3.80}$$

is positive definite, which is equivalent to [10]

$$\frac{zt}{U_0} < \frac{(U_0 n_c - \mu)\,[\mu - (n_c - 1)U_0]}{U_0 + \mu}. \tag{3.81}$$

If $zt/U_0$ is larger than the right-hand side of (3.81), then the fluctuation grows, and the approximate ground state exhibits non-zero ODLRO.

Figure 3.2 shows the result of numerical minimization [11] of (3.75), which agrees well with the boundary (3.81) obtained by the above simple argument. Note that here the ODLRO can be decomposed into the product of the expectation values of $a_x^\dagger$ and $a_y$, and we call them superfluid order parameters.

Although the analysis above is a simple one, various theoretical studies, including quantum Monte Carlo calculations [39, 40], have confirmed that the analysis shown above captures the qualitative feature of the phase transition well. For a summary and comparison of these studies, see Table 2 of [10].

The quantum phase transition between the Mott-insulator phase and the superfluid phase was experimentally realized [14], which is one of the cornerstones in cold atomic physics, opening up the possibility of quantum simulation, where various quantum many-body Hamiltonians can be implemented and compared with theoretical predictions.

[10] Here, we assume $\mu + U_0 > 0$.

[11] Precisely speaking, the result is obtained by the method called the decoupling approximation, which is equivalent to minimizing the Gutzwiller variational energy (3.75. This fact will be shown in section 4.4). The equivalence will be shown in section 4.4 for the spin-1 Bose-Hubbard model, but the same discussion applies to the scalar case.

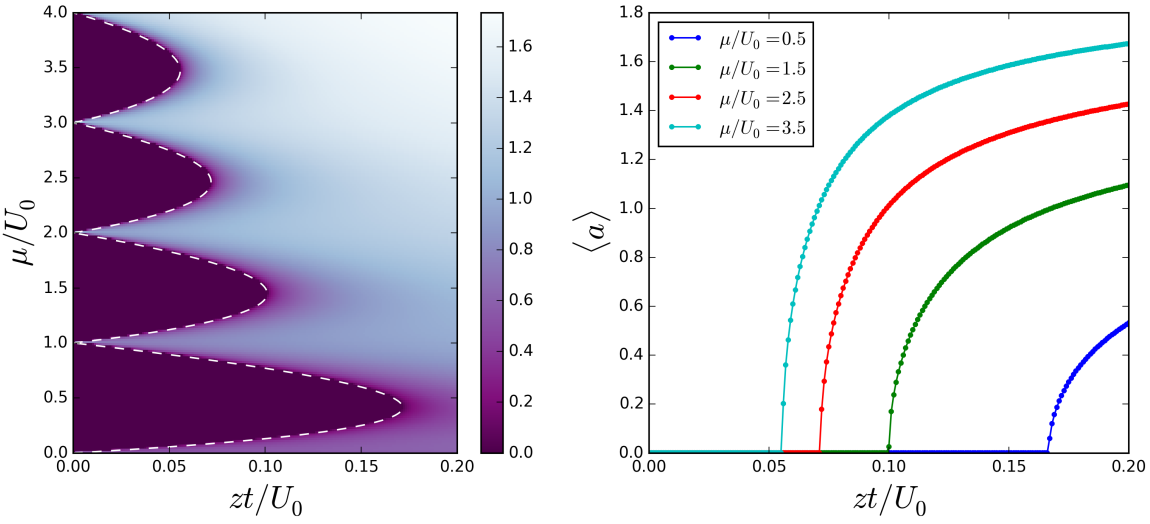


Figure 3.2: Ground-state phase diagram of the Bose-Hubbard model within the Gutzwiller variational ansatz. Left: Plotted in color is the superfluid order parameter $\langle a_x \rangle$, which is zero in the Mott-insulator phase, but non-zero in the superfluid phase. The white dashed curve denotes the boundary (3.81) obtained by the simple argument, which agrees well with the numerical result. Right: The hopping-amplitude $t$ dependence of the superfluid order parameter $\langle a \rangle$. It can be seen that the transition is continuous.

## 3.3 Spin-1 Bose-Hubbard model

### 3.3.1 Derivation

In this section, we derive the spin-1 Bose-Hubbard model starting from the Hamiltonian

$$\begin{aligned} H &= \int d\boldsymbol{r} \sum_{\sigma \in \mathcal{S}} \hat{\psi}^\dagger(\boldsymbol{r}, \sigma) \left[ -\frac{\hbar^2}{2M} \nabla^2 + U_T(\boldsymbol{r}) + U_L(\boldsymbol{r}) - p\sigma + q\sigma^2 \right] \hat{\psi}(\boldsymbol{r}, \sigma) \\ &\quad + \frac{1}{2} \int d\boldsymbol{r} \left[ c_0 : \hat{n}(\boldsymbol{r}) \hat{n}(\boldsymbol{r}) : \ + c_1 : \hat{\boldsymbol{F}}(\boldsymbol{r}) \cdot \hat{\boldsymbol{F}}(\boldsymbol{r}) : \right], \end{aligned} \tag{3.82}$$

where

$$\begin{aligned} & : \hat{n}(\boldsymbol{r}) \hat{n}(\boldsymbol{r}) : \\ := & \sum_{\sigma_1, \sigma_2 \in \mathcal{S}} \hat{\psi}^\dagger(\boldsymbol{r}, \sigma_1) \hat{\psi}^\dagger(\boldsymbol{r}, \sigma_2) \hat{\psi}(\boldsymbol{r}, \sigma_1) \hat{\psi}(\boldsymbol{r}, \sigma_2), \end{aligned} \tag{3.83}$$

$$\begin{aligned} & : \hat{\boldsymbol{F}}(\boldsymbol{r}) \cdot \hat{\boldsymbol{F}}(\boldsymbol{r}) : \\ := & \sum_{\sigma_1, \sigma_2, \tau_1, \tau_2 \in \mathcal{S}} \sum_{\alpha=1}^{3} S^{(\alpha)}_{\sigma_1, \tau_1} S^{(\alpha)}_{\sigma_2, \tau_2} \hat{\psi}^\dagger(\boldsymbol{r}, \sigma_1) \hat{\psi}^\dagger(\boldsymbol{r}, \sigma_2) \hat{\psi}(\boldsymbol{r}, \tau_1) \hat{\psi}(\boldsymbol{r}, \tau_2). \end{aligned} \tag{3.84}$$

Because the derivation can be done in almost the same way as the scalar case, here we only show the sketch of the derivation.

First, we define the creation/annihilation operators of spin-1 bosons at lattice points from

the Wannier functions:

$$a_{b,x,\sigma} := \int d\boldsymbol{r} W^*_{b,x}(\boldsymbol{r})\hat{\psi}(\boldsymbol{r},\sigma), \tag{3.85}$$

$$a^\dagger_{b,x,\sigma} := \int d\boldsymbol{r} W_{b,x}(\boldsymbol{r})\hat{\psi}^\dagger(\boldsymbol{r},\sigma), \tag{3.86}$$

which, from the orthonormality (3.27), satisfy the bosonic canonical commutation relations

$$[a_{b,x,\sigma}, a_{b',x',\sigma'}] = [a^\dagger_{b,x,\sigma}, a^\dagger_{b',x',\sigma'}] = 0, \quad [a_{b,x,\sigma}, a^\dagger_{b',x',\sigma'}] = \delta_{b,b'}\delta_{x,x'}\delta_{\sigma,\sigma'}. \tag{3.87}$$

Then, the Hamiltonian (3.82) can be rewritten as

$$\begin{aligned} H &= \sum_{b_1,b_2,x_1,x_2,\sigma_1,\sigma_2} (-t^{b_1,b_2}_{x_1,x_2} + U^{b_1,b_2}_{x_1,x_2}) a^\dagger_{b_1,x_1,\sigma_1} a_{b_2,x_2,\sigma_2} \\ &\quad + \sum_{b,x,\sigma} (-p\sigma + q\sigma^2) a^\dagger_{b,x,\sigma} a_{b,x,\sigma} \\ &\quad + \frac{1}{2} \sum_{b_1,b_2,b_3,b_4} \sum_{x_1,x_2,x_3,x_4} \sum_{\sigma,\tau} U^{b_1,b_2,b_3,b_4}_{0,x_1,x_2,x_3,x_4} a^\dagger_{b_1,x_1,\sigma} a^\dagger_{b_2,x_2,\tau} a_{b_3,x_3,\sigma} a_{b_4,x_4,\tau} \qquad (3.88) \\ &\quad + \frac{1}{2} \sum_{b_1,b_2,b_3,b_4} \sum_{x_1,x_2,x_3,x_4} \sum_{\sigma_1,\sigma_2,\tau_1,\tau_2} \sum_{\alpha} U^{b_1,b_2,b_3,b_4}_{2,x_1,x_2,x_3,x_4} S^{(\alpha)}_{\sigma_1,\tau_1} S^{(\alpha)}_{\sigma_2,\tau_2} \\ &\quad \times a^\dagger_{b_1,x_1,\sigma_1} a^\dagger_{b_2,x_2,\sigma_2} a_{b_3,x_3,\tau_1} a_{b_4,x_4,\tau_2}, \qquad (3.89) \end{aligned}$$

where

$$t^{b_1,b_2}_{x_1,x_2} := -\int d\boldsymbol{r} W^*_{b_1}(\boldsymbol{r}-\boldsymbol{r}_{x_1}) \left[ -\frac{\hbar^2}{2M}\nabla^2 + U_L(\boldsymbol{r}) \right] W_{b_2}(\boldsymbol{r}-\boldsymbol{r}_{x_2}), \tag{3.90}$$

$$U^{b_1,b_2}_{x_1,x_2} := \int d\boldsymbol{r} W^*_{b_1}(\boldsymbol{r}-\boldsymbol{r}_{x_1}) U_T(\boldsymbol{r}) W_{b_2}(\boldsymbol{r}-\boldsymbol{r}_{x_2}), \tag{3.91}$$

$$U^{b_1,b_2,b_3,b_4}_{0,x_1,x_2,x_3,x_4} := c_0 \int d\boldsymbol{r} W^*_{b_1}(\boldsymbol{r}-\boldsymbol{r}_{x_1}) W^*_{b_2}(\boldsymbol{r}-\boldsymbol{r}_{x_2}) W_{b_3}(\boldsymbol{r}-\boldsymbol{r}_{x_3}) W_{b_4}(\boldsymbol{r}-\boldsymbol{r}_{x_4}), \tag{3.92}$$

$$U^{b_1,b_2,b_3,b_4}_{2,x_1,x_2,x_3,x_4} := c_1 \int d\boldsymbol{r} W^*_{b_1}(\boldsymbol{r}-\boldsymbol{r}_{x_1}) W^*_{b_2}(\boldsymbol{r}-\boldsymbol{r}_{x_2}) W_{b_3}(\boldsymbol{r}-\boldsymbol{r}_{x_3}) W_{b_4}(\boldsymbol{r}-\boldsymbol{r}_{x_4}). \tag{3.93}$$

$(\because)$

Substituting the relations

$$\hat{\psi}(\boldsymbol{r},\sigma) = \sum_{b,x} W_{b,x}(\boldsymbol{r}) a_{b,x,\sigma}, \tag{3.94}$$

$$\hat{\psi}^\dagger(\boldsymbol{r},\sigma) = \sum_{b,x} W^*_{b,x}(\boldsymbol{r}) a^\dagger_{b,x,\sigma}, \tag{3.95}$$

which follows from the completeness relation (3.28), into (3.82) yields

$$
\begin{aligned}
H &= \sum_{b_1,b_2}\sum_{x_1,x_2}\sum_{\sigma}\left\{\int d\boldsymbol{r} W^*_{b_1,x_1}(\boldsymbol{r})\left[-\frac{\hbar^2}{2M}\nabla^2+U_L(\boldsymbol{r})\right]W_{b_2,x_2}(\boldsymbol{r})\right\} \\
&\quad \times a^\dagger_{b_1,x_1,\sigma}a_{b_2,x_2,\sigma} \\
&\quad +\sum_{b_1,b_2}\sum_{x_1,x_2}\sum_{\sigma}\left[\int d\boldsymbol{r} W^*_{b_1,x_1}(\boldsymbol{r})U_T(\boldsymbol{r})W_{b_2,x_2}(\boldsymbol{r})\right]a^\dagger_{b_1,x_1,\sigma}a_{b_2,x_2,\sigma} \\
&\quad +\sum_{b}\sum_{x}\sum_{\sigma}(-p\sigma+q\sigma^2)a^\dagger_{b,x,\sigma}a_{b,x,\sigma} \\
&\quad +\frac{c_0}{2}\sum_{b_1,b_2,b_3,b_4}\sum_{x_1,x_2,x_3,x_4}\sum_{\sigma,\tau}\int d\boldsymbol{r} W^*_{b_1,x_1}(\boldsymbol{r})W^*_{b_2,x_2}(\boldsymbol{r})W_{b_3,x_3}(\boldsymbol{r})W_{b_4,x_4}(\boldsymbol{r}) \\
&\quad \times a^\dagger_{b_1,x_1,\sigma}a^\dagger_{b_2,x_2,\tau}a_{b_3,x_3,\tau}a_{b_4,x_4,\tau} \\
&\quad +\frac{c_1}{2}\sum_{b_1,b_2,b_3,b_4}\sum_{x_1,x_2,x_3,x_4}\sum_{\sigma_1,\sigma_2,\tau_1,\tau_2}\sum_{\alpha}\int d\boldsymbol{r} W^*_{b_1,x_1}(\boldsymbol{r})W^*_{b_2,x_2}(\boldsymbol{r})W_{b_3,x_3}(\boldsymbol{r})W_{b_4,x_4}(\boldsymbol{r}) \\
&\quad \times S^{(\alpha)}_{\sigma_1,\tau_1}S^{(\alpha)}_{\sigma_2,\tau_2}a^\dagger_{b_1,x_1,\sigma_1}a^\dagger_{b_2,x_2,\sigma_2}a_{b_3,x_3,\tau_1}a_{b_4,x_4,\tau_2}. \qquad (3.96)
\end{aligned}
$$

■

By imposing exactly the same assumptions as in the scalar case, we obtain the spin-1 Bose-Hubbard model

$$
\begin{aligned}
H &= -\sum_{\substack{x,y\\ \text{neighboring}}}\sum_{\sigma}t_{x,y}a^\dagger_{x,\sigma}a_{y,\sigma}+\sum_x V_x\hat{n}_x+\sum_x\sum_\sigma(-p\sigma+q\sigma^2)\hat{n}_{x,\sigma} \\
&\quad +\frac{U_0}{2}\sum_x\hat{n}_x(\hat{n}_x-1)+\frac{U_2}{2}\sum_x\left(\boldsymbol{S}_x^2-2\hat{n}_x\right), \qquad (3.97)
\end{aligned}
$$

where

$$
\begin{aligned}
a_{x,\sigma} &:= a_{0,x,\sigma}=\int d\boldsymbol{r} W^*_{0,x}(\boldsymbol{r})\hat{\psi}(\boldsymbol{r},\sigma), && (3.98)\\
t_{x,y} &:= t^{0,0}_{x,y}=-\int d\boldsymbol{r} W^*_0(\boldsymbol{r}-\boldsymbol{r}_x)\left[-\frac{\hbar^2}{2M}\nabla^2+U_L(\boldsymbol{r})\right]W_0(\boldsymbol{r}-\boldsymbol{r}_y), && (3.99)\\
V_x &:= U_T(\boldsymbol{r}_x), && (3.100)\\
\hat{n}_{x,\sigma} &:= a^\dagger_{x,\sigma}a_{x,\sigma},\quad \hat{n}_x:=\sum_\sigma\hat{n}_{x,\sigma}, && (3.101)\\
U_0 &:= c_0\int d\boldsymbol{r}|W_0(\boldsymbol{r})|^4,\quad U_2:=c_1\int d\boldsymbol{r}|W_0(\boldsymbol{r})|^4, && (3.102)\\
S^{(\alpha)}_x &:= \sum_{\sigma,\tau}S^{(\alpha)}_{\sigma,\tau}a^\dagger_{x,\sigma}a_{x,\tau} && (3.103)
\end{aligned}
$$

(∵)

It is easy to confirm the result for terms except for the last term. Here we look at the last term. After the approximation, which is almost the same as the scalar

case, it becomes

$$\frac{1}{2}c_1 \int d\boldsymbol{r}|W_0(\boldsymbol{r})|^4 \sum_x \sum_{\alpha=1}^{3} \sum_{\sigma_1,\sigma_2,\tau_1,\tau_2} S^{(\alpha)}_{\sigma_1,\tau_1} S^{(\alpha)}_{\sigma_2,\tau_2} a^\dagger_{x,\sigma_1} a^\dagger_{x,\sigma_2} a_{x,\tau_1} a_{x,\tau_2} \tag{3.104}$$

The result follows from the fact that

$$\begin{aligned}
&\sum_{\alpha=1}^{3} \sum_{\sigma_1,\sigma_2,\tau_1,\tau_2} S^{(\alpha)}_{\sigma_1,\tau_1} S^{(\alpha)}_{\sigma_2,\tau_2} a^\dagger_{x,\sigma_1} a^\dagger_{x,\sigma_2} a_{x,\tau_1} a_{x,\tau_2} && (3.105)\\
=\ &\sum_{\alpha=1}^{3} \sum_{\sigma_1,\sigma_2,\tau_1,\tau_2} S^{(\alpha)}_{\sigma_1,\tau_1} S^{(\alpha)}_{\sigma_2,\tau_2} a^\dagger_{x,\sigma_1} \left(a_{x,\tau_1} a^\dagger_{x,\sigma_2} - \delta_{\tau_1,\sigma_2}\right) a_{x,\tau_2} && (3.106)\\
=\ &\sum_{\alpha=1}^{3} \left(S^{(\alpha)}_x\right)^2 - \sum_{\alpha=1}^{3} \sum_{\sigma,\tau,\rho} S^{(\alpha)}_{\sigma,\rho} S^{(\alpha)}_{\rho,\tau} a^\dagger_{x,\sigma} a_{x,\tau} && (3.107)\\
=\ &\boldsymbol{S}^2_x - 2\hat{n}_x, && (3.108)
\end{aligned}$$

where we used $\sum_{\alpha=1}^{3} \sum_\rho S^{(\alpha)}_{\sigma,\rho} S^{(\alpha)}_{\rho,\tau} = 2\delta_{\sigma,\tau}$.

■

Hereafter, we assume that the hopping amplitude $t_{x,y}$ for two neighboring sites does not depend on $x$ and $y$, and denote it by $t$. Also, in this chapter, we consider the case of $V_x = 0$ ($\forall x \in \Lambda$) and $p = q = 0$.

### 3.3.2 Ground states for the $t = 0$ case

First, we consider the $t = 0$ case to capture qualitative features of the ground state [28]. Because the Hamiltonian is now reduced to the sum of a local Hamiltonian at each site, we can consider the single-site grand Hamiltonian

$$K_{\rm ss} = \frac{U_0}{2}\hat{n}(\hat{n}-1) + \frac{U_2}{2}(\boldsymbol{S}^2 - 2\hat{n}) - \mu\hat{n}, \tag{3.109}$$

where we drop subscripts for lattice sites. From the fact that the grand Hamiltonian commutes with $\hat{n}$ and $\boldsymbol{S}$, we can diagonalize it using the simultaneous eigenstates of $\hat{n}, \boldsymbol{S}^2, S^{(3)}$, whose eigenvalues are $n, S(S+1), M$, respectively, where [24]

- for even $n$, $S$ can be $S = 0, 2, 4, \ldots, n$, and for each $S$, $M$ can be $M = -S, -S+1, \ldots, S$, and
- for odd $n$, $S$ can be $S = 1, 3, 5, \ldots, n$, and for each $S$, $M$ can be $M = -S, -S+1, \ldots, S$

For the state specified by $n, S, M$, the corresponding eigenvalue of the grand Hamiltonian can be written as

$$K(n,S) = \frac{U_0}{2}n(n-1) + \frac{U_2}{2}\left[S(S+1) - 2n\right] - \mu n. \tag{3.110}$$

Using this expression, we calculate ground states as follows.

**Ferromagnetic case**

For the ferromagnetic interaction ($U_2 < 0$), $K(n, S)$ can be minimized with respect to $S$ by taking $S = n$, which means that the ground state maximizes the magnitude of spin. The state with the particle number density $n$ attains the minimum only if

$$K(n+1, n+1) > K(n, n), \quad K(n-1, n-1) > K(n, n), \tag{3.111}$$

which is equivalent to

$$(n-1)(U_0 + U_2) < \mu < n(U_0 + U_2). \tag{3.112}$$

Note that $U_0 + U_2 > 0$ holds from the assumption of positive $a_0, a_2$ (see subsection 2.2.3).

**Antiferromagnetic case**

For the antiferromagnetic interaction ($U_2 > 0$), the value of $S$ which minimizes $K(n, S)$ depends on whether $n$ is even or odd. If $n$ is even, $S = 0$ is the minimizer, which means that the ground state forms a spin-singlet. On the other hand, if $n$ is odd, $S = 1$ is the minimizer.

The state with $n$ being odd and $S = 1$ is a ground state only if

$$K(n+1, 0) > K(n, 1), \quad K(n-1, 0) > K(n, 1), \tag{3.113}$$

which is equivalent to

$$(n-1)U_0 < \mu < nU_0 - 2U_2. \tag{3.114}$$

Note that $2U_2 < U_0$ holds from the assumption of positive $a_0, a_2$.

The state with $n$ being even and $S = 0$ is a ground state only if

$$K(n+1, 1) > K(n, 0), \quad K(n-1, 1) > K(n, 0), \tag{3.115}$$

which is equivalent to

$$(n-1)U_0 - 2U_2 < \mu < nU_0. \tag{3.116}$$

Figure 3.3 summarizes these results. Note that for the antiferromagnetic interaction, the odd Mott lobes shrink as $U_2/U_0$ is increased, and finally disappear in the limit of $U_2/U_0 \to 1/2$.

### 3.3.3 Superfluid to Mott-insulator phase transitions

Similarly to the scalar case, the spin-1 Bose Hubbard model also exhibits superfluid to Mott-insulator transitions when the hopping amplitude $t$ is changed. However, we will see that the nature of the phase transition is greatly affected by the presence, especially the sign, of the spin-dependent interaction.

**Ferromagnetic case**

For the ferromagnetic interaction, the superfluid to Mott-insulator phase transition is known to be quite similar to the scalar case; the phase diagram resembles that of the scalar case except for the value of the chemical potential, and the phase transition is also continuous. Figure 3.4 shows the phase diagrams obtained by the Gutzwiller variational

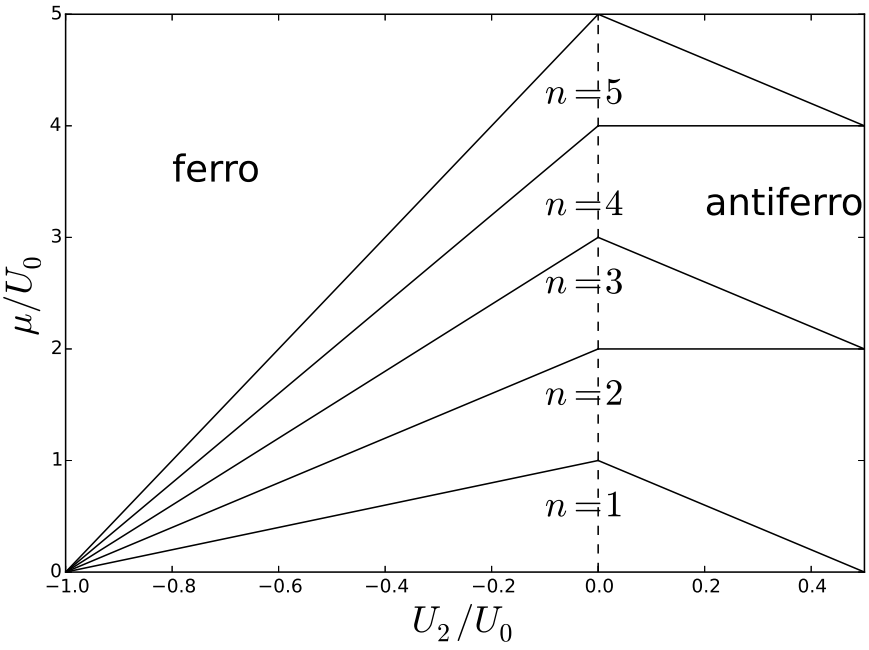


Figure 3.3: Phase diagram of spin-1 Bose-Hubbard model at the atomic limit ($t = 0$). Solid lines denote phase boundaries, while the dashed line denotes the boundary between the antiferromagnetic case and the ferromagnetic case. For the ferromagnetic interaction, the ground state exhibits ferromagnetism with $S = n$, while for the antiferromagnetic interaction, the ground state has spin $S = 0$ (even $n$) or $S = 1$ (odd $n$). It can be seen that, for the antiferromagnetic interaction, the odd $n$ region shrinks as $U_2/U_0$ is increased.

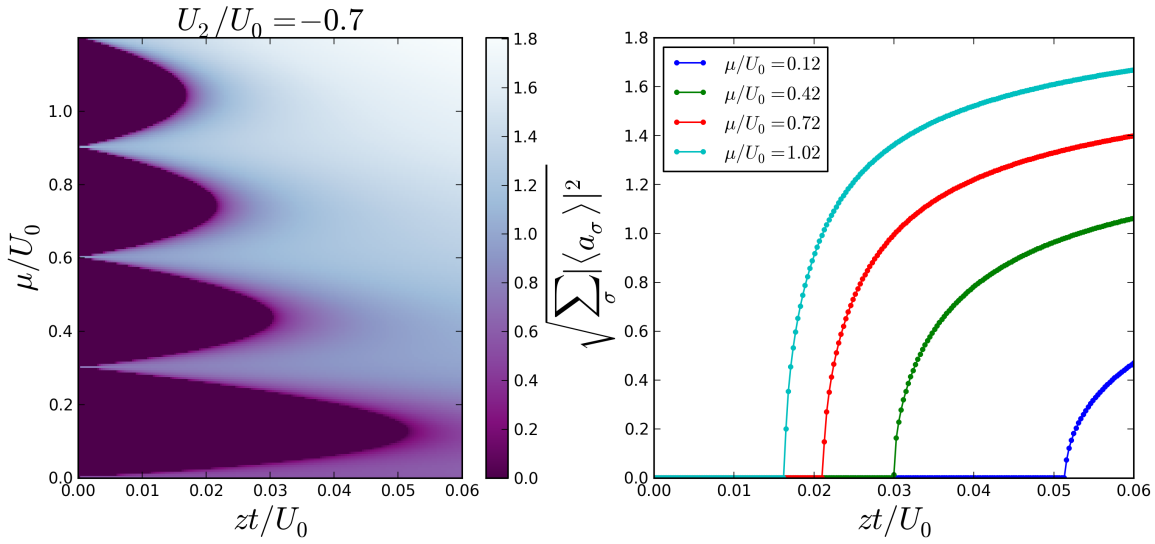


Figure 3.4: Ground-state phase diagrams of the ferromagnetic spin-1 Bose-Hubbard model, where $U_2/U_0 = -0.7$. Left: The $t-\mu$ phase diagram. Right: The $t$ dependence of the superfluid order parameter. In each panel, plotted as the superfluid order parameter is $\sqrt{\sum_\sigma \langle a_\sigma \rangle^2}$. The $t-\mu$ phase diagram resembles that of the scalar Bose-Hubbard model, and the phase transitions are continuous.

ansatz [12], and a quantum Monte Carlo study of a two-dimensional system has shown the same behavior (see figures 1 and 7 in [41] ). Also, it has rigorously been shown that the ground state exhibits ferromagnetism [42].

**Antiferromagnetic case**

For the antiferromagnetic interaction, the phase diagram changes drastically from the scalar case. First, as can be anticipated from figure 3.3, odd Mott lobes shrink compared with even Mott lobes. For even lobes, bosons form spin-singlets with $S = 0$, and for odd lobes, $S = 1$. Moreover, it is known from various calculations [27, 41] that the phase transition between an even Mott lobe and the superfluid phase is discontinuous for small values of $U_2/U_0$, while the transition between an odd Mott lobe and the superfluid phase is continuous. Figure 3.5 shows the phase diagrams obtained by the Gutzwiller variational ansatz [13].

[12] Precisely speaking, it is obtained by the decoupling approximation, which is equivalent to the Gutzwiller variational ansatz. The equivalence will be shown in section 4.4.

[13] See the previous footnote.

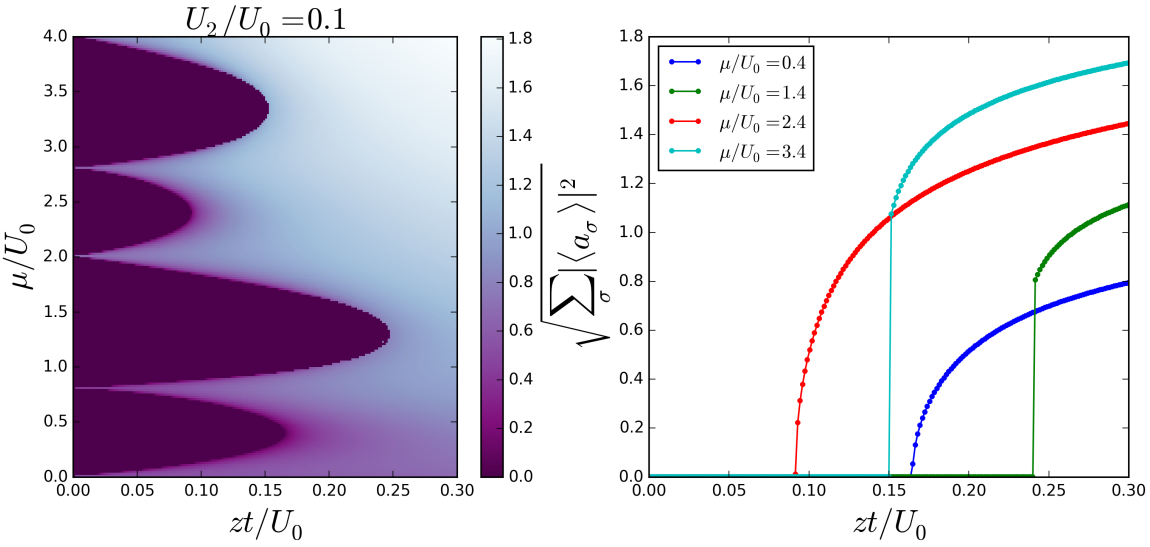


Figure 3.5: Ground-state phase diagrams of the antiferromagnetic spin-1 Bose-Hubbard model, where $U_2/U_0 = 0.1$. Left: The $t-\mu$ phase diagram, where odd Mott shrink compared with even lobes. Right: The $t$ dependence of the superfluid order parameter. In each panel, plotted as the superfluid order parameter is $\sqrt{\sum_\sigma \langle a_\sigma \rangle^2}$. It can be seen that the quantum phase transition between odd Mott lobes and the superfluid phase can be discontinuous.

# Chapter 4

# The model and analyses

In this chapter, we present the model, and discuss in detail the methods that we utilize for analyzing the model.

- In section 4.1, we present the model we analyze, and establish the notation. As discussed in the previous chapter, we are interested in the competition between the ferromagnetic interaction and a positive quadratic Zeeman effect, and we introduce such terms in the model.

- In section 4.2, we discuss an approximation method called the Gutzwiller variational ansatz, whose idea is to restrict our variational states (wave functions or density matrices) to products of local states.

  Although the method is conceptually straightforward, implementing this method directly for spinor systems is numerically inefficient. To cope with this problem, we instead use an equivalent and numerically low-cost [1] method, which will be described in the next section [2].

- In section 4.3, we describe an approximation method called the decoupling approximation, [3] in which we decouple hopping terms between different sites. The method will be shown to be equivalent to the Gutzwiller variational ansatz in the next section.

- In section 4.4, we show the equivalence between the Gutzwiller variational ansatz and the decoupling approximation. Based on this result, we employ the decoupling approximation as our method to analyze the model.

- In section 4.5, we turn to the problem of numerical implementation of the decoupling approximation, including the basic algorithms we use, concrete expressions for the matrix elements of the grand Hamiltonian, and some numerical tricks.

[1] This point will be discussed in subsection 4.5.1.

[2] The reason why a section on the Gutzwiller variational ansatz, which we do not use directly later, is included is that it is more conceptually transparent compared with the decoupling approximation described in the subsequent section. Based on the equivalence discussion in section 4.4, we use the decoupling approximation to do our calculations. Those who are not interested in the Gutzwiller variational ansatz can skip this section and section 4.4 altogether.

[3] Some authors use phrases with the word "Gutzwiller" to mean the decoupling approximation [43, 44]. However, here we use the word "Gutzwiller" only for the Gutzwiller variational ansataz, for clearly distinguishing the two methods.

## 4.1 The model

### 4.1.1 Setting

**Basic settings**

- Let $\Lambda$ be a finite lattice, on which we load our bosons, and let $|\Lambda|$ be the number of lattice sites.
- Define $\mathcal{B} \subset \Lambda \times \Lambda$ to be the set of all bonds **with order**, i.e., for different sites $x$ and $y$ ($x, y \in \Lambda$, $x \neq y$) we distinguish $(x, y)$ from $(y, x)$. We assume that bonds are symmetric, i.e., $(x, y) \in \mathcal{B}$ implies $(y, x) \in \mathcal{B}$.
- By $\mathcal{N}_x := \{y \in \Lambda | (x, y) \in \mathcal{B}\}$, we denote the neighborhood of a site $x \in \Lambda$, and by $z_x := |\mathcal{N}_x|$, we denote the number of sites neighboring the site $x$.
- We consider bosons with spin 1. Thus, for a given quantization axis, we denote the set of magnetic quantum numbers by $\mathcal{S} := \{-1, 0, 1\}$.

**Observables**

- We define the boson annihilation and creation operators by $a_{x,\sigma}$ and $a^\dagger_{x,\sigma}$, where $x \in \Lambda, \sigma \in \mathcal{S}$.
- Particle-number operators are denoted by

$$\hat{n}_{x,\sigma} := a^\dagger_{x,\sigma} a_{x,\sigma} \quad (x \in \Lambda, \sigma \in \mathcal{S}), \tag{4.1}$$

$$\hat{n}_x := \sum_{\sigma \in \mathcal{S}} \hat{n}_{x,\sigma} \quad (x \in \Lambda), \tag{4.2}$$

  where $\hat{n}_{x,\sigma}$ means the number of particles with magnetic quantum number $\sigma$ at site $x$, and $\hat{n}_x$ means the number of particles (regardless of their magnetic quantum number) at site $x$.
- We denote the spin operators by

$$\boldsymbol{S}_x := \left(S^{(1)}_x, S^{(2)}_x, S^{(3)}_x\right), \tag{4.3}$$

$$S^{(\alpha)}_x := \sum_{\sigma,\tau \in \mathcal{S}} S^{(\alpha)}_{\sigma,\tau} a^\dagger_{x,\sigma} a_{x,\tau} \quad (x \in \Lambda, \alpha \in \{1, 2, 3\}), \tag{4.4}$$

$$S^{\pm}_x := S^{(1)}_x \pm i S^{(2)}_x \quad (x \in \Lambda), \tag{4.5}$$

  where $S^{(\alpha)}_x$ means the operator of the $\alpha$ component of the spin at a site $x$. Spin matrices $S^{(\alpha)}$ ($\alpha \in \{1, 2, 3\}$) are defined by

$$S^{(1)} := \frac{1}{\sqrt{2}} \begin{pmatrix} 0 & 1 & 0 \\ 1 & 0 & 1 \\ 0 & 1 & 0 \end{pmatrix}, \quad S^{(2)} := \frac{i}{\sqrt{2}} \begin{pmatrix} 0 & -1 & 0 \\ 1 & 0 & -1 \\ 0 & 1 & 0 \end{pmatrix}, \quad S^{(3)} := \begin{pmatrix} 1 & 0 & 0 \\ 0 & 0 & 0 \\ 0 & 0 & -1 \end{pmatrix}, \tag{4.6}$$

where it is understood that matrix indices are in the order of $1, 0, -1$ [4], and $\alpha = 3$ corresponds to the direction of the given quantization axis. For the total spin, we define

$$\boldsymbol{S}_{\mathrm{tot}} := \left(S^{(1)}_{\mathrm{tot}}, S^{(2)}_{\mathrm{tot}}, S^{(3)}_{\mathrm{tot}}\right), \quad S^{(\alpha)}_{\mathrm{tot}} := \sum_{x\in\Lambda} S^{(\alpha)}_x \ (\alpha \in \{1,2,3\}), \quad S^{\pm}_{\mathrm{tot}} := \sum_{x\in\Lambda} S^{\pm}_x = S^{(1)}_{\mathrm{tot}} \pm i S^{(2)}_{\mathrm{tot}}. \tag{4.7}$$

**States**

- We define sets of particle configurations by

$$\mathcal{I} := \{\boldsymbol{n} = (n_{x,\sigma})_{x\in\Lambda,\sigma\in\mathcal{S}} \mid \forall x \in \Lambda,\ \forall \sigma \in \mathcal{S}\ (n_{x,\sigma} \geq 0)\}, \tag{4.8}$$

$$\mathcal{I}_N := \left\{ \boldsymbol{n} \in \mathcal{I} \;\middle|\; \sum_{x\in\Lambda,\sigma\in\mathcal{S}} n_{x,\sigma} = N \right\}, \tag{4.9}$$

  where $\mathcal{I}$ is the set of all configurations, and $\mathcal{I}_N$ is the set of all configurations whose total particle number are $N$.

- For a configuration $\boldsymbol{n} \in \mathcal{I}$, we define $n_x := \sum_{\sigma\in\mathcal{S}} n_{x,\sigma}$, $\boldsymbol{n}_x := (n_{x,1}, n_{x,0}, n_{x,-1})$, which refer to the local configuration at site $x$.

- For $x \in \Lambda, \sigma \in \mathcal{S}$, we define $\boldsymbol{e}_{x,\sigma} \in \mathcal{I}$ by $(\boldsymbol{e}_{x,\sigma})_{y,\tau} = \delta_{x,y}\delta_{\sigma,\tau}$, and for $\sigma \in \mathcal{S}$, we define $\boldsymbol{e}_\sigma$ by $(\boldsymbol{e}_\sigma)_\tau = \delta_{\sigma,\tau}$. In other words, they are "unit vectors" in configuration space.

- $\Phi_{\mathrm{vac}}$ denotes the vacuum state.

- We define our orthonormal basis composed of Fock states by

$$\Phi_{\boldsymbol{n}} := \prod_{\substack{x\in\Lambda \\ \sigma\in\mathcal{S}}} \frac{1}{\sqrt{n_{x,\sigma}!}} \left(a^\dagger_{x,\sigma}\right)^{n_{x,\sigma}} \Phi_{\mathrm{vac}}. \tag{4.10}$$

- We define our Hilbert space by

$$\mathcal{H}_N := \mathrm{Span}\{\Phi_{\boldsymbol{n}} \mid \boldsymbol{n} \in \mathcal{I}_N\} \tag{4.11}$$

$$\mathcal{H} := \bigoplus_{N=1}^{\infty} \mathcal{H}_N \tag{4.12}$$

### 4.1.2 The grand Hamiltonian

We work in the grand canonical ensemble with chemical potential $\mu$, and consider the following grand Hamiltonian $\hat{K}$

$$\hat{K} = -t \sum_{\substack{(x,y)\in\mathcal{B} \\ \sigma\in\mathcal{S}}} a^\dagger_{x,\sigma} a_{y,\sigma} + \frac{U_0}{2} \sum_{x\in\Lambda} \hat{n}_x(\hat{n}_x - 1) + \frac{U_2}{2} \sum_{x\in\Lambda} \left(\boldsymbol{S}^2_x - 2\hat{n}_x\right) + \sum_{x\in\Lambda}\sum_{\sigma\in\mathcal{S}} (-p\sigma + q\sigma^2)\hat{n}_{x,\sigma} - \mu \sum_{x\in\Lambda} \hat{n}_x. \tag{4.13}$$

The meanings and the properties of terms and coefficients are as follows:

[4] For example, $S^{(3)}_{\sigma,\tau}$ can be written as $S^{(3)}_{\sigma,\tau} = \sigma\delta_{\sigma,\tau}$.

- The first term $-t\sum_{\substack{(x,y)\in\mathcal{B}\\ \sigma\in\mathcal{S}}} a^\dagger_{x,\sigma}a_{y,\sigma}$ represents the hopping between different sites, and we call $t$ the hopping amplitude, or simply the hopping. We assume that $t > 0$.

- The second term $\frac{U_0}{2}\sum_{x\in\Lambda}\hat{n}_x(\hat{n}_x-1)$ means the spin-independent interaction, where the coefficient $U_0$ is defined by $U_0 = \frac{g_0+2g_2}{3}\int d\boldsymbol{r}|W_0(\boldsymbol{r})|^4$, and satisfies $U_0 > 0$ because we assume $g_0, g_2 > 0$ [5].

- The third term $\frac{U_2}{2}\sum_{x\in\Lambda}\left(\boldsymbol{S}_x^2 - 2\hat{n}_x\right)$ stands for the spin-dependent interaction. The nature of the interaction crucially depends on the sign of the coefficient $U_2$:

  - If $U_2 < 0$, it is energetically favorable to make the spin at each site larger, and the interaction is called the ferromagnetic interaction;
  - if $U_2 > 0$, it is energetically favorable to make the spin at each site smaller, and the interaction is called the antiferromagnetic interaction.

  Note that the ratio

  $$\frac{U_2}{U_0} = \frac{g_2-g_0}{g_0+2g_2} = \frac{\frac{g_2}{g_0}-1}{2\frac{g_2}{g_0}+1} = \frac{1}{2} - \frac{3}{2}\frac{1}{2\frac{g_2}{g_0}+1}, \tag{4.14}$$

  satisfies $U_2/U_0 \in (-1, \frac{1}{2})$ because $g_2/g_0 \in (0,\infty)$. In our analysis, we assume $U_2 < 0$.

- The fourth term $\sum_{x\in\Lambda}\sum_{\sigma\in\mathcal{S}}(-p\sigma+q\sigma^2)\hat{n}_{x,\sigma}$ represents the Zeeman energy induced by the external magnetic field. Here, we assume that we take the quantization axis in the direction of an applied external magnetic field.

  - The first term with the coefficient $p\in\mathbb{R}$ represents the linear Zeeman energy, and
  - the second term with the coefficient $q\in\mathbb{R}$ represents the quadratic Zeeman energy.

  In our setting, where the total magnetization along the axis of the applied magnetic field is conserved, the linear Zeeman energy can be gauged out. Thus, in our actual calculations, we set $p = 0$. Also, we assume $q > 0$.

Note that $t > 0$ and $U_0 > 0$ causes the competition between the kinetic energy and the repulsive interaction, and the assumption of $U_2 < 0$ and $q > 0$ ensures the competition between the ferromagnetic spin-dependent interaction and the positive quadratic Zeeman energy.

Later, we sometimes decompose the grand Hamiltonian into two parts: the hopping part and the local part which are defined by

$$\hat{K} = H_{\mathrm{hop}} + \sum_{x\in\Lambda} K_{\mathrm{loc},x}, \tag{4.15}$$

$$H_{\mathrm{hop}} := -t\sum_{\substack{(x,y)\in\mathcal{B}\\ \sigma\in\mathcal{S}}} a^\dagger_{x,\sigma}a_{y,\sigma}, \tag{4.16}$$

$$K_{\mathrm{loc},x} := \frac{U_0}{2}\hat{n}_x(\hat{n}_x-1) + \frac{U_2}{2}\left(\boldsymbol{S}_x^2 - 2\hat{n}_x\right) + \sum_{\sigma\in\mathcal{S}}(-p\sigma+q\sigma^2)\hat{n}_{x,\sigma} - \mu\hat{n}_x. \tag{4.17}$$

[5] $W_0$ is the Wannier function for the lowest band, and for the definitions of $g_0$ and $g_2$, see subsection 2.2.3.

## 4.2 The Gutzwiller variational ansatz

As a way to analyze the grand Hamiltonian presented in the last section, here we describe an approximation method called the "Gutzwiller variational ansatz" [37, 38]. The idea of this approximation is that we restrict our variational states (density matrices, for non-zero temperature cases) to products of local states. The rationale behind this restriction is that in both non-interacting and no-hopping limits, we can describe the corresponding ground states by this form of wave function

Although the method, being a variational method, is conceptually transparent, we have an equivalent and numerically efficient [6] approximation method, which will be described in the next section and will be used later.

### 4.2.1 The ground state

Gutzwiller variational ansatz for the ground state

To approximate the ground state, we use the following variational wave function $\Psi_{c,\Lambda}$

$$\Psi_{c,\Lambda} = \bigotimes_{x\in\Lambda} \sum_{\substack{n_{x,1},n_{x,0},n_{x,-1}\geq 0 \\ n_{x,1}+n_{x,0}+n_{x,-1}\leq n_{\max}}} c(\boldsymbol{n}_x)\Phi^{(x)}_{\boldsymbol{n}_x}, \tag{4.18}$$

where

- the states

$$\Phi^{(x)}_{\boldsymbol{n}_x} := \prod_{\sigma\in\mathcal{S}} \frac{1}{\sqrt{n_{x,\sigma}!}} \left(a^\dagger_{x,\sigma}\right)^{n_{x,\sigma}} \Phi^{(x)}_{\mathrm{vac}} \tag{4.19}$$

  are local Fock states, and $\Phi^{(x)}_{\mathrm{vac}}$ stands for the vacuum state of the Hilbert space of a single site $x$.

- Although the particle number can be infinite in principle, for simplicity we assume that the particle number at each site is not larger than a prescribed value $n_{\max}$.

Here, the function $c$ is the variational degree of freedom, and we search for such $c$ that minimizes the expectation value of $\hat{K}$

$$\left\langle \Psi_{c,\Lambda},\ \hat{K}\Psi_{c,\Lambda} \right\rangle \tag{4.20}$$

In short, as a variational wave function, we take the product of an identical local state, and we change this local state to attain the minimum of the variational energy [a] .

[a] Although we concentrate on spatially uniform cases, the Gutzwiller variational ansatz can be extended to non-uniform cases, where each local state is site-dependent, i.e., $c$ in the variational state (4.18) is replaced by site-dependent functions $c_x$, as was done in [11] for calculating spatial profile of the ground state of the scalar Bose-Hubbard model in a harmonic trap.

As was already stated, this form of the wave function can describe the ground states for both the non-interacting limit and the no-hopping (i.e., strong interaction) limit. For the no-

[6] This point will be discussed in subsection 4.5.1.

hopping limit, this is trivial. For the non-interacting limit, note that the exact ground-state wave function can be approximated by the product of local coherent states [7], which is of the above form.

### 4.2.2 Non-zero temperature

Before discussing the non-zero temperature version of the Gutzwiller variational ansatz, first note the following fact:

Variational principle for density matrices

For a Hermitian matrix $A$, define

$$f_A(X) := \mathrm{Tr}(XA) + \mathrm{Tr}(X \log X), \tag{4.21}$$

where the domain of $f$ is defined to be

$$\{X : \text{ matrices with the same shape as } A \mid X : \text{positive semidefinite}, \quad \mathrm{Tr}X = 1\}, \tag{4.22}$$

i.e., the set of all density matrices.
Then, it is known [45] that

$$X_A := \frac{e^{-A}}{\mathrm{Tr}e^{-A}} \tag{4.23}$$

is the unique minimizer of the function $f_A$, and

$$f_A(X_A) = -\mathrm{Tr}e^{-A} \tag{4.24}$$

If we set $A$ to be $\beta\times$ (grand) Hamiltonian, the minimizer is the (grand) canonical ensemble, and the minimum $\times\frac{1}{\beta}$ corresponds to the free energy.

Gutzwiller variational ansatz for non-zero temperature

To approximate the equilibrium state, we use the following type of variational density matrices:

$$\rho_{\mathrm{tot}} = \bigotimes_{x\in\Lambda} \rho \tag{4.25}$$

where $\rho$ is a density matrix of the one-site system.
We choose $\rho$ which minimizes the function

$$J_{\hat{K}}(\rho_{\mathrm{tot}}) := \frac{1}{\beta} f_{\beta\hat{K}}(\rho_{\mathrm{tot}}) = \mathrm{Tr}(\rho_{\mathrm{tot}}\hat{K}) + \frac{1}{\beta}\mathrm{Tr}(\rho_{\mathrm{tot}} \log \rho_{\mathrm{tot}}) \tag{4.26}$$

[7] For an arbitrary few-body observable (i.e., observables which can be written as a product of $l$ annihilation/creation operators, where $l \in \mathbb{N}$ is much smaller than the total particle number, or linear combination of them ), the expectation values with respect to this state and the exact ground state coincide in the thermodynamic limit, provided that we take $\phi$, the coherent state eigenvalue, to be the square root of the particle number density.

## 4.3 The decoupling approximation

In this section, we describe an approximation method called the decoupling approximation [46, 47], in which we decouple the hopping term between different sites. As it will be clear in the next section, the method is equivalent to the Gutzwiller variational ansatz, but the decoupling approximation is much more numerically efficient [8].

### 4.3.1 The decoupling procedure

In the decoupling approximation, we approximate the hopping term as follows :

$$\begin{aligned} a^\dagger_{x,\sigma}a_{y,\sigma} &= \left[\ \phi^*_{x,\sigma} + \left(a^\dagger_{x,\sigma} - \phi^*_{x,\sigma}\right)\right]\left[\phi_{y,\sigma} + (a_{y,\sigma} - \phi_{y,\sigma})\right] && (4.27)\\ &= \phi^*_{x,\sigma}\phi_{y,\sigma} + \phi^*_{x,\sigma}\left(a_{y,\sigma} - \phi_{y,\sigma}\right) + \phi_{y,\sigma}\left(a^\dagger_{x,\sigma} - \phi^*_{x,\sigma}\right) \\ &\quad + \left(a_{y,\sigma} - \phi_{y,\sigma}\right)\left(a^\dagger_{x,\sigma} - \phi^*_{x,\sigma}\right) && (4.28)\\ &\simeq \phi^*_{x,\sigma}\phi_{y,\sigma} + \phi^*_{x,\sigma}\left(a_{y,\sigma} - \phi_{y,\sigma}\right) + \phi_{y,\sigma}\left(a^\dagger_{x,\sigma} - \phi^*_{x,\sigma}\right) && (4.29)\\ &= \phi_{y,\sigma}a^\dagger_{x,\sigma} + \phi^*_{x,\sigma}a_{y,\sigma} - \phi^*_{x,\sigma}\phi_{y,\sigma} && (4.30)\end{aligned}$$

where $\phi_{x,\sigma}$, called "superfluid order parameters", or the expectation value of $a_{x,\sigma}$, will be determined self-consistently later. In deriving the third line, we have neglected the last term in the second line by assuming that the fluctuation represented by the term is small.

Because we consider uniform systems only, we assume that the superfluid order parameters $\phi_{x,\sigma}$ do not depend on the position $x$:

$$\phi_{x,\sigma} = \phi_\sigma \tag{4.31}$$

Also, we assume that $z_x$ does not depend on the site $x$ [9] and write $z$. Then, we have

$$\begin{aligned} \sum_{(x,y)\in\mathcal{B}} a^\dagger_{x,\sigma}a_{y,\sigma} &\simeq \sum_{(x,y)\in\mathcal{B}}\left(\phi_\sigma a^\dagger_{x,\sigma} + \phi^*_\sigma a_{y,\sigma} - |\phi_\sigma|^2\right) && (4.32)\\ &= z\phi_\sigma\sum_{x\in\Lambda}a^\dagger_{x,\sigma} + z\phi^*_\sigma\sum_{y\in\Lambda}a_{y,\sigma} - z|\Lambda||\phi_\sigma|^2 && (4.33)\\ &= z\sum_{x\in\Lambda}\left(\phi_\sigma a^\dagger_{x,\sigma} + \phi^*_\sigma a_{x,\sigma} - |\phi_\sigma|^2\right) && (4.34)\end{aligned}$$

and

$$\begin{aligned} K \simeq \sum_{x\in\Lambda} &\left[-zt\sum_{\sigma\in\mathcal{S}}\left(\phi_\sigma a^\dagger_{x,\sigma} + \phi^*_\sigma a_{x,\sigma} - |\phi_\sigma|^2\right) + \frac{U_0}{2}\hat{n}_x(\hat{n}_x - 1) + \frac{U_2}{2}\left(\boldsymbol{S}^2_x - 2\hat{n}_x\right)\right. && (4.35)\\ &\left. + \sum_{\sigma\in\mathcal{S}}(-p\sigma + q\sigma^2)\hat{n}_{x,\sigma} - \mu\hat{n}_x\right]. && (4.36)\end{aligned}$$

Thus, the problem reduces to the single-site problem with the grand Hamiltonian $\hat{K}_{\rm dc}(\boldsymbol{\phi})$ given by

[8] For detail, see subsection 4.5.1.

[9] This assumption holds for different types of lattices including the $d$-dimensional cubic lattice and the triangular lattice

The decoupled grand Hamiltonian

$$\begin{aligned}\hat{K}_{\mathrm{dc}}(\boldsymbol{\phi}) &:= -zt\sum_{\sigma\in\mathcal{S}}\left(\phi_\sigma a_\sigma^\dagger + \phi_\sigma^* a_\sigma - |\phi_\sigma|^2\right) + \frac{U_0}{2}\hat{n}(\hat{n}-1) + \frac{U_2}{2}\left(\boldsymbol{S}^2 - 2\hat{n}\right) \\ &\quad + \sum_{\sigma\in\mathcal{S}}(-p\sigma + q\sigma^2)\hat{n}_\sigma - \mu\hat{n}, \end{aligned} \tag{4.37}$$

where $\boldsymbol{\phi}$ collectively represents $\phi_1, \phi_0, \phi_{-1}$, and we omit the index $x$ which represents sites.

**The ground state**

The approximate ground state under the decoupling approximation is obtained self-consistently as follows:

The approximate ground state

Choose a set of superfluid order parameters $\boldsymbol{\phi}$ such that the ground state of $\hat{K}_{\mathrm{dc}}(\boldsymbol{\phi})$, $\psi_{\boldsymbol{\phi}}$ satisfies the self-consistent condition

$$\phi_\sigma = \langle \psi_{\boldsymbol{\phi}}, a_\sigma \psi_{\boldsymbol{\phi}} \rangle \quad (\forall \sigma \in \mathcal{S}). \tag{4.38}$$

If we have multiple $\boldsymbol{\phi}$'s that satisfy the condition (4.38), then we choose the one whose corresponding ground state $\psi_{\boldsymbol{\phi}}$ gives the smallest value of $\left\langle \psi_{\boldsymbol{\phi}}, \hat{K}_{\mathrm{dc}}(\boldsymbol{\phi})\psi_{\boldsymbol{\phi}} \right\rangle$. Then, $\Psi_{\mathrm{tot}} := \bigotimes_{x\in\Lambda} \psi_{\boldsymbol{\phi}}$ is the approximate ground state.

**Non-zero temperature**

The approximate density matrix

Choose a set of superfluid order parameters $\boldsymbol{\phi}$ such that the density matrix $\rho_{\boldsymbol{\phi}}$, defined by

$$\rho_{\boldsymbol{\phi}} := \frac{1}{\Xi_{\boldsymbol{\phi}}} e^{-\beta \hat{K}_{\mathrm{dc}}(\boldsymbol{\phi})}, \quad \Xi_{\boldsymbol{\phi}} := \mathrm{Tr} e^{-\beta \hat{K}_{\mathrm{dc}}(\boldsymbol{\phi})}, \tag{4.39}$$

satisfies the self-consistent condition

$$\phi_\sigma = \mathrm{Tr}(a_\sigma \rho_{\boldsymbol{\phi}}). \tag{4.40}$$

If we have multiple $\boldsymbol{\phi}$'s that satisfy the condition (4.40), then we choose the one which gives the smallest value of the free energy $-\frac{1}{\beta}\log \Xi_{\boldsymbol{\phi}}$. Then, $\rho_{\mathrm{tot}} := \bigotimes_{x\in\Lambda} \rho_{\boldsymbol{\phi}}$ is the approximate equilibrium state.

### 4.3.2 Rephrasing the self-consistency condition in terms of the minimum of the (free) energy functional

In the last subsection, we have given the self-consistent conditions that determine the approximate states.

Here, we show that these conditions can be rephrased in terms of the minimum condition of the (free) energy functional, which will be used later to visualize and clarify the properties of phase transitions [48, 49].

**The ground state**

The minimum condition for the energy functional

Define the energy functional $K$ by

$$K(\boldsymbol{\phi}) := \min_{\psi} \left\langle \psi, \hat{K}_{\mathrm{dc}}(\boldsymbol{\phi})\psi \right\rangle . \tag{4.41}$$

For each $\boldsymbol{\phi}$, let $\psi_{\boldsymbol{\phi}}$ be the state $\psi$ that gives the minimum of $\left\langle \psi, \hat{K}_{\mathrm{dc}}(\boldsymbol{\phi})\psi \right\rangle$, i.e.,

$$\psi_{\boldsymbol{\phi}} = \mathrm{argmin}_{\psi} \left\langle \psi, \hat{K}_{\mathrm{dc}}(\boldsymbol{\phi})\psi \right\rangle . \tag{4.42}$$

Note that $\psi_{\boldsymbol{\phi}}$ is the ground state of the decoupled grand Hamiltonian $\hat{K}_{\mathrm{dc}}(\boldsymbol{\phi})$:

$$\hat{K}_{\mathrm{dc}}(\boldsymbol{\phi})\psi_{\boldsymbol{\phi}} = K(\boldsymbol{\phi})\psi_{\boldsymbol{\phi}}. \tag{4.43}$$

Assume that $\psi_{\boldsymbol{\phi}}$ is differentiable with respect to $\boldsymbol{\phi}$. Under these assumptions, the following two are equivalent:

- $\boldsymbol{\phi}^0$ is a stationary point of $K$.
- $\psi_{\boldsymbol{\phi}^0}$ satisfies the self-consistent condition $\langle \psi_{\boldsymbol{\phi}^0}, a_\sigma \psi_{\boldsymbol{\phi}^0} \rangle = \phi^0_\sigma$ $(\forall \sigma \in \mathcal{S})$.

$(\because)$

The result follows directly from the Hellmann-Feynman theorem.
Let

$$x_\sigma := \mathrm{Re}\phi_\sigma, \quad y_\sigma := \mathrm{Im}\phi_\sigma. \tag{4.44}$$

Then,

$$\begin{aligned}
\frac{\partial K}{\partial x_\sigma}(\boldsymbol{\phi}) &= \left\langle \psi_{\boldsymbol{\phi}}, \frac{\partial \hat{K}_{\mathrm{dc}}}{\partial x_\sigma}(\boldsymbol{\phi})\psi_{\boldsymbol{\phi}} \right\rangle && (4.45)\\
&= -zt\left( \left\langle \psi_{\boldsymbol{\phi}}, a^\dagger_\sigma \psi_{\boldsymbol{\phi}} \right\rangle + \langle \psi_{\boldsymbol{\phi}}, a_\sigma \psi_{\boldsymbol{\phi}} \rangle - 2x_\sigma \right), && (4.46)\\
\frac{\partial K}{\partial y_\sigma}(\boldsymbol{\phi}) &= \left\langle \psi_{\boldsymbol{\phi}}, \frac{\partial \hat{K}_{\mathrm{dc}}}{\partial y_\sigma}(\boldsymbol{\phi})\psi_{\boldsymbol{\phi}} \right\rangle && (4.47)\\
&= -zt\left( i\left\langle \psi_{\boldsymbol{\phi}}, a^\dagger_\sigma \psi_{\boldsymbol{\phi}} \right\rangle - i\langle \psi_{\boldsymbol{\phi}}, a_\sigma \psi_{\boldsymbol{\phi}} \rangle - 2y_\sigma \right) && (4.48)
\end{aligned}$$

Thus, it follows that

$$\boldsymbol{\phi}^0 \text{ is a stationary point of } K. \tag{4.49}$$

$$\iff \quad \frac{\partial K}{\partial x_\sigma}(\boldsymbol{\phi}^0) = \frac{\partial K}{\partial y_\sigma}(\boldsymbol{\phi}^0) = 0 \quad (\forall \sigma \in \mathcal{S}) \tag{4.50}$$

$$\iff \quad \forall \sigma \in \mathcal{S} \ : \\ \left\langle \psi_{\boldsymbol{\phi}^0}, a_\sigma \psi_{\boldsymbol{\phi}^0} \right\rangle + \left\langle \psi_{\boldsymbol{\phi}^0}, a_\sigma^\dagger \psi_{\boldsymbol{\phi}^0} \right\rangle = 2x_\sigma^0 \text{ and} \\ \left\langle \psi_{\boldsymbol{\phi}^0}, a_\sigma \psi_{\boldsymbol{\phi}^0} \right\rangle - \left\langle \psi_{\boldsymbol{\phi}^0}, a_\sigma^\dagger \psi_{\boldsymbol{\phi}^0} \right\rangle = 2iy_\sigma^0 \tag{4.51}$$

$$\iff \quad \left\langle \psi_{\boldsymbol{\phi}^0}, a_\sigma \psi_{\boldsymbol{\phi}^0} \right\rangle = x_\sigma^0 + iy_\sigma^0 = \phi_\sigma^0 \tag{4.52}$$

■

Using this property, [48] and [26] analytically calculated phase boundaries between the Mott insulator phase and the superfluid phase for the scalar Bose-Hubbard model and the spin-1 antiferromagnetic Bose-Hubbard model, respectively, by evaluating $K(\boldsymbol{\phi})$ perturbatively, where the hopping term is treated as a perturbation, up to fourth order in superfluid order parameters [10].

**Non-zero temperature**

The minimum condition for the free energy functional

Define

$$J(\boldsymbol{\phi}) := -\frac{1}{\beta} \log \Xi_{\boldsymbol{\phi}}, \quad \Xi_{\boldsymbol{\phi}} := \mathrm{Tr} e^{-\beta \hat{K}_{\mathrm{dc}}(\boldsymbol{\phi})}. \tag{4.53}$$

Then, the following two statements are equivalent:

- $\boldsymbol{\phi}^0$ is a stationary point of $J$.
- $\boldsymbol{\phi}^0$ satisfies the self-consistent condition $\phi_\sigma^0 = \mathrm{Tr}(a_\sigma \rho_{\boldsymbol{\phi}^0})$.

($\because$)

Let

$$x_\sigma := \mathrm{Re}\phi_\sigma, \quad y_\sigma := \mathrm{Im}\phi_\sigma. \tag{4.54}$$

Then,

$$\frac{\partial J}{\partial x_\sigma}(\boldsymbol{\phi}) = -\frac{1}{\beta}\frac{\partial}{\partial x_\sigma} \log \Xi_{\boldsymbol{\phi}} = -\frac{1}{\beta \Xi_{\boldsymbol{\phi}}} \frac{\partial \Xi_{\boldsymbol{\phi}}}{\partial x_\sigma} \tag{4.55}$$

$$= -\frac{1}{\beta \Xi_{\boldsymbol{\phi}}} \mathrm{Tr}\left[ \frac{\partial}{\partial x_\sigma} e^{-\beta \hat{K}_{\mathrm{dc}}(\boldsymbol{\phi})} \right] = \frac{1}{\Xi_{\boldsymbol{\phi}}} \mathrm{Tr}\left[ \frac{\partial \hat{K}_{\mathrm{dc}}(\boldsymbol{\phi})}{\partial x_\sigma} e^{-\beta \hat{K}_{\mathrm{dc}}(\boldsymbol{\phi})} \right] \tag{4.56}$$

$$= \frac{1}{\Xi_{\boldsymbol{\phi}}} \mathrm{Tr}\left[ -zt(a_\sigma^\dagger + a_\sigma - 2x_\sigma) e^{-\beta \hat{K}_{\mathrm{dc}}(\boldsymbol{\phi})} \right] \tag{4.57}$$

$$= \mathrm{Tr}\left[ -zt(a_\sigma^\dagger + a_\sigma - 2x_\sigma) \rho_{\boldsymbol{\phi}} \right], \tag{4.58}$$

[10] However, the result in [26] for even Mott lobe does not coincide with the result obtained by direct minimization of the Gutzwiller variational energy, as pointed out in [27], because the sixth order terms should be considered to describe the first order phase transition within the decoupling approximation, which occurs for even Mott lobes.

$$\frac{\partial J}{\partial y_\sigma}(\boldsymbol{\phi}) = -\frac{1}{\beta}\frac{\partial}{\partial y_\sigma}\log \Xi_{\boldsymbol{\phi}} = -\frac{1}{\beta \Xi_{\boldsymbol{\phi}}}\frac{\partial \Xi_{\boldsymbol{\phi}}}{\partial y_\sigma} \tag{4.59}$$

$$= -\frac{1}{\beta \Xi_{\boldsymbol{\phi}}}\mathrm{Tr}\left[\frac{\partial}{\partial y_\sigma} e^{-\beta \hat{K}_{\mathrm{dc}}(\boldsymbol{\phi})}\right] = \frac{1}{\Xi_{\boldsymbol{\phi}}}\mathrm{Tr}\left[\frac{\partial \hat{K}_{\mathrm{dc}}(\boldsymbol{\phi})}{\partial y_\sigma} e^{-\beta \hat{K}_{\mathrm{dc}}(\boldsymbol{\phi})}\right] \tag{4.60}$$

$$= \frac{1}{\Xi_{\boldsymbol{\phi}}}\mathrm{Tr}\left[-zt(a_\sigma^\dagger + a_\sigma - 2x_\sigma) e^{-\beta \hat{K}_{\mathrm{dc}}(\boldsymbol{\phi})}\right] \tag{4.61}$$

$$= \mathrm{Tr}\left[-zt(ia_\sigma^\dagger - ia_\sigma - 2y_\sigma)\rho_{\boldsymbol{\phi}}\right]. \tag{4.62}$$

Thus, it follows that

$$\boldsymbol{\phi}^0 \text{ is a stationary point of } J. \tag{4.63}$$

$$\iff \quad \frac{\partial J}{\partial x_\sigma}(\boldsymbol{\phi}^0) = \frac{\partial J}{\partial x_\sigma}(\boldsymbol{\phi}^0) = 0 \quad (\forall \sigma \in \mathcal{S}). \tag{4.64}$$

$$\iff \quad \forall \sigma \in \mathcal{S} \ : \\ \mathrm{Tr}(a_\sigma^\dagger \rho_{\boldsymbol{\phi}^0}) + \mathrm{Tr}(a_\sigma \rho_{\boldsymbol{\phi}^0}) = 2x_\sigma^0 \text{ and} \\ -\mathrm{Tr}(a_\sigma^\dagger \rho_{\boldsymbol{\phi}^0}) + \mathrm{Tr}(a_\sigma \rho_{\boldsymbol{\phi}^0}) = 2iy_\sigma^0. \tag{4.65}$$

$$\iff \quad \mathrm{Tr}(a_\sigma \rho_{\boldsymbol{\phi}^0}) = x_\sigma^0 + iy_\sigma^0 = \phi_\sigma^0. \tag{4.66}$$

■

## 4.4 The equivalence of the Gutzwiller variational ansatz and the decoupling approximation

In this section, we show that the decoupling approximation and the Gutzwiller variational ansatz are basically equivalent.

### 4.4.1 The ground state

The equivalence for the ground-state case

We assume that at most $n_{\max}$ particles can populate each single site.

1. Let $\bigotimes_{x\in\Lambda}\psi^0$ be a state obtained by the Gutzwiller variational ansatz. Then, $\psi^0$ satisfies the self-consistent condition of the decoupling approximation, i.e., $\psi^0$ is the ground state of $\hat{K}_{\mathrm{dc}}(\boldsymbol{\phi}^0)$, where $\phi_\sigma^0 := \langle \psi^0, a_\sigma \psi^0 \rangle$.

2. For an arbitrary superfluid order parameter $\boldsymbol{\phi}$ and an arbitrary single-site state $\psi$ that satisfy $\langle \psi, a_\sigma \psi \rangle = \phi_\sigma \ \ (\forall \sigma \in \mathcal{S})$, the following equality holds:

$$\left\langle \bigotimes_{x\in\Lambda}\psi, \hat{K}\bigotimes_{x\in\Lambda}\psi \right\rangle = |\Lambda| \left\langle \psi, \hat{K}_{\mathrm{dc}}(\boldsymbol{\phi})\psi \right\rangle. \tag{4.67}$$

From these two statements, it follows that a state obtained by the Gutzwiller variational ansatz can be obtained by the decoupling approximation.

(∵)

Recall that the grand Hamiltonian can be written as

$$\hat{K} = H_{\mathrm{hop}} + \sum_{x\in\Lambda} K_{\mathrm{loc},x} \tag{4.68}$$

Let $\psi$ be an arbitrary single-site state, and $\boldsymbol{\phi}$ be an arbitrary superfluid order parameter. We rewrite $\left\langle \bigotimes_{x\in\Lambda}\psi, \hat{K}\bigotimes_{x\in\Lambda}\psi \right\rangle$ and $\langle\psi, K_{\mathrm{dc}}(\boldsymbol{\phi})\psi\rangle$, and derive an equality connecting these two quantities.

On one hand, we have

$$\left\langle \bigotimes_{x\in\Lambda}\psi, \hat{K}\bigotimes_{x\in\Lambda}\psi \right\rangle = |\Lambda|\left(-zt\sum_{\sigma\in\mathcal{S}}\left\langle a_\sigma^\dagger\right\rangle\langle a_\sigma\rangle + \langle K_{\mathrm{loc}}\rangle\right) \tag{4.69}$$

where $\langle\cdot\rangle := \langle\psi,\ \cdot\ \psi\rangle$ and subscripts standing for sites are omitted.

On the other hand, we also have

$$\langle\psi, K_{\mathrm{dc}}(\boldsymbol{\phi})\psi\rangle = -zt\sum_{\sigma\in\mathcal{S}}\left(\phi_\sigma\langle a_\sigma^\dagger\rangle + \phi_\sigma^*\langle a_\sigma\rangle - |\phi_\sigma|^2\right) + \langle K_{\mathrm{loc}}\rangle \tag{4.70}$$

The hopping term can be rewritten as

$$\begin{aligned}\phi_\sigma\langle a_\sigma^\dagger\rangle + \phi_\sigma^*\langle a_\sigma\rangle - |\phi_\sigma|^2 &= \langle a_\sigma^\dagger\rangle\langle a_\sigma\rangle - \left(\langle a_\sigma\rangle - \phi_\sigma\right)\left(\langle a_\sigma^\dagger\rangle - \phi_\sigma^*\right) &(4.71)\\ &= \langle a_\sigma^\dagger\rangle\langle a_\sigma\rangle - |\langle a_\sigma\rangle - \phi_\sigma|^2, &(4.72)\end{aligned}$$

which yields

$$\left\langle\psi, \hat{K}_{\mathrm{dc}}(\boldsymbol{\phi})\psi\right\rangle = -zt\sum_{\sigma\in\mathcal{S}}\langle a_\sigma^\dagger\rangle\langle a_\sigma\rangle + \langle K_{\mathrm{loc}}\rangle + zt\sum_{\sigma\in\mathcal{S}}|\langle a_\sigma\rangle - \phi_\sigma|^2. \tag{4.73}$$

By comparing (4.69) and (4.73), we obtain

$$\left\langle\psi, \hat{K}_{\mathrm{dc}}(\boldsymbol{\phi})\psi\right\rangle = \frac{1}{|\Lambda|}\left\langle \bigotimes_{x\in\Lambda}\psi, \hat{K}\bigotimes_{x\in\Lambda}\psi \right\rangle + zt\sum_{\sigma\in\mathcal{S}}\left|\langle\psi, a_\sigma\psi\rangle - \phi_\sigma\right|^2. \tag{4.74}$$

The result 2 follows directly from this equality.

We show the result 1. Define

$$\phi_\sigma^0 := \langle\psi^0, a_\sigma\psi^0\rangle \quad (\forall\sigma\in\mathcal{S}). \tag{4.75}$$

If suffices to show that $\psi^0 = \operatorname{argmin}\left\langle\psi, \hat{K}_{\mathrm{dc}}(\boldsymbol{\phi}^0)\psi\right\rangle$. Let $\psi$ be an arbitrary single-site state. Then, from the equality (4.74), we have

$$\begin{aligned}\left\langle\psi, \hat{K}_{\mathrm{dc}}(\boldsymbol{\phi}^0)\psi\right\rangle &= \frac{1}{|\Lambda|}\left\langle \bigotimes_{x\in\Lambda}\psi, \hat{K}\bigotimes_{x\in\Lambda}\psi \right\rangle + zt\sum_{\sigma\in\mathcal{S}}\left|\langle\psi, a_\sigma\psi\rangle - \phi_\sigma^0\right|^2 &(4.76)\\ &\geq \frac{1}{|\Lambda|}\left\langle \bigotimes_{x\in\Lambda}\psi^0, \hat{K}\bigotimes_{x\in\Lambda}\psi^0 \right\rangle + zt\sum_{\sigma\in\mathcal{S}}\left|\langle\psi, a_\sigma\psi\rangle - \phi_\sigma^0\right|^2 &(4.77)\\ &\geq \frac{1}{|\Lambda|}\left\langle \bigotimes_{x\in\Lambda}\psi^0, \hat{K}\bigotimes_{x\in\Lambda}\psi^0 \right\rangle &(4.78)\\ &= \left\langle\psi^0, \hat{K}_{\mathrm{dc}}(\boldsymbol{\phi}^0)\psi^0\right\rangle, &(4.79)\end{aligned}$$

from which the result 1 follows.

■

### 4.4.2 Non-zero temperature

The equivalence for the non-zero temperature case

We assume that at most $n_{\max}$ particles can populate each single site. We also assume that the approximate ground states in the Gutzwiller variational ansatz and the decoupling approximation can be determined uniquely in each procedure.
For an arbitrary single-site state $\rho$, define

$$j_{\boldsymbol{\phi}}(\rho) := \mathrm{Tr}[\rho \hat{K}_{\mathrm{dc}}(\boldsymbol{\phi})] + \frac{1}{\beta}\mathrm{Tr}\rho\log\rho. \tag{4.80}$$

Recall that

$$J_{\hat{K}}(\rho_{\mathrm{tot}}) := \mathrm{Tr}(\rho_{\mathrm{tot}}\hat{K}) + \frac{1}{\beta}\mathrm{Tr}(\rho_{\mathrm{tot}}\log\rho_{\mathrm{tot}}). \tag{4.81}$$

1. Let $\bigotimes_{x\in\Lambda}\rho^0$ be the state obtained by the Gutzwiller variational ansatz, i.e., $\bigotimes_{x\in\Lambda}\rho^0$ be the state that minimizes $J_{\hat{K}}\left(\bigotimes_{x\in\Lambda}\rho\right)$. Then, $\rho^0$ satisfies the self-consistent condition of the decoupling approximation, i.e., for $\phi^0_\sigma := \mathrm{Tr}(\rho^0 a_\sigma)$, the following relation holds:
$$\rho^0 = \frac{e^{-\beta\hat{K}_{\mathrm{dc}}(\boldsymbol{\phi}^0)}}{\mathrm{Tr}e^{-\beta\hat{K}_{\mathrm{dc}}(\boldsymbol{\phi}^0)}}. \tag{4.82}$$
It should also be noted that
$$j_{\boldsymbol{\phi}^0}(\rho^0) = -\frac{1}{\beta}\log\left[\mathrm{Tr}e^{-\beta\hat{K}_{\mathrm{dc}}(\boldsymbol{\phi}^0)}\right] = J(\boldsymbol{\phi}^0) \tag{4.83}$$
holds, where $J$ is defined in (4.53).

2. For an arbitrary superfluid order parameter $\boldsymbol{\phi}$ and an arbitrary single-site density matrix $\rho$ that satisfy the self-consistent condition $\mathrm{Tr}(\rho a_\sigma) = \phi_\sigma$ $(\forall\sigma\in\mathcal{S})$, we have
$$j_{\boldsymbol{\phi}}(\rho) = \frac{1}{|\Lambda|}J_{\hat{K}}\left(\bigotimes_{x\in\Lambda}\rho\right). \tag{4.84}$$

From these two statements, it follows that the state obtained by the Gutzwiller variational ansatz is equal to the state obtained by the decoupling approximation.

(∵)

Recall that the grand Hamiltonian can be written as

$$\hat{K} = H_{\mathrm{hop}} + \sum_{x\in\Lambda} K_{\mathrm{loc},x} \tag{4.85}$$

We denote $\mathrm{Tr}(\rho\,\cdot)$ by $\langle\cdot\rangle$.

Let $\rho$ be an arbitrary single-site state, and $\boldsymbol{\phi}$ be an arbitrary superfluid order parameter. Like the ground-state case, we begin by rewriting $J_{\hat{K}}(\bigotimes_{x\in\Lambda}\rho)$ and $j_{\boldsymbol{\phi}}(\rho)$, and derive an equality connecting these two quantities.

On one hand, we have

$$J_{\hat{K}}\left(\bigotimes_{x\in\Lambda}\rho\right) = \mathrm{Tr}\left(\bigotimes_{x\in\Lambda}\rho\hat{K}\right)+\frac{1}{\beta}\mathrm{Tr}\left[\bigotimes_{x\in\Lambda}\rho\log\left(\bigotimes_{x\in\Lambda}\rho\right)\right] \tag{4.86}$$

$$= |\Lambda|\left(-zt\sum_{\sigma\in\mathcal{S}}\langle a_\sigma^\dagger\rangle\langle a_\sigma\rangle+\langle K_{\mathrm{loc}}\rangle+\frac{1}{\beta}\mathrm{Tr}\rho\log\rho\right), \tag{4.87}$$

where subscripts standing for sites are omitted. On the other hand,

$$j_{\boldsymbol{\phi}}(\rho) = -zt\sum_{\sigma\in\mathcal{S}}(\phi_\sigma\langle a_\sigma^\dagger\rangle+\phi_\sigma^*\langle a_\sigma\rangle-|\phi_\sigma|^2)+\langle K_{\mathrm{loc}}\rangle+\frac{1}{\beta}\mathrm{Tr}\rho\log\rho \tag{4.88}$$

holds.

The hopping term can be rewritten as

$$\phi_\sigma\langle a_\sigma^\dagger\rangle+\phi_\sigma^*\langle a_\sigma\rangle-|\phi_\sigma|^2 = \langle a_\sigma^\dagger\rangle\langle a_\sigma\rangle-(\langle a_\sigma\rangle-\phi_\sigma)\left(\langle a_\sigma^\dagger\rangle-\phi_\sigma^*\right) \tag{4.89}$$

$$= \langle a_\sigma^\dagger\rangle\langle a_\sigma\rangle-|\langle a_\sigma\rangle-\phi_\sigma|^2 \tag{4.90}$$

which gives

$$j_{\boldsymbol{\phi}}(\rho) = -zt\sum_{\sigma\in\mathcal{S}}\langle a_\sigma^\dagger\rangle\langle a_\sigma\rangle+\langle K_{\mathrm{loc}}\rangle+\frac{1}{\beta}\mathrm{Tr}\rho\log\rho+zt\sum_{\sigma\in\mathcal{S}}|\mathrm{Tr}(\rho a_\sigma)-\phi_\sigma|^2 \tag{4.91}$$

$$= \frac{1}{|\Lambda|}J_{\hat{K}}\left(\bigotimes_{x\in\Lambda}\rho\right)+zt\sum_{\sigma\in\mathcal{S}}|\mathrm{Tr}(\rho a_\sigma)-\phi_\sigma|^2. \tag{4.92}$$

The result 2 follows directly from this equality.

To show the result 1, it suffices to show that $\rho^0$ minimizes $j_{\boldsymbol{\phi}^0}(\cdot)$ because this condition and the variational principle for density matrices [11] yields

$$\rho^0 = \frac{e^{-\beta\hat{K}_{\mathrm{dc}}(\boldsymbol{\phi}^0)}}{\mathrm{Tr}e^{-\beta\hat{K}_{\mathrm{dc}}(\boldsymbol{\phi}^0)}}. \tag{4.93}$$

In addition,

$$j_{\boldsymbol{\phi}^0}(\rho^0) = -\frac{1}{\beta}\log\left[\mathrm{Tr}e^{-\beta\hat{K}_{\mathrm{dc}}(\boldsymbol{\phi})}\right] = J(\boldsymbol{\phi}^0) \tag{4.94}$$

holds immediately from the form of $\rho^0$. Thus, we concentrate on showing that $\rho^0$ minimizes $j_{\boldsymbol{\phi}^0}(\cdot)$.

Let $\rho$ be an arbitrary single-site density matrix. Then, it follows that

$$j_{\boldsymbol{\phi}^0}(\rho) = \frac{1}{|\Lambda|}J_{\hat{K}}\left(\bigotimes_{x\in\Lambda}\rho\right)+zt\sum_{\sigma\in\mathcal{S}}\left|\mathrm{Tr}(\rho a_\sigma)-\phi_\sigma^0\right|^2 \quad (\because (4.92)) \tag{4.95}$$

$$\geq \frac{1}{|\Lambda|}J_{\hat{K}}\left(\bigotimes_{x\in\Lambda}\rho^0\right)+zt\sum_{\sigma\in\mathcal{S}}\left|\mathrm{Tr}(\rho a_\sigma)-\phi_\sigma^0\right|^2$$

$$(\because \rho^0 \text{ minimizes } J_{\hat{K}}\left(\textstyle\bigotimes_{x\in\Lambda}\cdot\right)) \tag{4.96}$$

$$\geq \frac{1}{|\Lambda|}J_{\hat{K}}\left(\bigotimes_{x\in\Lambda}\rho^0\right) \tag{4.97}$$

$$= j_{\boldsymbol{\phi}^0}(\rho^0) \quad (\because \text{equality (4.92) and } \phi_\sigma^0=\mathrm{Tr}(\rho^0 a_\sigma)) \tag{4.98}$$

[11] See the box enclosing 4.23).

which shows that $\rho^0$ minimizes $j_{\phi^0}(\cdot)$.

■

## 4.5 Numerical calculation

So far, we have discussed two approximation methods and equivalence between them, and concentrated on their conceptual aspects. In this section, we turn to a more practical problem, i.e., the problem of solving the self-consistent equations. Here, we discuss the details of numerical methods that are used to solve the self-consistent equations.

- In 4.5.1, we discuss costs required for solving the Gutzwiller variational ansatz and the decoupling approximation, and describe why we use the decoupling approximation rather than the conceptually straightforward Gutzwiller approximation.
- Subsection 4.5.2 describes the basic framework of the calculation.
- In 4.5.3, we show concrete forms of matrix elements of the decoupled grand Hamiltonian, and their derivation. Matrix elements shown here will be plugged into programs to numerically solve the self-consistent equations.
- In 4.5.4, the method of accurately determining phase boundaries, a binary search algorithm, will be described.
- In 4.5.5, we briefly touch on some numerical tricks that are used for the calculation of the non-zero temperature case.
- Subsection 4.5.6 is a short note on the implementation.

### 4.5.1 Why do we use the decoupling approximation?

Before delving into the detailed discussion on how to numerically solve the self-consistent equations, we first make a few comments on the numerical costs required to deal with the Gutzwiller variational ansatz and the decoupling approximation, and thereby clarify why we employ the decoupling approximation rather than the conceptually straightforward Gutzwiller variational ansatz.

- In numerically solving the variational problem with the Gutzwiller variational ansatz, we have to carry out minimization over high-dimensional space; $d_{n_{\max}}$-dimension for the zero temperature case, and $d_{n_{\max}}(d_{n_{\max}}+1)/2$-dimensional space for the non-zero temperature case, where $d_{n_{\max}}$ is the dimension of the Hilbert space corresponding the single-site system with its particle number less than or equal to $n_{\max}$. The concrete expression for $d_{n_{\max}}$ is given by
$$d_{n_{\max}} = \frac{1}{6}(n_{\max}+1)(n_{\max}+2)(n_{\max}+3), \tag{4.99}$$
because the number of ways of allocating $n_{\max}$ particles to four states, i.e., three spin indices $(1, 0, -1)$ and a state "none", is
$$\frac{(n_{\max}+3)!}{n_{\max}!3!} = \frac{1}{6}(n_{\max}+1)(n_{\max}+2)(n_{\max}+3). \tag{4.100}$$

For example, we have

| $n_{\max}$ | 1 | 2 | 3 | 4 | 5 | 6 | 7 |
|---|---|---|---|---|---|---|---|
| $d_{n_{\max}}$ | 4 | 10 | 20 | 35 | 56 | 84 | 120 |

.

- On the other hand, in implementing the decoupling approximation, we have to care about only three variables, i.e., superfluid order parameters. This number, three, of course does not depend on $n_{\max}$.

Thus, it can be seen that for typical value of $n_{\max} \geq 2$, the decoupling approximation is much easier to handle, and we choose this method to numerically obtain the approximate ground (or equilibrium) state.

### 4.5.2 The basic procedure

We solved the self-consistent equations iteratively as follows:

1. Choose the initial value of $\boldsymbol{\phi}$ randomly.
2. Diagonalize $K(\boldsymbol{\phi})$, and
   - for the ground-state case, obtain its ground state $\tilde{\psi}$.
   - for non-zero temperature case, obtain the corresponding density matrix $\tilde{\rho} = e^{-\beta K(\boldsymbol{\phi})}/\mathrm{Tr}e^{-\beta K(\boldsymbol{\phi})}$.
3. From the obtained state, calculate $\boldsymbol{\phi}$ by $\phi_\sigma = \left\langle \tilde{\psi}, a_\sigma \tilde{\psi} \right\rangle$ or $\phi_\sigma = \mathrm{Tr}\left(\tilde{\rho} a_\sigma\right)$ .
4. Iterate 2 and 3 until $\boldsymbol{\phi}$ converges within a prescribed numerical precision.

To avoid being trapped by local solutions, we start the iteration from randomly chosen different initial values ($\boldsymbol{\phi}$), and select the solution with the lowest grand energy. In performing the numerical calculation, the maximum particle number per site $n_{\max}$, whose specific value will be chosen to be large enough that the physics will not be affected [12].

### 4.5.3 Matrix elements

For the numerical calculation, we need matrix elements of $\hat{K}_{\mathrm{dc}}(\boldsymbol{\phi})$ (for a given value of $\boldsymbol{\phi}$) with respect to a specific set of basis. Here, we take local (i.e. single-site) Fock states as our basis, and give the expression for the matrix elements.

Recall that the decoupled grand Hamiltonian $\hat{K}_{\mathrm{dc}}(\boldsymbol{\phi})$ is

$$\begin{aligned} \hat{K}_{\mathrm{dc}}(\boldsymbol{\phi}) \;:=\; & -zt\sum_{\sigma\in\mathcal{S}}\left(\phi_\sigma a_\sigma^\dagger + \phi_\sigma^* a_\sigma - |\phi_\sigma|^2\right) + \frac{U_0}{2}\hat{n}(\hat{n}-1) + \frac{U_2}{2}\left(\boldsymbol{S}^2 - 2\hat{n}\right) \\ & + \sum_{\sigma\in\mathcal{S}}(-p\sigma + q\sigma^2)\hat{n}_\sigma - \mu\hat{n} \end{aligned} \tag{4.101}$$

[12] Specific values of $n_{\max}$ will be shown in the next chapter.

In this section, we use the following simplified notations (because we only consider single-site problem here) :

$$\boldsymbol{n} = (n_\sigma)_{\sigma\in\mathcal{S}}, \tag{4.102}$$

$$\Phi_{\boldsymbol{n}} = \prod_{\sigma\in\mathcal{S}} \frac{1}{\sqrt{n_\sigma!}} (a_\sigma^\dagger)^{n_\sigma} \Phi_{\mathrm{vac}}, \tag{4.103}$$

$$n := \sum_{\sigma\in\mathcal{S}} n_\sigma. \tag{4.104}$$

Then, the matrix elements are given by

Matrix elements of the decoupled grand Hamiltonian

$$\begin{aligned}
&\left\langle \Phi_{\boldsymbol{n}}, \hat{K}_{\mathrm{dc}}(\boldsymbol{\phi})\Phi_{\boldsymbol{n}'} \right\rangle \\
=\ & -zt \sum_{\sigma\in\mathcal{S}} \left( \sqrt{n_\sigma}\phi_\sigma \delta_{\boldsymbol{n}-\boldsymbol{e}_\sigma,\boldsymbol{n}'} + \sqrt{n_\sigma+1}\ \phi_\sigma^* \delta_{\boldsymbol{n}+\boldsymbol{e}_\sigma,\boldsymbol{n}'} - |\phi_\sigma|^2 \delta_{\boldsymbol{n},\boldsymbol{n}'} \right) \\
&+ \left[ \frac{U_0}{2} n(n-1) + \sum_{\sigma\in\mathcal{S}} (-p\sigma + q\sigma^2) n_\sigma - \mu n \right] \delta_{\boldsymbol{n},\boldsymbol{n}'} \\
&+ \frac{U_2}{2} \left\{ \left[ (n_1 - n_{-1})^2 + (2n_0 - 1)(n_1 + n_{-1}) \right] \delta_{\boldsymbol{n},\boldsymbol{n}'} \right. \\
&+ 2\sqrt{n_0(n_0-1)(n_1+1)(n_{-1}+1)} \delta_{\boldsymbol{n}+\boldsymbol{e}_1+\boldsymbol{e}_{-1}-2\boldsymbol{e}_0,\boldsymbol{n}'} \\
&\left. + 2\sqrt{n_1 n_{-1}(n_0+1)(n_0+2)} \delta_{\boldsymbol{n}-\boldsymbol{e}_1-\boldsymbol{e}_{-1}+2\boldsymbol{e}_0,\boldsymbol{n}'} \right\}
\end{aligned} \tag{4.105}$$

$$\begin{aligned}
=\ & -zt \sum_{\sigma\in\mathcal{S}} \left( \sqrt{n_\sigma}\phi_\sigma \delta_{\boldsymbol{n}-\boldsymbol{e}_\sigma,\boldsymbol{n}'} + \sqrt{n_\sigma+1}\ \phi_\sigma^* \delta_{\boldsymbol{n}+\boldsymbol{e}_\sigma,\boldsymbol{n}'} - |\phi_\sigma|^2 \delta_{\boldsymbol{n},\boldsymbol{n}'} \right) \\
&+ \left\{ \frac{U_0}{2} n(n-1) + \sum_{\sigma\in\mathcal{S}} (-p\sigma + q\sigma^2) n_\sigma - \mu n \right. \\
&\left. + \frac{U_2}{2} \left[ (n_1 - n_{-1})^2 + (2n_0 - 1)(n_1 + n_{-1}) \right] \right\} \delta_{\boldsymbol{n},\boldsymbol{n}'} \\
&+ U_2 \left[ \sqrt{n_0(n_0-1)(n_1+1)(n_{-1}+1)} \delta_{\boldsymbol{n}+\boldsymbol{e}_1+\boldsymbol{e}_{-1}-2\boldsymbol{e}_0,\boldsymbol{n}'} \right. \\
&\left. + \sqrt{n_1 n_{-1}(n_0+1)(n_0+2)} \delta_{\boldsymbol{n}-\boldsymbol{e}_1-\boldsymbol{e}_{-1}+2\boldsymbol{e}_0,\boldsymbol{n}'} \right].
\end{aligned} \tag{4.106}$$

$(\because)$

**hopping term**

It is easy to show

$$\left\langle \Phi_{\boldsymbol{n}}, a_\sigma^\dagger \Phi_{\boldsymbol{n}'} \right\rangle = \langle a_\sigma \Phi_{\boldsymbol{n}}, \Phi_{\boldsymbol{n}'} \rangle = \sqrt{n_\sigma} \langle \Phi_{\boldsymbol{n}-\boldsymbol{e}_\sigma}, \Phi_{\boldsymbol{n}'} \rangle = \sqrt{n_\sigma} \delta_{\boldsymbol{n}-\boldsymbol{e}_\sigma,\boldsymbol{n}'}, \tag{4.107}$$

$$\langle \Phi_{\boldsymbol{n}}, a_\sigma \Phi_{\boldsymbol{n}'} \rangle = \left\langle a_\sigma^\dagger \Phi_{\boldsymbol{n}}, \Phi_{\boldsymbol{n}'} \right\rangle = \sqrt{n_\sigma+1} \langle \Phi_{\boldsymbol{n}+\boldsymbol{e}_\sigma}, \Phi_{\boldsymbol{n}'} \rangle = \sqrt{n_\sigma+1} \delta_{\boldsymbol{n}+\boldsymbol{e}_\sigma,\boldsymbol{n}'}, \tag{4.108}$$

from which we obtain

$$\begin{aligned}
&\left\langle \Phi_{\boldsymbol{n}}, -zt \sum_{\sigma\in\mathcal{S}} \left(\phi_\sigma a_\sigma^\dagger + \phi_\sigma^* a_\sigma - |\phi_\sigma|^2\right) \Phi_{\boldsymbol{n}'} \right\rangle \\
= \; & -zt \sum_{\sigma\in\mathcal{S}} \left(\sqrt{n_\sigma}\phi_\sigma \delta_{\boldsymbol{n}-\boldsymbol{e}_\sigma,\boldsymbol{n}'} + \sqrt{n_\sigma+1}\phi_\sigma^* \delta_{\boldsymbol{n}+\boldsymbol{e}_\sigma,\boldsymbol{n}'} - |\phi_\sigma|^2 \delta_{\boldsymbol{n},\boldsymbol{n}'}\right). \qquad (4.109)
\end{aligned}$$

**local term (except for the spin-dependent interaction term)**

This term can be easily treated because it is diagonal:

$$\begin{aligned}
&\left\langle \Phi_{\boldsymbol{n}}, \left[\frac{U_0}{2}\hat{n}(\hat{n}-1) + \sum_{\sigma\in\mathcal{S}}(-p\sigma + q\sigma^2)\hat{n}_\sigma - \mu\hat{n}\right] \Phi_{\boldsymbol{n}'} \right\rangle \\
= \; & \left[\frac{U_0}{2}n(n-1) + \sum_{\sigma\in\mathcal{S}}(-p\sigma + q\sigma^2)n_\sigma - \mu n\right] \delta_{\boldsymbol{n},\boldsymbol{n}'}. \qquad (4.110)
\end{aligned}$$

**spin-dependent interaction term**

Note that the term can be rewritten as

$$\boldsymbol{S}^2 - 2\hat{n} = \sum_{\substack{\sigma_1,\tau_1,\\ \sigma_2,\tau_2\in\mathcal{S}}} \sum_{\alpha=1}^{3} S^{(\alpha)}_{\sigma_1,\tau_1} S^{(\alpha)}_{\sigma_2,\tau_2} a_{\sigma_1}^\dagger a_{\sigma_2}^\dagger a_{\tau_1} a_{\tau_2} \qquad (4.111)$$

(See equation (3.105).).

$$\begin{aligned}
&\left\langle \Phi_{\boldsymbol{n}}, \left(\boldsymbol{S}^2 - 2\hat{n}\right) \Phi_{\boldsymbol{n}'} \right\rangle \\
= \; & \left\langle \left(\boldsymbol{S}^2 - 2\hat{n}\right) \Phi_{\boldsymbol{n}}, \Phi_{\boldsymbol{n}'} \right\rangle \qquad (4.112) \\
= \; & \sum_{\substack{\sigma_1,\tau_1,\\ \sigma_2,\tau_2\in\mathcal{S}}} \left[\sum_{\alpha=1}^{3} S^{(\alpha)}_{\sigma_1,\tau_1} S^{(\alpha)}_{\sigma_2,\tau_2}\right] \left\langle a_{\sigma_1}^\dagger a_{\sigma_2}^\dagger a_{\tau_1} a_{\tau_2} \Phi_{\boldsymbol{n}}, \Phi_{\boldsymbol{n}'} \right\rangle \qquad (4.113) \\
= \; & \sum_{\substack{\sigma_1,\tau_1,\\ \sigma_2,\tau_2\in\mathcal{S}}} \left[\frac{1}{2}\sqrt{(1+\sigma_1)(2-\sigma_1)(1-\sigma_2)(2+\sigma_2)}\delta_{\sigma_1-1,\tau_1}\delta_{\sigma_2+1,\tau_2}\right. \\
& + \frac{1}{2}\sqrt{(1-\sigma_1)(2+\sigma_1)(1+\sigma_2)(2-\sigma_2)}\delta_{\sigma_1+1,\tau_1}\delta_{\sigma_2-1,\tau_2} \\
& \left. + \sigma_1\sigma_2\delta_{\sigma_1,\tau_1}\delta_{\sigma_2,\tau_2}\right] \left\langle a_{\sigma_1}^\dagger a_{\sigma_2}^\dagger a_{\tau_1} a_{\tau_2} \Phi_{\boldsymbol{n}}, \Phi_{\boldsymbol{n}'} \right\rangle \qquad (4.114) \\
& \left(\because \text{ From a straightforward expansion of } \sum_{\alpha=1}^{3} S^{(\alpha)}_{\sigma_1,\tau_1} S^{(\alpha)}_{\sigma_2,\tau_2}\right) \\
= \; & \sum_{\substack{\sigma_1,\tau_1,\\ \sigma_2,\tau_2\in\mathcal{S}}} \left[\sqrt{(1+\sigma_1)(2-\sigma_1)(1-\sigma_2)(2+\sigma_2)}\delta_{\sigma_1-1,\tau_1}\delta_{\sigma_2+1,\tau_2}\right. \\
& \left. + \sigma_1\sigma_2\delta_{\sigma_1,\tau_1}\delta_{\sigma_2,\tau_2}\right] \\
& \times \left\langle a_{\sigma_1}^\dagger a_{\sigma_2}^\dagger a_{\tau_1} a_{\tau_2} \Phi_{\boldsymbol{n}}, \Phi_{\boldsymbol{n}'} \right\rangle \qquad (4.115) \\
= \; & \sum_{\substack{\sigma_1,\tau_1,\\ \sigma_2,\tau_2\in\mathcal{S}}} \sqrt{(1+\sigma_1)(2-\sigma_1)(1-\sigma_2)(2+\sigma_2)}\delta_{\sigma_1-1,\tau_1}\delta_{\sigma_2+1,\tau_2} \left\langle a_{\sigma_1}^\dagger a_{\sigma_2}^\dagger a_{\tau_1} a_{\tau_2} \Phi_{\boldsymbol{n}}, \Phi_{\boldsymbol{n}'} \right\rangle \\
& + \sum_{\sigma_1,\sigma_2\in\mathcal{S}} \sigma_1\sigma_2 \left\langle a_{\sigma_1}^\dagger a_{\sigma_2}^\dagger a_{\sigma_1} a_{\sigma_2} \Phi_{\boldsymbol{n}}, \Phi_{\boldsymbol{n}'} \right\rangle. \qquad (4.116)
\end{aligned}$$

The second term can be rewritten as follows

$$\begin{aligned}
&\sum_{\sigma_1,\sigma_2\in\mathcal{S}} \sigma_1\sigma_2 \left\langle a^\dagger_{\sigma_1} a^\dagger_{\sigma_2} a_{\sigma_1} a_{\sigma_2} \Phi_{\boldsymbol{n}}, \Phi_{\boldsymbol{n}'} \right\rangle \\
= &\sum_{\sigma_1,\sigma_2\in\mathcal{S}} \sigma_1\sigma_2 \left\langle \left(a^\dagger_{\sigma_1} a_{\sigma_1} a^\dagger_{\sigma_2} a_{\sigma_2} - \delta_{\sigma_1,\sigma_2} a^\dagger_{\sigma_1} a_{\sigma_2}\right) \Phi_{\boldsymbol{n}}, \Phi_{\boldsymbol{n}'} \right\rangle && (4.117)\\
= &\sum_{\sigma_1,\sigma_2\in\mathcal{S}} \sigma_1\sigma_2 \left(n_{\sigma_1} n_{\sigma_2} - \delta_{\sigma_1,\sigma_2} n_{\sigma_1}\right) \left\langle \Phi_{\boldsymbol{n}}, \Phi_{\boldsymbol{n}'} \right\rangle && (4.118)\\
= &\left[ \left( \sum_{\sigma\in\mathcal{S}} \sigma n_\sigma \right)^2 - \sum_{\sigma\in\mathcal{S}} \sigma^2 n_\sigma \right] \delta_{\boldsymbol{n},\boldsymbol{n}'} && (4.119)\\
= &\left[ (n_1 - n_{-1})^2 - (n_1 + n_{-1}) \right] \delta_{\boldsymbol{n},\boldsymbol{n}'}. && (4.120)
\end{aligned}$$

For the first term, note that the summand is zero when $\sigma_1 = -1$ or $\sigma_2 = 1$, which enables us to write

$$\begin{aligned}
&\sum_{\substack{\sigma_1,\tau_1,\\ \sigma_2,\tau_2\in\mathcal{S}}} \sqrt{(1+\sigma_1)(2-\sigma_1)(1-\sigma_2)(2+\sigma_2)}\delta_{\sigma_1-1,\tau_1}\delta_{\sigma_2+1,\tau_2} \left\langle a^\dagger_{\sigma_1} a^\dagger_{\sigma_2} a_{\tau_1} a_{\tau_2} \Phi_{\boldsymbol{n}}, \Phi_{\boldsymbol{n}'} \right\rangle \\
= &\sum_{\sigma_1=0}^{1} \sum_{\sigma_2=-1}^{0} \sqrt{(1+\sigma_1)(2-\sigma_1)(1-\sigma_2)(2+\sigma_2)} \left\langle a^\dagger_{\sigma_1} a^\dagger_{\sigma_2} a_{\sigma_1-1} a_{\sigma_2+1} \Phi_{\boldsymbol{n}}, \Phi_{\boldsymbol{n}'} \right\rangle && (4.121)\\
= &\, 2\left\langle a^\dagger_1 a^\dagger_0 a_0 a_1 \Phi_{\boldsymbol{n}}, \Phi_{\boldsymbol{n}'} \right\rangle + 2\left\langle a^\dagger_1 a^\dagger_{-1} a_0 a_0 \Phi_{\boldsymbol{n}}, \Phi_{\boldsymbol{n}'} \right\rangle \\
&+2\left\langle a^\dagger_0 a^\dagger_0 a_{-1} a_1 \Phi_{\boldsymbol{n}}, \Phi_{\boldsymbol{n}'} \right\rangle + 2\left\langle a^\dagger_0 a^\dagger_{-1} a_{-1} a_0 \Phi_{\boldsymbol{n}}, \Phi_{\boldsymbol{n}'} \right\rangle && (4.122)\\
= &\, 2n_0(n_1 + n_{-1})\delta_{\boldsymbol{n},\boldsymbol{n}'} \\
&+2\sqrt{n_0(n_0-1)(n_1+1)(n_{-1}+1)} \left\langle \Phi_{\boldsymbol{n}+\boldsymbol{e}_1+\boldsymbol{e}_{-1}-2\boldsymbol{e}_0}, \Phi_{\boldsymbol{n}'} \right\rangle \\
&+2\sqrt{n_1 n_{-1}(n_0+1)(n_0+2)} \left\langle \Phi_{\boldsymbol{n}-\boldsymbol{e}_1-\boldsymbol{e}_{-1}+2\boldsymbol{e}_0}, \Phi_{\boldsymbol{n}'} \right\rangle && (4.123)\\
= &\, 2n_0(n_1 + n_{-1})\delta_{\boldsymbol{n},\boldsymbol{n}'} \\
&+2\sqrt{n_0(n_0-1)(n_1+1)(n_{-1}+1)}\delta_{\boldsymbol{n}+\boldsymbol{e}_1+\boldsymbol{e}_{-1}-2\boldsymbol{e}_0,\boldsymbol{n}'} \\
&+2\sqrt{n_1 n_{-1}(n_0+1)(n_0+2)}\delta_{\boldsymbol{n}-\boldsymbol{e}_1-\boldsymbol{e}_{-1}+2\boldsymbol{e}_0,\boldsymbol{n}'}. && (4.124)
\end{aligned}$$

Thus, we finally arrive at

$$\begin{aligned}
&\left\langle \Phi_{\boldsymbol{n}}, \left(\boldsymbol{S}^2 - 2\hat{n}\right) \Phi_{\boldsymbol{n}'} \right\rangle \\
= &\left[ (n_1 - n_{-1})^2 + (2n_0 - 1)(n_1 + n_{-1}) \right] \delta_{\boldsymbol{n},\boldsymbol{n}'} \\
&+2\sqrt{n_0(n_0-1)(n_1+1)(n_{-1}+1)}\delta_{\boldsymbol{n}+\boldsymbol{e}_1+\boldsymbol{e}_{-1}-2\boldsymbol{e}_0,\boldsymbol{n}'} \\
&+2\sqrt{n_1 n_{-1}(n_0+1)(n_0+2)}\delta_{\boldsymbol{n}-\boldsymbol{e}_1-\boldsymbol{e}_{-1}+2\boldsymbol{e}_0,\boldsymbol{n}'}. && (4.125)
\end{aligned}$$

■

### 4.5.4 Binary search

We are mainly interested in the $t-\mu$ phase diagrams. To obtain the phase diagram in the $t-\mu$ space, we solve the self-consistent equations for each point of the mesh in the parameter space.

As to phase boundaries, they can be obtained by plotting the superfluid order parameters calculated for each point in the mesh, and choosing the point where the order parameters changes from 0 to non-zero values. However, there is a more accurate way to determine the phase boundary; a binary search algorithm that we describe below.

Usually, superfluid order parameters grow monotonically with the hopping amplitude $t$ (This property is numerically confirmed for the parameter ranges we considered. ). Then, we can use binary search to locate the phase boundary across which the value of $\phi_\sigma$ (for a specific $\sigma$) changes from 0 to a non-zero value, and distinguish discontinuous phase transitions from continuous phase transitions as follows (Here, we denote $zt/U_0$ by $x$):

1. Fix the value of chemical potential .
2. Choose a sufficiently large $x_r$, and set $x_l = 0$. It is assumed that, at $x = x_l$, we have $\phi_\sigma = 0$, and at $x = x_r$ we have $\phi_\sigma \neq 0$.
3. Set $x_c := (x_r + x_l)/2$. Solve the self-consistent equation at $x = x_c$, and obtain $\phi_\sigma$. What we do next depends on whether $\phi_\sigma = 0$ or not [13].
   - If $\phi_\sigma \neq 0$, the desired value of $x$ is located at the left of $x_c$, and we substitute $x_c$ for $x_r$.
   - If $\phi_\sigma = 0$, the desired value of $x$ is located at the right of $x_c$, and we substitute $x_c$ for $x_l$.
4. Iterate step 3 until $x$ converges within a prescribed numerical precision [14]. The final value of $x_c$ represents the location of the boundary.
5. Whether the phase transition is continuous or not can be judged as follows: Define $\phi_r$ and $\phi_l$ as the values of $\phi_\sigma$ corresponding to the final value of $x_r$ and $x_l$. If the phase transition is continuous, we have $|\phi_r| \simeq |\phi_l|$. On the other hand, if the phase transition is discontinuous, $|\phi_r|$ deviates from $|\phi_l|$. [15]

### 4.5.5 Some notes on the non-zero temperature case

For the non-zero temperature case, its numerical calculation requires a few tricks.

#### Expression instead of trace

We denoted the expectation value of an observable $O$ with respect to a density matrix by a trace of the product of $O$ and a matrix exponential. However, we use the following implementation because it is faster:

1. First, diagonalize the decoupled grand Hamiltonian, and denote eigenvalues and the corresponding eigenvectors by $\lambda_1, \lambda_2, \ldots, \lambda_n$ and $\psi^1, \psi^2, \ldots, \psi^n$. Define $U := (\psi^1, \psi^2, \ldots, \psi^n)$, where each $\psi^i$ is regarded as a column vector. Denote the $j$-th component of the eigenvector $\psi^i$ by $\psi^i_j$, from which $U_{ij} = \psi^j_i$ holds.

[13] Because we have inevitable numerical error in numerical calculations, the condition $\phi_\sigma \neq 0$ is replaced by $|\phi_\sigma| > \phi_{\text{thresh}}$, where we took $\phi_{\text{thresh}} = 10^{-4}$.

[14] We took the criteria to be $10^{-4}$

[15] In our calculation, we take this threshold to be $\sim 10^{-2}$

2. Then, $\langle O \rangle$, the expectation value of $O$ can be expressed as

$$\begin{aligned}
\langle O \rangle &= \frac{\mathrm{Tr} O e^{-\beta K}}{\mathrm{Tr} e^{-\beta K}} = \frac{\sum_i \langle \psi^i, O\psi^i \rangle e^{-\beta \lambda_i}}{\sum_i e^{-\beta \lambda_i}} && (4.126)\\
&= \frac{\sum_{i,j,k} (\psi^i_j)^* O_{jk} \psi^i_k e^{-\beta \lambda_i}}{\sum_i e^{-\beta \lambda_i}} && (4.127)\\
&= \frac{\sum_{i,j,k} U^*_{ji} O_{jk} U_{ki} e^{-\beta \lambda_i}}{\sum_i e^{-\beta \lambda_i}} && (4.128)\\
&= \frac{\sum_{i,j,k} (U^\dagger)_{ij} O_{jk} U_{ki} e^{-\beta \lambda_i}}{\sum_i e^{-\beta \lambda_i}} && (4.129)\\
&= \frac{\sum_i (U^\dagger O U)_{ii} e^{-\beta \lambda_i}}{\sum_i e^{-\beta \lambda_i}}. && (4.130)
\end{aligned}$$

3. In addition, the thermodynamic potential $J$ can be calculated from

$$J := -\frac{1}{\beta} \log \left( \sum_i e^{-\beta \lambda_i} \right). \tag{4.131}$$

**Subtracting the ground-state energy**

Although the above expressions are analytically correct, they will cause problems when they are directly implemented. This is because, for large $\beta$ (i.e., low temperature),

- if all the eigenvalues $\lambda_i$ are large, the Boltzmann factors are so small that numerically they are judged to be zero, which causes the zero division problem.
- if there are small (i.e., negatively large) eigenvalues $\lambda_i$, the Boltzmann factor will cause overflow.

To remedy this situation, we subtract the ground energy from eigenvalues as follows: Define

$$\varepsilon := \min_i \lambda_i \tag{4.132}$$

and, rewrite

$$\langle O \rangle = \frac{\sum_i (U^\dagger O U)_{ii} e^{-\beta \lambda_i}}{\sum_i e^{-\beta \lambda_i}} = \frac{\sum_i (U^\dagger O U)_{ii} e^{-\beta (\lambda_i - \varepsilon)}}{\sum_i e^{-\beta (\lambda_i - \varepsilon)}} \tag{4.133}$$

and

$$\begin{aligned}
J &= -\frac{1}{\beta} \log \left( e^{-\beta \varepsilon} \sum_i e^{-\beta (\lambda_i - \varepsilon)} \right) && (4.134)\\
&= \varepsilon - \frac{1}{\beta} \log \left( \sum_i e^{-\beta (\lambda_i - \varepsilon)} \right). && (4.135)
\end{aligned}$$

.

### 4.5.6 Implementation

Methods described so far are implemented by python, with numpy and scipy. Especially, as to the diagonalization routine, scipy `eigh` function is utilized. Data visualizations are done by matplotlib.

All calculations are run on my laptop or cluster computers of the Ueda group.

# Chapter 5

# Phase diagrams in the presence of a quadratic Zeeman effect

In this chapter, we present the results obtained by the method described in the previous chapter.

- In section 5.1, we first present the results for the ground state i.e., $T = 0$ case. It will be shown that, by exerting external magnetic field, we have two distinct superfluid phases in addition to the Mott-insulator phase, and, for the parameter set corresponding to $^7$Li, discontinuous phase transitions between two superfluid phases occur.
- In section 5.2, we present the results for the non-zero temperature case will be presented. It will be shown that discontinuous phase transitions similar to those found at $T = 0$ also occur at for low temperatures.
- Based on these results, in section 5.3, we compare our results with previous studies, and discuss their physical implications.

## 5.1 Ground-state phase diagrams

In this section, we discuss ground-state phase diagrams, i.e. the $T = 0$ case.

- First, in subsection 5.1.1, we show the $t-\mu$ plane phase diagrams, which show the presence of two superfluid phases.
- Then, the $t$ dependence and the $q$ dependence are examined in subsections 5.1.2 and 5.1.3, where discontinuous phase transitions between the two superfluid phases are clearly seen.
- Finally, in subsection 5.1.4, we present $t - \mu$ phase diagram which was obtained by the binary search algorithm described in section 4.5.4, and shows whether the transition is continuous or discontinuous.

In calculating results throughout this subsection, the maximum number of particles per site, $n_{\max}$, is taken to be $n_{\max} = 7$, which is confirmed to be sufficient for numerical convergence in the parameter regime studied here (see appendix A).

### 5.1.1 $t - \mu$ plane phase diagrams

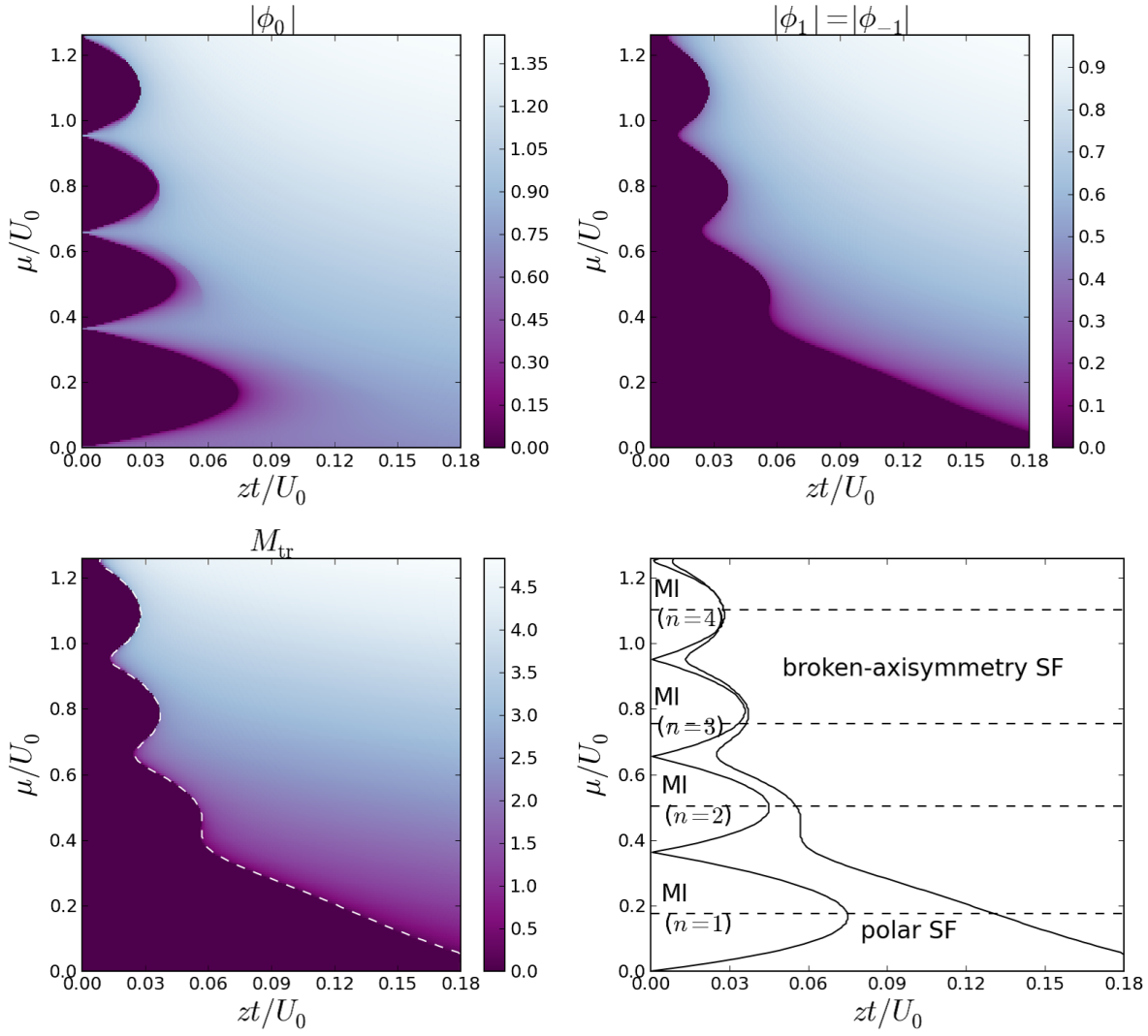


Figure 5.1: Ground-state phase diagrams for $(U_2/U_0, q/U_0) = (-0.7, 0.1)$ ($^7$Li ). Upper left: $|\phi_0|$, upper right: $|\phi_1|$, lower left: transverse magnetization $M_{\rm tr} := \sqrt{\langle S^{(1)}\rangle^2 + \langle S^{(2)}\rangle^2}$, where the white dashed curve shows the boundary obtained from the data of $\phi_1$, which coincides with the boundary across which $M_{\rm tr}$ changes from zero to non-zero, and lower right: the entire phase diagram, where dashed lines represent the slices taken in figure 5.3, SF stands for superfluid, MI stands for Mott-insulator, and $n$ in each Mott-lobe represents particle number densities. Contrary to the case without a quadratic Zeeman effect, there are two phases (polar and BA) in superfluid phase, and the lower-left plot shows that transverse magnetization arises in the BA phase. The magnetization parallel to an applied magnetic field is always zero (within numerical errors).

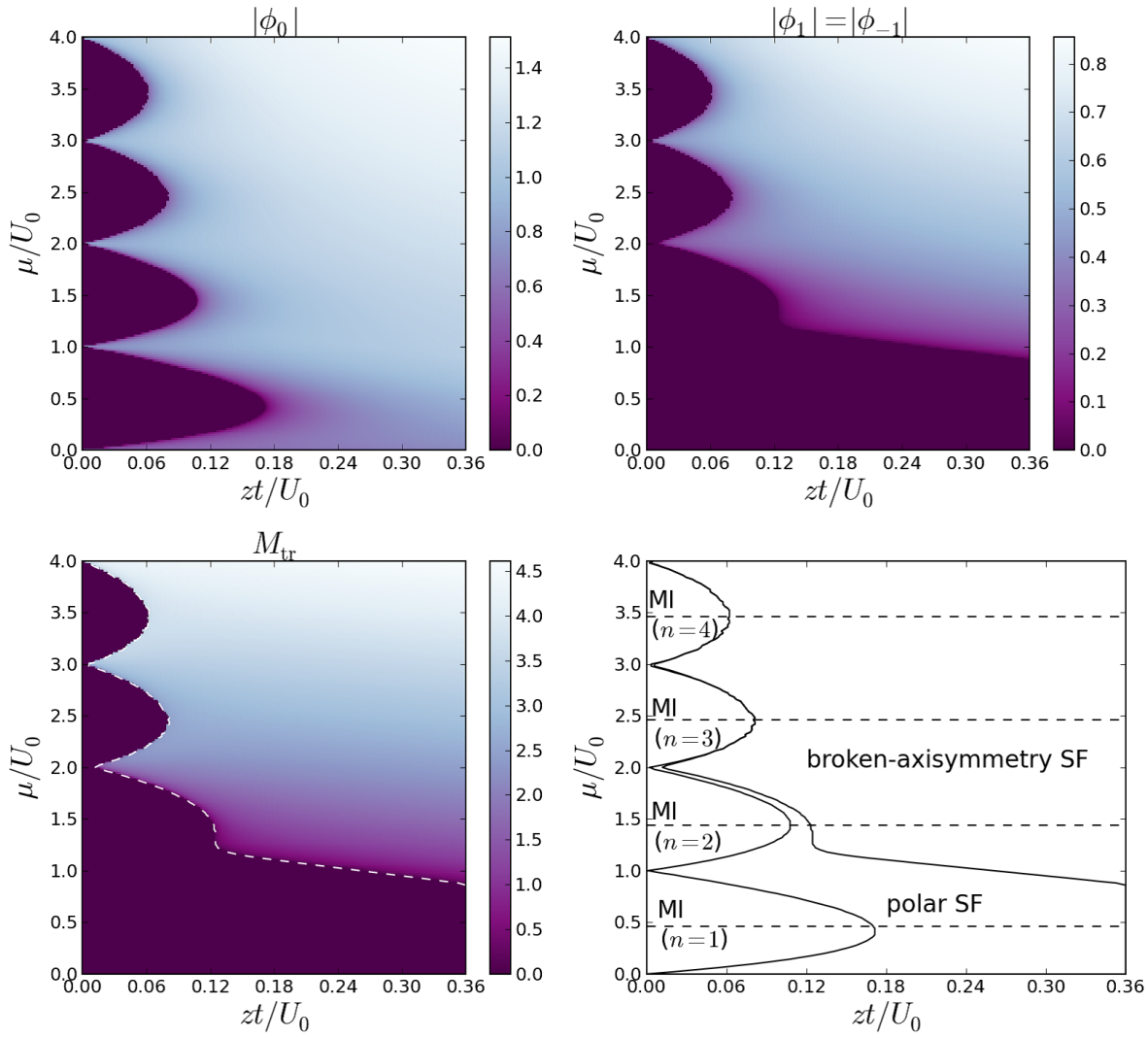


Figure 5.2: Ground-state phase diagrams for $(U_2/U_0, q/U_0) = (-0.005, 0.0085)$ ($^{87}$Rb ). The same description as figure 5.1 applies.

Figures 5.1 and 5.2 show the obtained observables and phase diagrams in the $t - \mu$ plane for $(U_2/U_0, q/U_0) = (-0.7, 0.1)$ and $(-0.005, 0.0085)$, respectively. Note that the former parameter set corresponds to the hyperfine spin-1 manifold of $^7$Li, while the latter to the hyperfine spin-1 manifold of $^{87}$Rb.

In each figure:

- The upper panels show the magnitude of superfluid order parameters $|\phi_\sigma|$. Note that because of the inversion symmetry [1], we have $|\phi_1| = |\phi_{-1}|$.
- We find that no longitudinal magnetization arise along the axis of the external magnetic field, and thus we only plot the transverse magnetization $M_{\rm tr} := \sqrt{\langle S^{(1)} \rangle^2 + \langle S^{(2)} \rangle^2}$, which is shown in the lower left panel of each figure. The white dashed curve is the boundary

[1] In performing the self-consistent calculation, we did not make any assumptions about the relation between $\phi_1$ and $\phi_{-1}$. The relation $|\phi_1| = |\phi_{-1}|$ is confirmed from the obtained data.

across which $|\phi_1|$ changes from zero to non-zero value [2].

- The lower right panel shows the phase diagram obtained from the data of superfluid order parameters $(\phi_1, \phi_0, \phi_{-1})$. Dashed lines correspond to slices taken in figure 5.3.

From the lower left panel, it can be seen that the white curve coincides with the boundary across which $M_{\rm tr}$ changes from zero to non-zero value. Thus, we have two distinct superfluid phases in our system, and following the convention for the mean-field theory of weakly interacting spin-1 bosons, we call

- the superfluid phase in which only the 0 component is superfluid and no magnetization is present, the polar superfluid phase, and
- the superfluid phase in which all the $1, 0, -1$ components are superfluid and transverse magnetization is present, the broken-axisymmetry superfluid phase.

### 5.1.2 Hopping amplitude ($t$) dependence

#### Discontinuous phase transitions

Although the obtained $t - \mu$ phase diagrams for $^7$Li and $^{87}$Rb apparently look similar, a closer look reveals that order parameters behave in quantitatively different ways.

[2] Numerically, we set a threshold value.

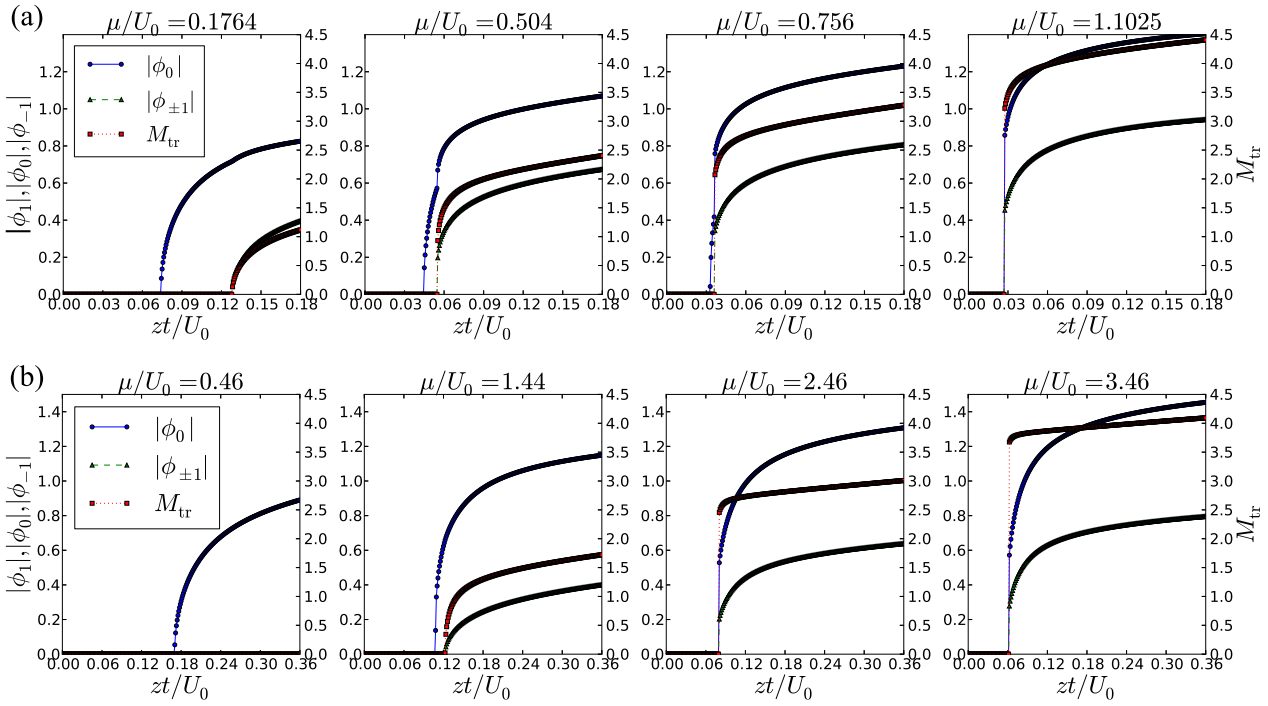


Figure 5.3: The hopping dependence of order parameters (for fixed chemical potential $\mu$). The left scales show $|\phi_\sigma|$, the magnitude of superfluid order parameters , and the right scales show the transverse magnetization $M_{\rm tr}$. The parameters used are (a) $U_2/U_0 = -0.7$, $q/U_0 = 0.1$, and (b) $U_2/U_0 = -0.005$, $q/U_0 = 0.0085$. For phase transitions between the polar and the broken-axisymmetry superfluid phases, the panel (a) shows discontinuous phase transitions, while panel (b) shows continuous phase transitions. Discontinuous phase transitions between the broken-axisymmetry superfluid phase and the Mott-insulator phase should be interpreted with caution (see text for details).

Figure 5.3 shows the hopping amplitude ($t$) dependence of order parameters $\phi_\sigma$ and $M_{\rm tr}$, where the left scales show $\phi_\sigma$ and the right scales show $M_{\rm tr}$. The upper panels show the results for $^7$Li, while the lower panels show the results for $^{87}$Rb. Slices are taken along the dashed lines shown in the lower right panels in figures 5.1 and 5.2.

It can be seen that, for $^7$Li, i.e., in the upper panels, we have discontinuous phase transitions **between two superfluid phases**, while for $^{87}$Rb, i.e., in the lower panels, we only have continuous phase transitions between superfluid phases in the parameter range we consider. Although we have discontinuous phase transition between the broken-axisymmetry superfluid phase and the Mott-insulator phase for both cases, this result should be interpreted with caution (See subsection 5.3.1).

### The energy functional: metastability

To clearly visualize and confirm the observed discontinuous phase transitions from a different point of view, here we show plots of energy functional $K(\boldsymbol{\phi})$, which is defined by

$$K(\boldsymbol{\phi}) := \min_{\psi} \left\langle \psi, \hat{K}_{\rm dc}(\boldsymbol{\phi})\psi \right\rangle \tag{5.1}$$

Recall that in section 4.3 we have shown that stationary points of $K$ correspond to solutions to the self-consistent equations of the decoupling approximation. Thus, if $K$ has multiple local minima, it indicates that we have discontinuous phase transitions.

Figure 5.4 shows the plot of $K$ as a function of [3] $|\phi_1|$ and $|\phi_0|$. For clarity, we only plotted values below a certain threshold value. The values of $K$ are shifted so that 0 in the grayscale bars correspond to the threshold value, and the bars are in an arbitrary unit. The white circle in each panel indicates the global minima.

The left panel corresponds to the polar superfluid phase, while the right panel to the broken-axisymmetry superfluid phase. It can be clearly seen from the figure that $K$ has two local minima, whose presence shows metastability and accompanying discontinuous phase transitions.

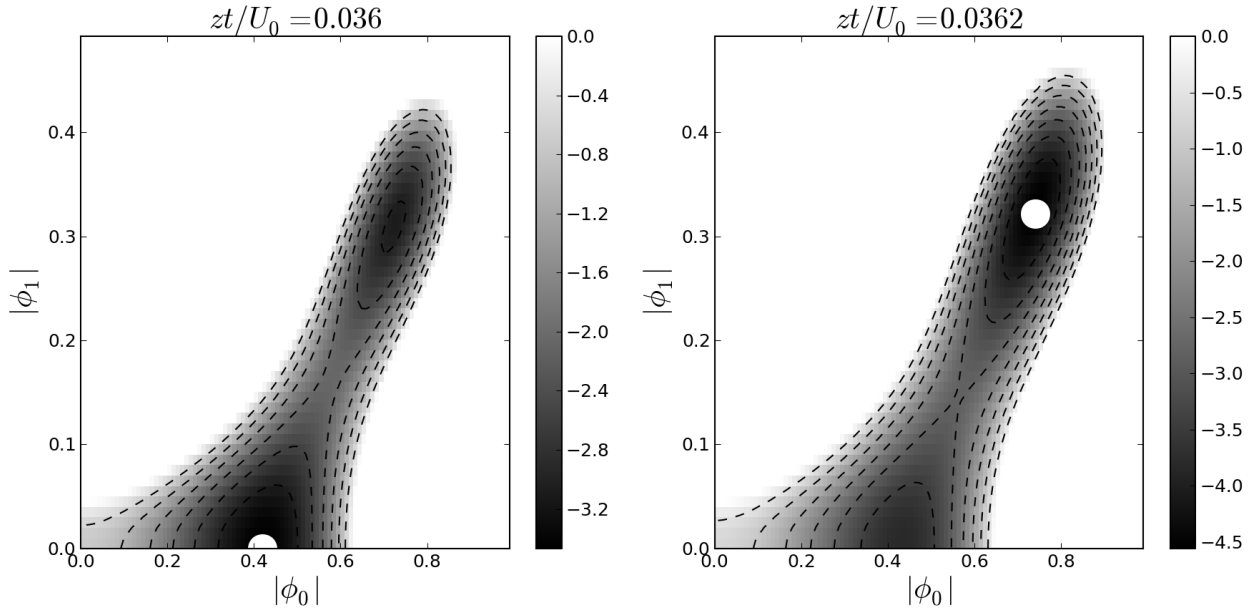


Figure 5.4: $K(\boldsymbol{\phi}) := \min_{\psi}\langle\psi, K(\boldsymbol{\phi})\psi\rangle$, where, by the assumption of the inversion symmetry $|\phi_1| = |\phi_{-1}|$, $\boldsymbol{\phi}$ can be written as $(|\phi_1|e^{i\theta}, |\phi_0|, |\phi_1|e^{i\theta})$ and the minimum with respect to $\theta$ has already been taken numerically. White circles stand for global minima. For clarity, values above a given threshold value are not plotted, and the grayscale bars are in an arbitrary unit. It can be seen that there are two local minima, indicating metastability and the ensuing discontinuous phase transition. $U_2/U_0 = -0.7, q/U_0 = 0.1$ and $\mu/U_0 = 0.756$.

### 5.1.3 Quadratic Zeeman energy ($q$) dependence

Discontinuous phase transitions between two superfluid phases can also be observed when the external magnetic field is varied. The upper panel of figure 5.5 shows that with an increase in the quadratic Zeeman coefficient $q$, the system undergoes a discontinuous phase transition from the broken-axisymmetry superfluid phase to the polar superfluid phase. The lower panels of figure 5.5 also show metastability and the accompanying discontinuous phase transition.

[3] Here we assume the inversion symmetry $|\phi_1| = |\phi_{-1}|$. Then, by using a global phase shift and a rotation around the applied external magnetic field, we can write $\boldsymbol{\phi} = (|\phi_1|e^{i\theta}, |\phi_0|, |\phi_1|e^{i\theta})$, where $\theta \in \mathbb{R}$. The minimum with respect to $\theta$ has already been taken numerically before plotting $K$.

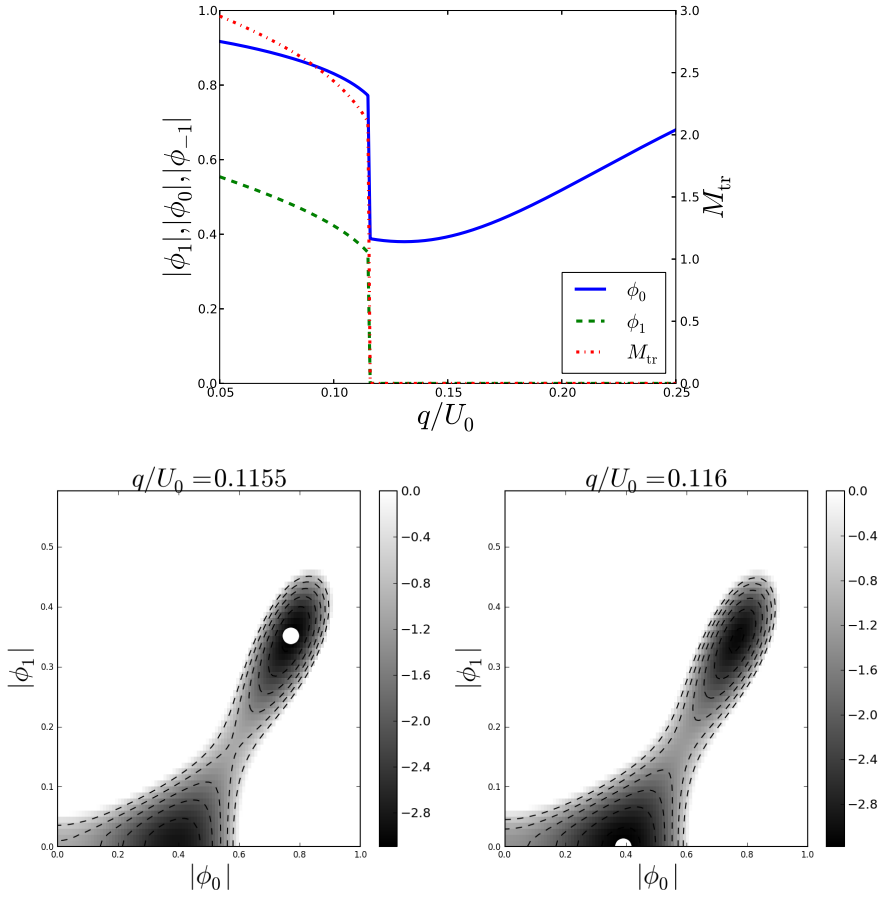


Figure 5.5: Upper : Superfluid order parameters (left scale) and the transverse magnetization (right scale) as functions of $q/U_0$ for $U_2/U_0 = -0.7, zt/U_0 = 0.0372$, and $\mu/U_0 = 0.819$. A discontinuous phase transition occurs at $q/U_0 \simeq 0.116$. Lower : $K(\boldsymbol{\phi})$ (see the caption of figure 5.4 for detail).

### 5.1.4 $t-\mu$ phase diagrams (revisited)

So far, we have seen that, within our approximation scheme of the decoupling approximation, the spin-1 Bose-Hubbard model with the quadratic Zeeman effect has discontinuous phase transitions between the broken-axisymmetry superfluid phase and other phases.

Based on this observation, in figure 5.6, we show phase boundaries obtained by the binary search method described in subsection 4.5.4. In the figure, black circles indicate the boundaries across which discontinuous phase transitions take place, and white circles indicate the boundaries across which continuous phase transitions occur.

It can be seen that the increase in $q$ results in the increase of the polar superfluid phase region, and that the discontinuous phase transitions occur between two superfluid phases, and between the broken-axisymmetry phase and the Mott-insulator phase (although the latter should be interpreted with caution[4]). Also, we can see that discontinuous phase transitions occur only when the transition point is close to the Mott-insulator phase.

[4]See subsection 5.3.1.

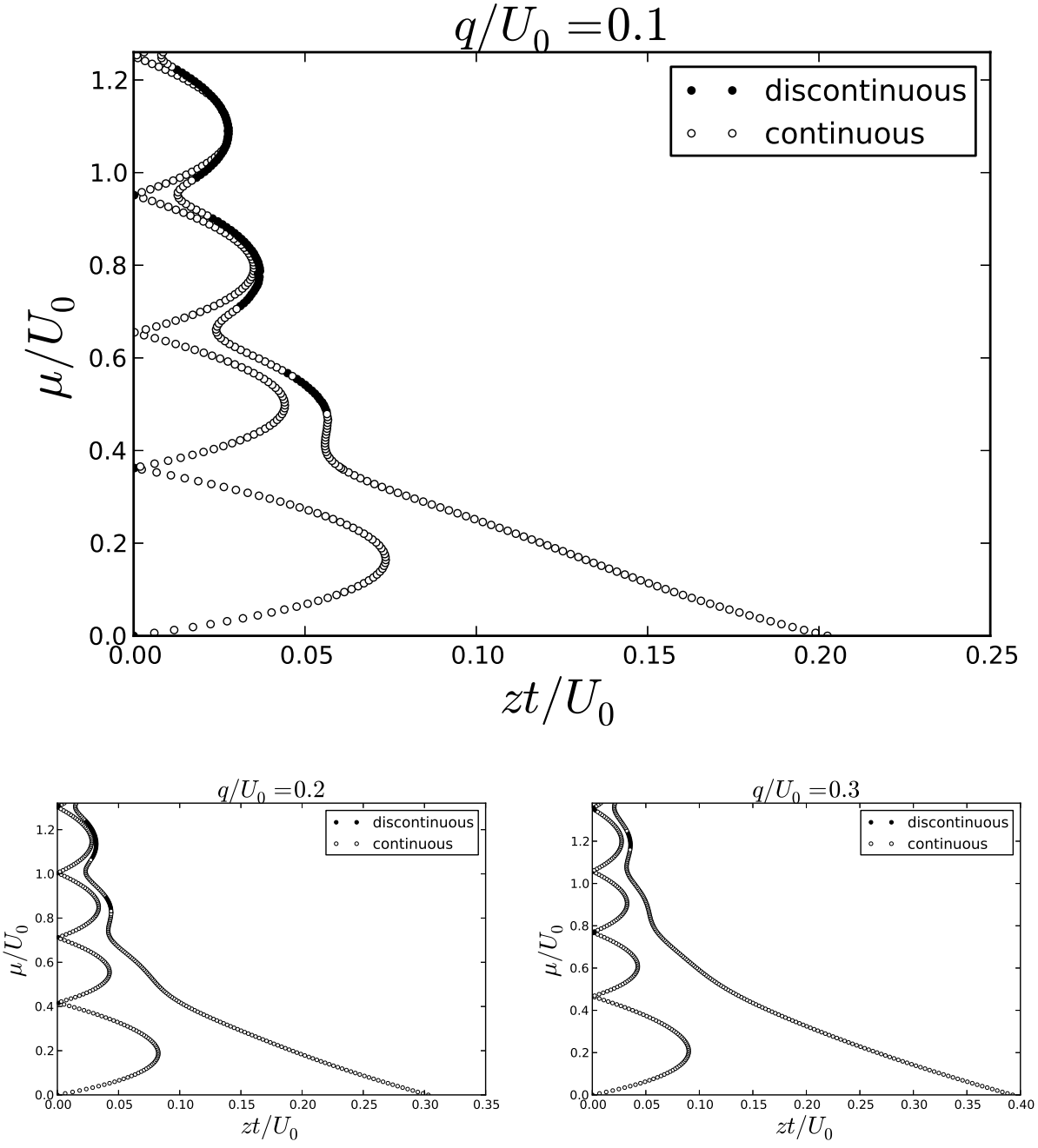


Figure 5.6: The ground-state phase diagram for $(U_2/U_0, q/U_0) = (-0.7, 0.1), (-0.7, 0.2)$, and $(-0.7, 0.3)$, where phase boundaries are determined by the binary search algorithm described in section 4.5.4. White circles denote the boundary across which continuous phase transitions occur, while black circles denote the boundary across which discontinuous phase transitions occur. It can be seen that discontinuous phase transitions between two superfluid phases occur when the boundary is close to Mott lobes.

## 5.2 Phase diagrams at non-zero temperature

In this section, we show the results for the non-zero temperature case, and compare them with those for the zero temperature case. Throughout this section, we consider smaller particle-number densities compared with the previous section to decrease the numerical cost. For that aim, we take $\mu$ to be smaller compared with the previous section, and set $n_{\max} = 5$ and $(U_2/U_0, q/U_0) = (-0.7, 0.02)$. The choice $n_{\max} = 5$ is confirmed to be sufficient (see appendix A).

As was done in the last section, we examine the $t - \mu$ phase diagrams, the $t$ dependence, the $q$ dependence, and finally the effect of temperature.

### 5.2.1 $t - \mu$ phase diagrams

Figure 5.7 shows the obtained observables and phase diagram in the $t - \mu$ plane, where the temperature is $k_B T/U_0 = 0.02$. The panels are read in the same way as the panels in figure 5.1.

Similarly to the zero-temperature case, it can be seen that, the system possesses the normal bose liquid phase [5] and the two superfluid phases, i.e., the polar superfluid phase and the broken-axisymmetry phase.

[5] The normal bose liquid phase corresponds to the Mott-insulator phase in the ground state. The distinction comes from the fact that, for non-zero temperatures, compressibility takes a non-zero value.

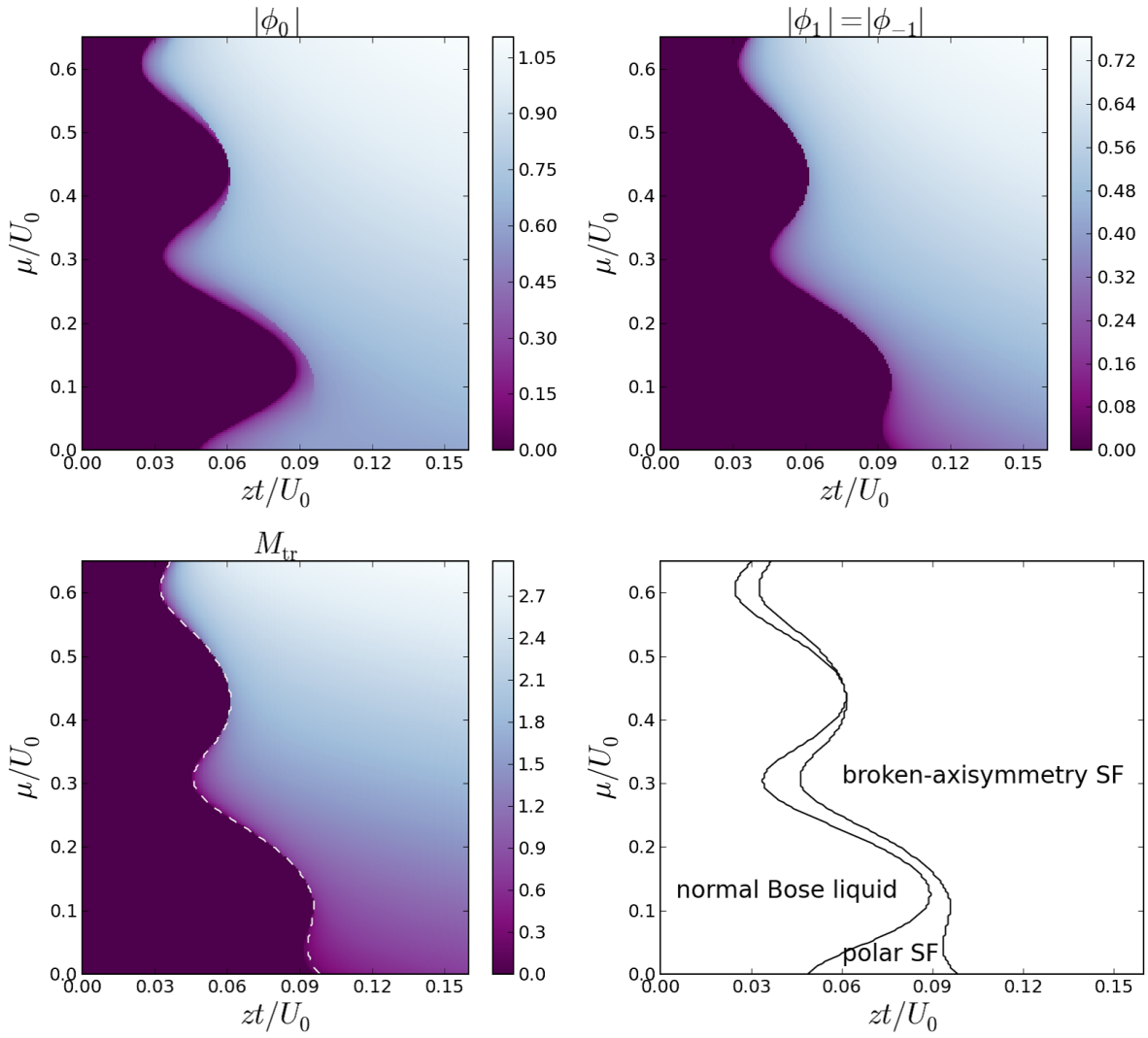


Figure 5.7: Equilibrium state phase diagrams for $(U_2/U_0, q/U_0, k_BT/U_0) = (-0.7, 0.02, 0.02)$ ($^7$Li ). Upper left: $\phi_0$, upper right: $\phi_1$, lower left: transverse magnetization $M_{\rm tr} := \sqrt{\langle S^{(1)}\rangle^2 + \langle S^{(2)}\rangle^2}$, where the white dashed curve shows the boundary obtained from the data of $\phi_1$, which coincides with the boundary across which $M_{\rm tr}$ changes from zero to non-zero, and lower right: the entire phase diagram, where SF stands for superfluid. The magnetization parallel to an applied magnetic field is always zero (within numerical errors).

### 5.2.2 Hopping amplitude ($t$) dependence

The upper panel in figure 5.8 shows the hopping amplitude ($t$) dependence of the order parameters $\phi_\sigma$ and $M_{\rm tr}$, where the left scales show $\phi_\sigma$ and the right scales show $M_{\rm tr}$. It can be seen that we have discontinuous phase transitions **between the two superfluid phases**.

The lower panels visualize this discontinuous phase transition more clearly. In analogy with figure 5.4, we plot the thermodynamic potential $J(\boldsymbol{\phi})$ defined by

$$J(\boldsymbol{\phi}) := -\frac{1}{\beta}\log \mathrm{Tr} e^{-\beta \hat{K}_{\rm dc}(\boldsymbol{\phi})}. \tag{5.2}$$

In section 4.3, we have shown that stationary points of $J$ correspond to self-consistent solutions obtained by the decoupling approximation. Thus, the presence of multiple local minima indicates the occurrence of metastability and the accompanying discontinuous phase transition. Plotted in the lower panels are $J$ as a function of $|\phi_0|$ and $|\phi_1|$, where the white circle indicates the global minimum in each panel. The presence of two local minima, one corresponding to the polar superfluid phase and the other corresponding to the broken-axisymmetry phase can clearly be seen.

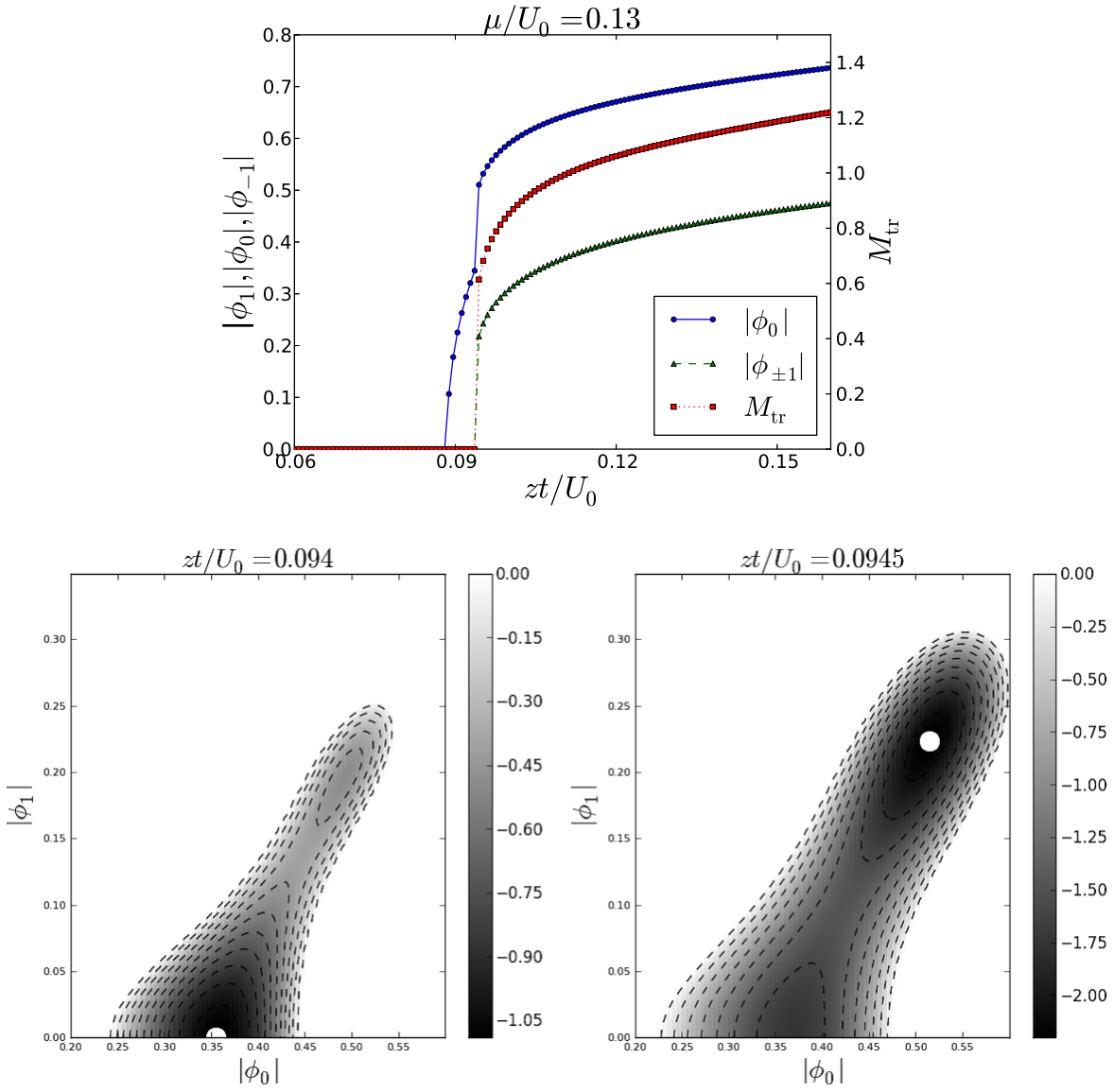


Figure 5.8: Phase transitions at non-zero temperature. Upper : Superfluid order parameters (left scale) and transverse magnetization (right scale) as functions of $zt/U_0$. A discontinuous phase transition occurs at $zt/U_0 \simeq 0.094$. Lower : $J(\boldsymbol{\phi})$. By the assumption of the inversion symmetry $|\phi_1| = |\phi_{-1}|$, $\boldsymbol{\phi}$ can be written as $(|\phi_1|e^{i\theta}, |\phi_0|, |\phi_1|e^{i\theta})$ and the minimum with respect to $\theta$ has already been taken numerically. White circles stand for the global minima. For clarity, values above certain thresholds are not plotted, and the grayscale bars are in an arbitrary unit. In all panels, $U_2/U_0 = -0.7, q/U_0 = 0.02, \mu/U_0 = 0.13$, and $k_BT/U_0 = 0.02$.

### 5.2.3 Quadratic Zeeman energy ($q$) dependence

In figure 5.9, we examine the $q$ dependence of the order parameters. The upper panel shows the occurrence of the discontinuous phase transition at $q/U_0 \simeq 0.0256$, and the lower panels visualize the presence metastability.

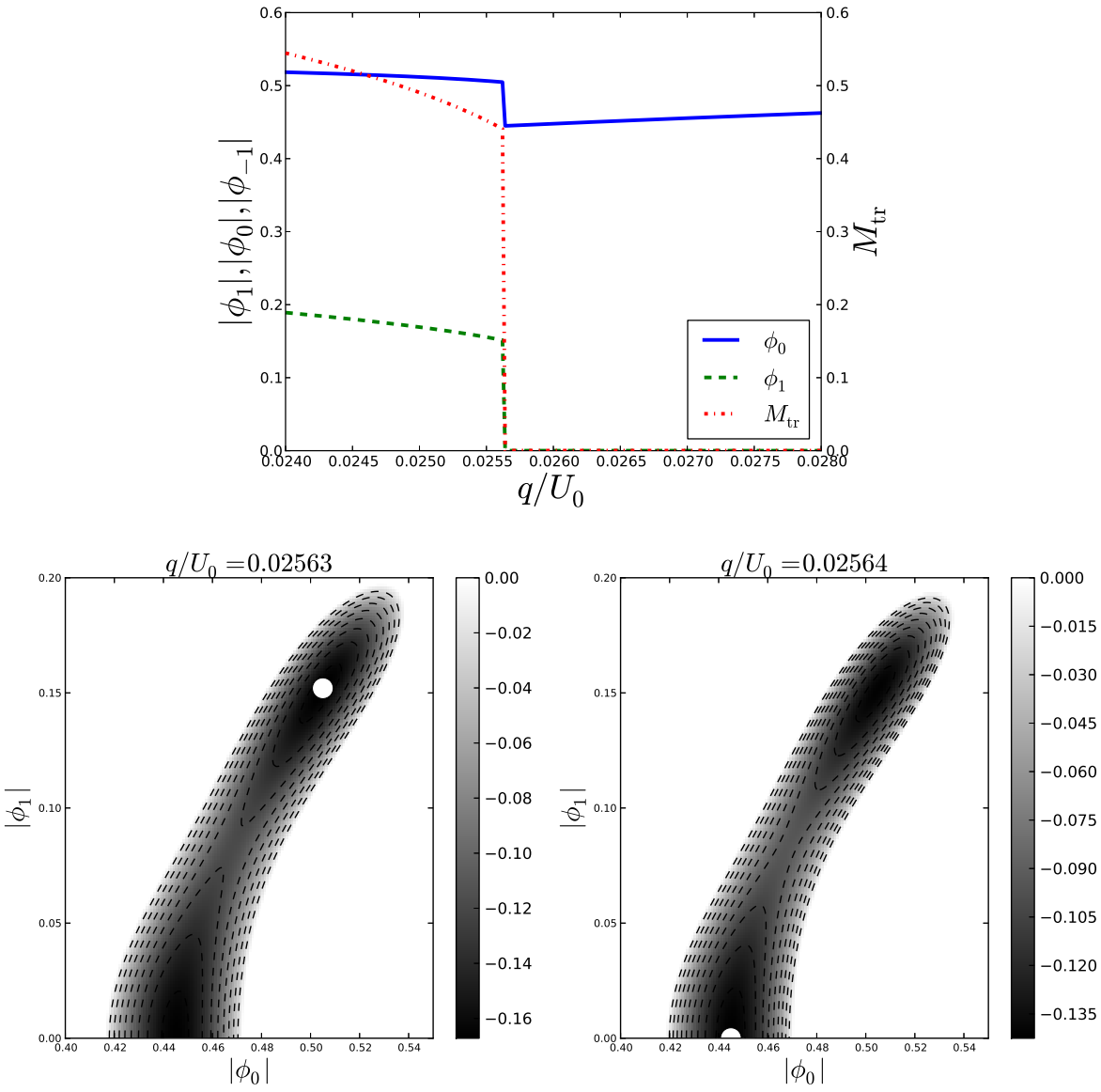


Figure 5.9: Upper : Superfluid order parameters (left scale) and the transverse magnetization (right scale) as functions of $q/U_0$. A discontinuous phase transition occurs at $q/U_0 \simeq 0.0256$. Lower : Lower : $J(\boldsymbol{\phi})$. For detail, see the caption of figure 5.8. In all panels, $U_2/U_0 = -0.7, zt/U_0 = 0.095, \mu/U_0 = 0.13$, and $k_BT/U_0 = 0.02$.

### 5.2.4 The effect of temperature

Finally, we examine how the temperature affects the nature of phase transitions in this system.

Figure 5.10 shows the $t-\mu$ phase diagrams obtained by the binary search algorithm described in section 4.5.4, where white circles show the continuous phase transition boundary, and black

circles show the discontinuous phase transitions boundary. The temperature is varied between 0 (the upper left panel) and $k_BT/U_0 = 0.05$ (the lower right panel).

For a sufficiently low temperature, the phase diagram resembles that of the zero-temperature case, where we can see two superfluid phases and the normal bose liquid phase, and discontinuous phase transitions occur between the two superfluid phases, when the boundary is close to the normal bose liquid phase. However, by raising the temperature, we can see that the region of discontinuous phase transition shrinks, and finally disappear, i.e., phase transitions between different phases become continuous.

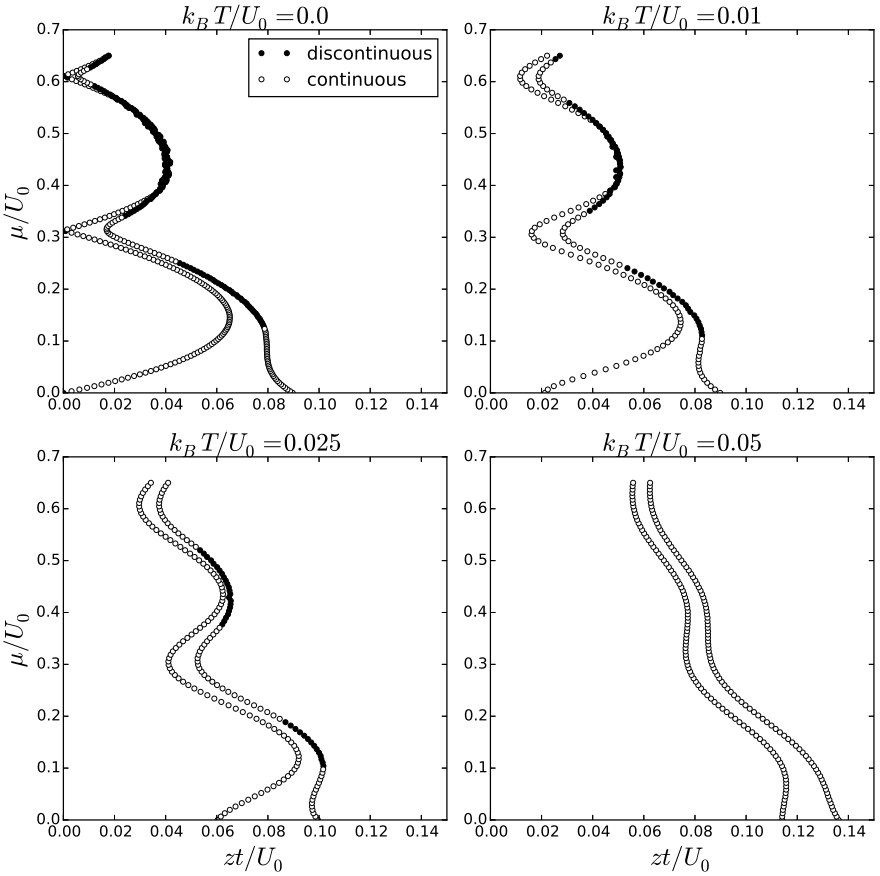


Figure 5.10: The non-zero temperature phase diagrams for $(U_2/U_0, q/U_0) = (-0.7, 0.02)$, where phase boundaries are determined by the binary search algorithm described in section 4.5.4. White circles denote the boundary across which continuous phase transitions occur, while black circles denote the boundary across which discontinuous phase transitions occur. It can be seen that, as the temperature is increased, discontinuous phase transition region shrink, and finally disappear.

## 5.3 Discussions

### 5.3.1 On the Mott-insulator phase

Our calculation shows that the Mott phase exhibits no magnetization and that the phase transitions between the Mott phase and the broken-axisymmetry superfluid phase are discontinuous.

However, as already stated, this result should be interpreted with caution. This is because the decoupling approximation cannot treat the effect of the hopping term in the Mott-insulator phase correctly, which can be easily seen from the decoupled grand Hamiltonian (4.37); in the Mott-insulator phase, where $\phi_\sigma = 0$, the hopping term vanishes, and its effect is completely ignored.

A previous study treated the unit-filling Mott-insulator phase by an effective spin model and a field theory [30], which shows that, inside the Mott lobe, there are two phases, namely, the XY-FM phase and the Ising nematic phase, where the rotational symmetry around an applied external magnetic field is broken in the former phase, but not in the latter phase. The presence of such a phase transition inside a Mott lobe suggests that the discontinuous phase transition from the Mott-insulator phase to the BA superfluid phase predicted in our calculation might be an artifact of the decoupling approximation. Further analyses about these phase transitions and the entire phase diagram remains to be explored.

### 5.3.2 Comparison with previous results on spin-1 bosons

We have found that the ferromagnetic spin-1 bosons in optical lattices can exhibit, in addition to the Mott-insulator phase, two superfluid phases and that discontinuous phase transitions occur between these two superfluid phases when various parameters including the hopping amplitude and the quadratic Zeeman energy are varied. Although the presence of two superfluid phases is expected from previous studies on ferromagnetic spin-1 bosons without a lattice (see figure 2.2), where the presence of two superfluid phases is shown on the basis of mean-field theory for weak interaction, the discontinuous phase transition we have found for the system with lattices is in clear contrast to the prediction for the system without a lattice; mean-field analyses for the latter system predict continuous phase transitions between these two superfluid phases.

We note that discontinuous phase transitions between two superfluid phases occur only when the boundary is close to the Mott-insulator phase, and that continuous phase transitions occur when the hopping is so large that the boundary is far from the Mott-insulator phase. (See figures 5.6. ). This is not only consistent with the fact that the corresponding phase transitions are continuous for weakly interacting bosons, in which almost all the particles participate in the superfluidity, but it also suggests that the presence of a considerable portion of the non-superfluid component is crucial for the occurrence of discontinuous phase transitions, highlighting the role of the interplay between the spatial degrees of freedom and the spin degrees of freedom.

### 5.3.3 On the experimental realization

The discontinuous phase transitions between two superfluid phases predicted in our calculation can be experimentally observed by examining the presence of hysteresis, as was recently reported for the antiferromagnetic spin-1 bosons in an optical lattice [29]. Here, we discuss this topic, using experimental parameters of $^7$Li ($F = 1$), where $U_2/U_0 \simeq -0.7$, for the three-dimensional cubic lattice.

**model parameters**

First, we note that, for the three-dimensional cubic lattice, the model parameters can be expressed as (equations (23) and (57) in [10])

$$U_0 = 4\sqrt{2\pi}E_R\frac{a_0+2a_2}{3\lambda}x^{3/4}, \tag{5.3}$$

$$U_2 = 4\sqrt{2\pi}E_R\frac{a_2-a_0}{3\lambda}x^{3/4}, \tag{5.4}$$

$$t = \frac{4}{\sqrt{\pi}}E_R x^{3/4}e^{-2\sqrt{x}}, \tag{5.5}$$

where

- $a_0$ and $a_2$ stands for the $s$-wave scattering length of the total spin-0, and 2 channels, respectively,
- the optical lattice potential $U_L(\boldsymbol{r})$ is expressed as $U_L(\boldsymbol{r}) = V_0\sum_{i=1}^{3}\sin^2(\boldsymbol{k}_i\cdot\boldsymbol{r})$, and $|\boldsymbol{k}_i| =: k$, $\lambda := 2\pi/k$ (note that the lattice spacing is not $\lambda$, but $\lambda/2$.),
- $E_R := \hbar^2k^2/(2M)$, where $M$ is the mass of the bosonic atom, and
- $x := V_0/E_R$.

Here we calculate the value of $U_0$ for later calculations.

For $^7$Li ($F=1$), we have [31]

$$a_0 = 39.1a_B, \quad a_2 = 4.9a_B, \tag{5.6}$$

$$\lambda = 1064\text{nm}, \quad \frac{V_0}{E_R} \leq 100, \tag{5.7}$$

which gives

$$U_0 \simeq 1.37\times10^{-31}\times x^{3/4}\text{J}. \tag{5.8}$$

$(\cdot.\cdot)$

Using parameters given above and the values of physical constants

$$\text{Planck constant} \quad h \simeq 6.626\times10^{-34}\text{J}\cdot\text{s}, \tag{5.9}$$

$$\text{Atomic mass} \quad M_0 \simeq 1.6606\times10^{-27}\text{kg}, \tag{5.10}$$

$$\text{Bohr radius} \quad a_B = \frac{4\pi\varepsilon_0\hbar^2}{m_e e^2} \simeq 0.529\times10^{-10}\text{m}, \tag{5.11}$$

we have

$$
\begin{aligned}
& U_0 \\
= \; & 4\sqrt{2\pi}E_R\frac{a_0+2a_2}{3\lambda}x^{3/4} && (5.12)\\
= \; & 4\sqrt{2\pi}\frac{\hbar^2k^2}{2M}\frac{a_0+2a_2}{3\lambda}x^{3/4} && (5.13)\\
= \; & \frac{2}{3}\sqrt{2\pi}\frac{h^2}{M}\frac{a_0+2a_2}{\lambda^3}x^{3/4} && (5.14)\\
= \; & \frac{2}{3}\sqrt{2\pi}\times\frac{6.63^2\times10^{-68}\mathrm{J}^2\cdot\mathrm{s}^2}{7\times1.66\times10^{-27}\mathrm{kg}} \\
& \times\frac{(39.1+2\times4.9)\times0.529\times10^{-10}\mathrm{m}}{1.06^3\times10^{-18}\mathrm{m}^3}\times x^{3/4} && (5.15)\\
= \; & \frac{2}{3}\sqrt{2\pi}\times\frac{6.63^2\times(39.1+2\times4.9)\times0.529}{7\times1.66\times1.06^3}\times10^{-68-10+27+18}\times x^{3/4}\mathrm{J} && (5.16)\\
\simeq \; & 137.3\times10^{-33}\times x^{3/4}\mathrm{J} && (5.17)\\
\simeq \; & 1.37\times10^{-31}\times x^{3/4}\mathrm{J}. && (5.18)
\end{aligned}
$$

■

Note that, once scattering lengths and the lattice wave length are given, the value of $x$ determine $t/U_0$ as $\frac{t}{U_0}\simeq e^{-2\sqrt{x}}\times2.767\times10^2$.

$(\because)$

$$
\begin{aligned}
\frac{t}{U_0} &= \frac{3}{\pi\sqrt{2}}e^{-2\sqrt{x}}\frac{\lambda}{a_0+2a_2} && (5.19)\\
&\simeq e^{-2\sqrt{x}}\times\frac{3}{\pi\sqrt{2}}\frac{1.06\times10^{-6}}{(39.1+2\times4.9)\times0.529\times10^{-10}} && (5.20)\\
&\simeq e^{-2\sqrt{x}}\times2.767\times10^2. && (5.21)
\end{aligned}
$$

■

Thus, for the three-dimensional cubic lattice, where $z=6$, if we fix $zt/U_0\sim0.1$, which is a typical value for observing the phase transitions mentioned in earlier sections, then $x$ must be $x\sim20-30$.

### The strength of the magnetic field

Because the magnetization parallel to an applied magnetic field is conserved [6], and hence the linear Zeeman effect can be gauged out, the quadratic Zeeman effect can be easily tuned with an external magnetic field.

The value of $q/U_0\simeq0.1$ used in previous sections corresponds to $B\sim0.6$G.

[6]For alkali atoms, it is known (see table I of [18]) that the magnetic dipolar-dipolar interaction, which breaks the angular momentum conservation, is sufficiently small so that the total angular momentum is conserved for typical experimental time scales. For example, [32] experimentally showed that, for $F=1$ manifold of $^{87}$Rb, the magnetization along the axis of the applied magnetic field is conserved for approximately 1 second.

(∵)

The definition of the quadratic Zeeman energy is (see (2.41))

$$q = \frac{1}{16}\frac{(g\mu_B B)^2}{\Delta E_{\rm hf}}, \tag{5.22}$$

where

- $g \simeq 2$ is the electronic spin $g$ factor,
- $\mu_B \simeq 9.27 \times 10^{-24}$ J T$^{-1}$ is the Bohr magneton,
- $B$ is the strength of the external magnetic field,
- $\Delta E_{\rm hf}$ is the hyperfine energy splitting.

For $^7$Li , we have $\Delta E_{\rm hf} \simeq h \times 0.804$GHz (See table 2.1. ), which gives

$$\begin{aligned} q &= \frac{1}{16} \times \frac{(2 \times 9.27 \times 10^{-24}{\rm J T}^{-1} B)^2}{0.804 \times 10^9 {\rm s}^{-1} \times 6.63 \times 10^{-34}{\rm J \cdot s}} && (5.23)\\ &= \frac{9.27^2}{4 \times 0.804 \times 6.63} \times 10^{-48-9+34} (B{\rm T}^{-1})^2 {\rm J} && (5.24)\\ &\simeq 4.03 \times 10^{-23} (B{\rm T}^{-1})^2 {\rm J} && (5.25) \end{aligned}$$

Thus, we have

$$\begin{aligned} \frac{q}{U_0} &\simeq \frac{4.03 \times 10^{-23} (B{\rm T}^{-1})^2}{1.37 \times 10^{-31} \times x^{3/4}} && (5.26)\\ &\simeq 2.94 \times 10^8 \times x^{-\frac{3}{4}} (B{\rm T}^{-1})^2, && (5.27) \end{aligned}$$

and hence

$$B = \sqrt{\frac{q}{U_0} \times \frac{x^{3/4}}{2.94}} \times 10^{-4}{\rm T} \tag{5.28}$$

If we use $x \simeq 20$, $q/U_0 \simeq 0.1$, then, the magnetic field should be

$$B \sim 0.6 \times 10^{-4}{\rm T} = 0.6{\rm G} \tag{5.29}$$

■

The required value of magnetic field (several hundred mG) is experimentally realizable [32].

**Temperature**

As to the temperature, the system should be cooled as low as $k_B T/U_0 \sim 0.3$, which corresponds to $T \sim$3 nK.

(∵)

From (5.8) for $U_0$ and the value of the Boltzmann constant $k_B \simeq 1.3806 \times 10^{-23}$J/K, we have

$$\begin{aligned} \frac{U_0}{k_B} &\simeq \frac{1.37 x^{3/4} \times 10^{-31}{\rm J}}{1.38 \times 10^{-23}{\rm J/K}} && (5.30)\\ &\simeq 0.993 x^{3/4} \times 10^{-8}{\rm K}. && (5.31) \end{aligned}$$

and

$$T = \frac{k_B T}{U_0} \times \frac{U_0}{k_B} \tag{5.32}$$

$$\simeq \frac{k_B T}{U_0} \times 0.993 x^{3/4} \times 10^{-8}\mathrm{K}, \tag{5.33}$$

which, for $x \simeq 20$, gives

$$T \simeq \frac{k_B T}{U_0} \times 0.993 x^{3/4} \times 10^{-8}\mathrm{K} \tag{5.34}$$

$$\simeq \frac{k_B T}{U_0} \times 9.39 \times 10^{-8}\mathrm{K}. \tag{5.35}$$

Thus, $k_B T/U_0 \sim 0.03$ corresponds to $T \sim 3\mathrm{nK}$.

■

Although the temperature is much lower than usual BEC transition temperature (hundreds of nanokelvin), it is not experimentally unreachable, as exemplified by the realization of cold atomic systems with temperature less than 6 nK [50].

**Initial state preparation**

In our results, the magnetization along the axis of the applied magnetic field is always zero, which correspond to experimental settings where initial states have zero magnetization (note that the magnetization along the axis of the applied magnetic field is conserved).

Such initial states, including pure $\sigma = 0$ condensate, can be prepared by several experimental techniques, as described in literatures [32, 51]

**Measurement**

Discontinuous phase transitions predicted in our study can be experimentally tested by examining the presence of hysteresis, which signifies metastability and accompanying discontinuous phase transitions.

Similar measurements were recently performed for the spin-1 hyperfine spin manifold of $^{23}$Na [29], which is described by the antiferromagnetic spin-1 Bose-Hubbard model. In the experiment, the depth of the optical lattice is changed in two ways; in the first case, the lattice depth was gradually raised to the value at which TOF imaging was performed, and in the second case, the lattice depth was first raised to a large enough value and then lowered to the value at which TOF imaging was performed. It was shown that the transition points for two cases estimated from the condensate fraction as a function of the final lattice depth, which is calculated from the TOF image, do not coincide with each other, signifying the presence of hysteresis.

In addition to TOF imaging, the transverse magnetization can also be directly measured, as was done in [51] for $F = 1$ $^{87}$Rb.

# Chapter 6

# Summary and outlook

## 6.1 Summary

In this thesis, we have studied the ground-state and nonzero-temperature phase diagrams of the ferromagnetic spin-1 Bose-Hubbard model with an external magnetic field, which describes spin-1 atoms such as $^7$Li and $^{87}$Rb in an optical lattice. In addition to the competing effect of the kinetic-energy term and the repulsive interaction term, which induces the phase transition between the superfluid phase and the Mott insulator phase, the model also involves yet another competition between the ferromagnetic interaction and the positive quadratic Zeeman energy, which is known to give rise to two superfluid phases in the corresponding weakly interacting spin-1 system without a lattice.

As a mean to analyze the system, we described the Gutzwiller variational ansatz, whose essence is to restrict variational states to products of local states. The rationale of this approximation is that the ground states for both the no-hopping and non-interacting limits can be written in this form, and that it is natural to expect that this form of state can also capture the physics of intermediate parameter region, in which phase transitions occur. However, in our actual calculations, we have employed the decoupling approximation, which was shown to be equivalent to, and much more numerically efficient compared with the Gutzwiller variational ansatz In the decoupling approximation, we decouple the hopping term which connects different lattice sites, and reduce the problem to a single-site problem with mean-field order parameters, which are to be determined self-consistently. To obtain the phase diagrams, we have numerically solved the resulting self-consistent equations by iteratively diagonalizing the single-site Hamiltonian which include the mean-field order parameter.

For the zero-temperature case, we have found, in addition to the Mott insulator phase, two superfluid phases; the polar phase, which shows no magnetization, and the broken-axisymmetry phase, which exhibits nonzero transverse magnetization. Further, we have found that, for the strong spin-dependent interaction corresponding to the $^7$Li, the phase transition between these two superfluid phases can be discontinuous, i.e., the superfluid order parameters and the transverse magnetization have nonzero jumps at the transition point on some part of the phase boundary in the $t - \mu$ phase diagram. Discontinuous phase transitions are also found when the quadratic Zeeman energy is varied, in clear contrast to the mean-field theory prediction for weakly interacting spin-1 bosons without an optical lattice, where the corresponding phase transition is known to be continuous. To clarify that these discontinuous phase transitions seen in our calculations are not due to numerical artifacts, we have also examined the energy function as a function of the superfluid order parameters, and confirmed metastability and

ensuing discontinuous phase transitions. We have found that discontinuous phase transitions between the two superfluid phases occur only when the boundary is close to the Mott insulator phase, which is consistent with the mean-field theory prediction for weakly interacting spin-1 bosons in which almost all particles participate in a superfluid.

For the nonzero-temperature case, we have found that the system also exhibits the above mentioned properties, i.e., two superfluid phases with different magnetic properties and discontinuous phase transitions between these two phases, for low enough temperatures. However, with the increase of temperature, the region of discontinuous phase transition gradually shrinks, and for higher temperature, the phase transitions become continuous.

## 6.2 Outlook

### 6.2.1 Quantum Monte Carlo calculation

As we already pointed out, the decoupling approximation on which we rely has the drawback of completely neglecting the effect of the hopping term in the Mott insulator phase. Thus, physics inside Mott lobes cannot be properly predicted by the decoupling approximation. To firmly verify the discontinuous phase transitions between two superfluid phases predicted in our research, and to explore the whole phase diagram including the Mott insulator phase, various quantum Monte Carlo methods [52] are promising, because bosonic systems are free of the sign problem.

The idea of quantum Monte Carlo methods [1] is to sample quantum states according to the weight represented by the Boltzmann factor and evaluate observables using many samples of quantum states. Important properties of quantum Monte Carlo methods are that it is exact except for statistical errors which converge to zero as the sample number is increased, and that it is numerically much more efficient compared with the exact diagonalization, which requires exponentially large computational resource as the particle number increases.

Recently, quantum Monte Carlo calculations of spin-1 Bose-Hubbard model in two-dimensional square lattice was performed in 2013 [41], confirming various properties predicted by diverse methods including the decoupling approximation; for the ferromagnetic interaction, the model exhibits ferromagnetism over the entire phase diagram, and the phase transition between the Mott insulator phase and the superfluid phase is continuous, while for the antiferromagnetic interaction, the phase transitions is continuous for odd Mott lobes, but discontinuous for even Mott lobes, when $U_2/U_0$ is small enough. The same method are expected to be directly applicable to the system with an external magnetic field.

### 6.2.2 Experiment

The discontinuous phase transitions predicted in our calculation can be probed experimentally by examining the presence of metastability and the accompanying hysteresis, as was recently done [29] for the spin-1 hyperfine spin manifold of $^{23}$Na, which is described by the antiferromagnetic spin-1 Bose-Hubbard model. There, Jiang et al. performed TOF imaging after varying the lattice depth in two ways; in the first case, the lattice depth is monotonically raised, and in the second case, the lattice depth is first raised to large enough value, and then lowered. It was

[1] Here we exclude variational Monte Carlo, which is nothing but a variational method.

shown that the transition points for two cases calculated from the TOF image do not coincide with each other, signifying the presence of hysteresis.

Recently, experimental efforts to realize ultracold spinor $^7$Li gas are actively underway [31], and the temperature required to observe the discontinuous phase transitions is predicted to be not far beyond the current experimental techniques. It is our hope that the predictions made in this the present thesis will be tested experimentally in the near future.

# Appendix A

# $n_{\max}$ dependence

As was described in chapter 4, in our calculations, we assume that the particle number at each site is not larger than a prescribed value $n_{\max}$.

Here, we show that the truncation does not change the physics within the decoupling approximation, by showing that phase diagrams do not change when $n_{\max}$ is further increased.

## A.1 $T = 0$ case

First, we show results for ground-state cases.

Figure A.1 shows the $t - \mu$ phase diagram for $(U_2/U_0, q/U_0) = (-0.7, 0.1)$ (c.f. figure 5.6, where $n_{\max} = 7$), and figure A.2 shows the $t - \mu$ phase diagram for $(U_2/U_0, q/U_0) = (-0.7, 0.02)$ (c.f. figure 5.10, where $n_{\max} = 5$).

Both figures show that increasing $n_{\max}$ beyond the values used in chapter 5 does not change the phase diagrams significantly, showing that the values used in 5 are sufficient.

## A.2 $T > 0$ case

Here, we show results for nonzero temperature.

Figure A.3 shows the $t - \mu$ phase diagram for $(U_2/U_0, q/U_0, k_B T/U_0) = (-0.7, 0.02, 0.025)$.

It can be seen that increasing $n_{\max}$ beyond $n_{\max}$, which is the value used in chapter 5, does not change the phase diagrams significantly, showing that $n_{\max}$ is sufficient.

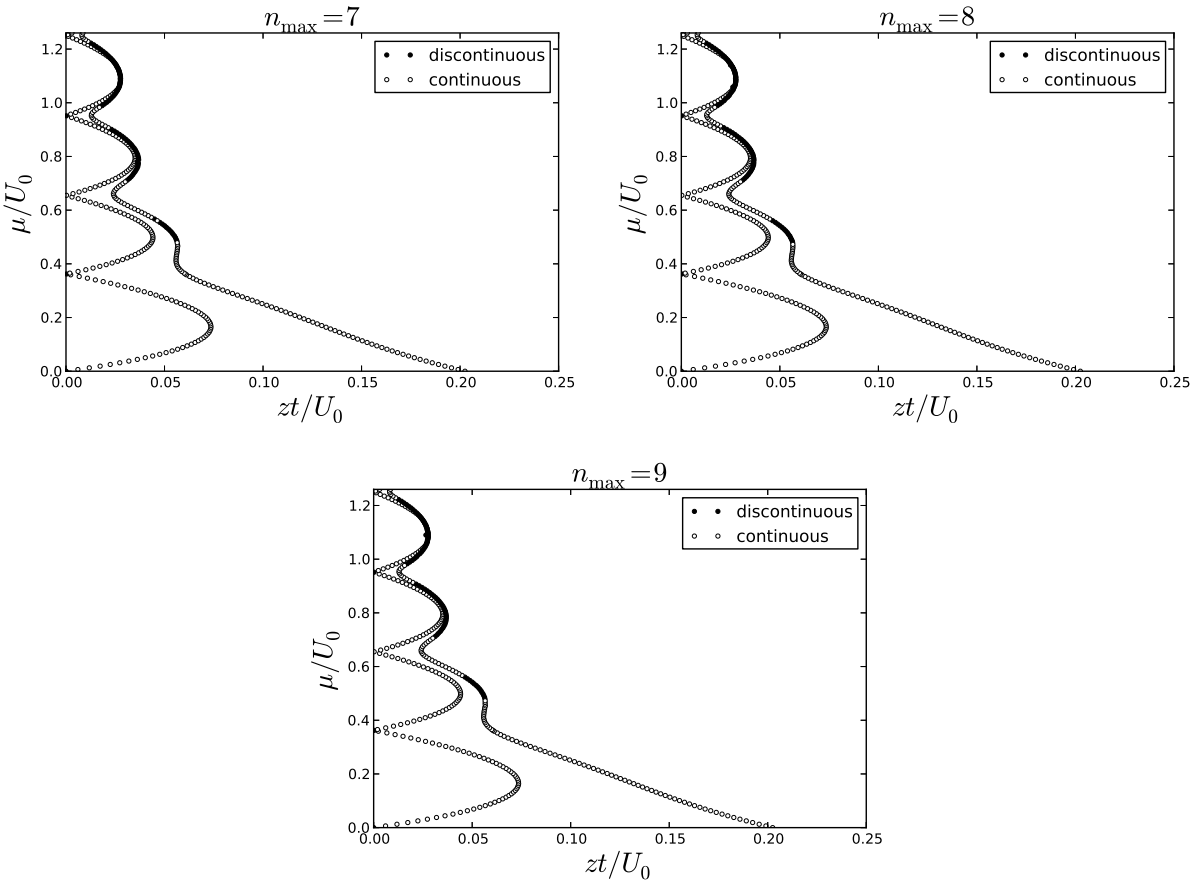


Figure A.1: Ground-state $t-\mu$ phase diagrams for different values of $n_{\max}$, which are shown in the figure. White circles denote the boundary across which continuous phase transitions occur, while black circles denote the boundary across which discontinuous phase transitions occur. No significant change can be seen with the increase of $n_{\max}$, signifying that the value $n_{\max} = 7$, which was used in section 5.1, is sufficient for capturing the physics of the system within the decoupling approximation. $U_2/U_0 = -0.7$ and $q/U_0 = 0.1$.

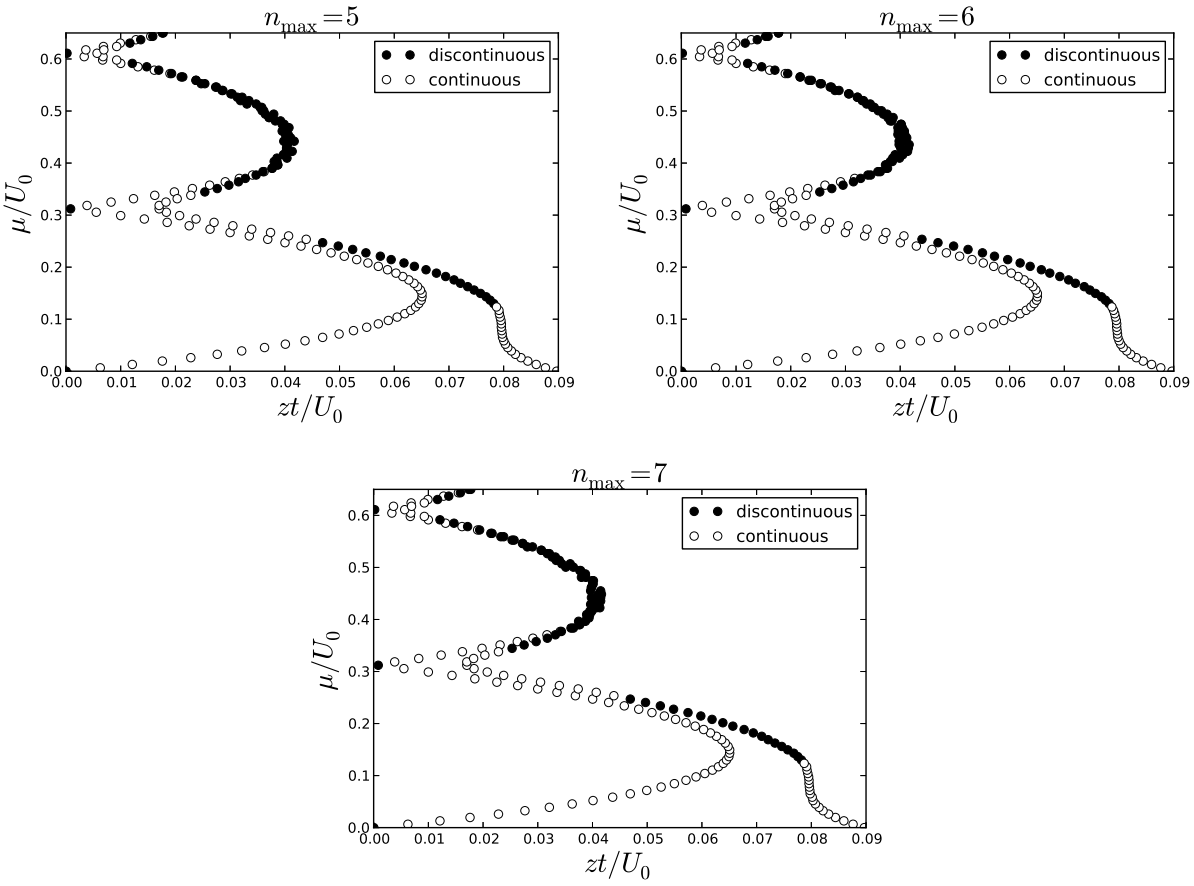


Figure A.2: Ground-state $t-\mu$ phase diagrams for different values of $n_{\max}$, which are shown in the figure. White circles denote the boundary across which continuous phase transitions occur, while black circles denote the boundary across which discontinuous phase transitions occur. No significant change can be seen with the increase of $n_{\max}$, signifying that the value $n_{\max} = 5$, which was used in section 5.2, is sufficient for capturing the physics of the system within the decoupling approximation. $U_2/U_0 = -0.7$ and $q/U_0 = 0.02$.

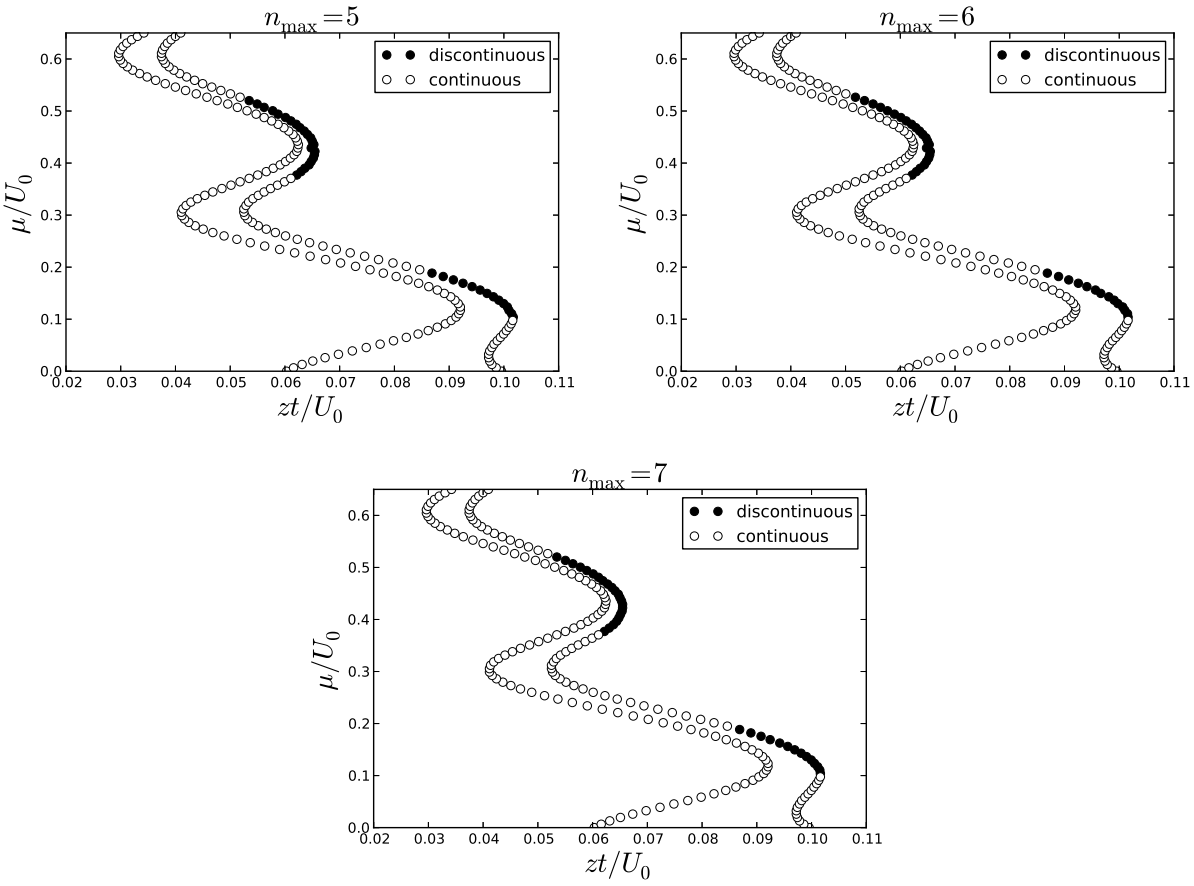


Figure A.3: Nonzero temperature $t-\mu$ phase diagrams for different values of $n_{\max}$, which are shown in the figure. White circles denote the boundary across which continuous phase transitions occur, while black circles denote the boundary across which discontinuous phase transitions occur. No significant change can be seen with the increase of $n_{\max}$, signifying that the value $n_{\max}=5$, which was used in section 5.2, is sufficient for capturing the physics of the system within the decoupling approximation. $U_2/U_0=-0.7$, $q/U_0=0.02$, and $k_BT/U_0=0.025$.

# Bibliography


[1] Albert Einstein, Quantentheorie des einatomigen idealen Gases, Sitzungsberichte der Preussischen Akademie der Wissenschaften, Physikalisch-mathematische Klasse, 261 (1924).

[2] Albert Einstein, Quantentheorie des einatomigen idealen Gases. 2. Abhandlung, Sitzungsberichte der Preussischen Akademie der Wissenschaften, Physikalisch-mathematische Klasse, 3 (1925).

[3] M. H. Anderson, J. R. Ensher, M. R. Matthews, C. E. Wieman, E. A. Cornell, Observation of Bose-Einstein Condensation in a Dilute Atomic Vapor, Science, **269**, 198 (1995).

[4] K. B. Davis, M. -O. Mewes, M. R. Andrews, N. J. van Druten, D. S. Durfee, D. M. Kurn, and W. Ketterle, Bose-Einstein Condensation in a Gas of Sodium Atoms, Phys. Rev. Lett. **75**, 3969 (1995),

[5] `https://www.nobelprize.org/nobel_prizes/physics/laureates/2001/index.html`

[6] C. J. Pethick and H. Smith, *Bose-Einstein Condensation in Dilute Gases, 2nd edition*, Cambridge University Press (2008).

[7] Lev P. Pitaevskii and Sandro Stringari, *Bose-Einstein Condensation*, Clarendon Press (2003)

[8] Immanuel Bloch, Jean Dalibard, and Wilhelm Zwerger, Many-body physics with ultracold gases Rev. Mod. Phys. **80**, 885 (2008).

[9] Maciej Lewenstein, Anna Sanpera, and Veronica Ahufinger, *Ultracold Atoms in Optical Lattices: Simulating Quantum Many-Body Systems*, Oxford University Press (2012).

[10] Konstantin V. Krutitsky, Ultracold bosons with short-range interaction in regular optical lattices, Phys. Rep. **607**, 1 (2016).

[11] D. Jaksch, C. Bruder, J. I. Cirac, C. W. Gardiner, and P. Zoller, Cold Bosonic Atoms in Optical Lattices, Phys. Rev. Lett. **81**, 3108 (1998).

[12] H. A. Gersch and G. C. Knollman, Quantum Cell Model for Bosons, Phys. Rev. **129**, 959 (1963).

[13] Matthew P. A. Fisher, Peter B. Weichman, G. Grinstein, and Daniel S. Fisher, Boson localization and the superfluid-insulator transition, Phys. Rev. B **40**, 546 (1989).

[14] Markus Greiner, Olaf Mandel, Tilman Esslinger, Theodor W. Hänsch and Immanuel Bloch, Quantum phase transition from a superfluid to a Mott insulator in a gas of ultracold atoms, Nature, **415**, 39 (2002).

[15] D. M. Stamper-Kurn, M. R. Andrews, A. P. Chikkatur, S. Inouye, H.-J. Miesner, J. Stenger, and W. Ketterle, Optical Confinement of a Bose-Einstein Condensate, Phys. Rev. Lett. **80**, 2027 (1998).

[16] M. D. Barrett, J. A. Sauer, and M. S. Chapman, All-Optical Formation of an Atomic Bose-Einstein Condensate, Phys. Rev. Lett. **87**, 010404 (2001).

[17] Yuki Kawaguchi and Masahito Ueda, Spinor Bose-Einstein condensates, Phys. Rep. **520**, 253 (2012).

[18] Dan M. Stamper-Kurn and Masahito Ueda, Spinor Bose gases: Symmetries, magnetism, and quantum dynamics, Rev. Mod. Phys. **85**, 1191 (2013).

[19] Tin-Lun Ho, Spinor Bose condensates in optical trap, Phys. Rev. Lett. **81**, 742 (1998).

[20] Tetsuo Ohmi and Kazushige Machida, Bose-Einstein condensation with internal degrees of freedom in alkali atom gases, J. Phys. Soc. Japan **67**, 1822 (1998).

[21] J. Stenger, S. Inouye, D. M. Stamper-Kurn, H.-J. Miesner, A. P. Chikkatur and W. Ketterle, Spin domains in ground-state Bose-Einstein condensates, *Nature* **396**, 345 (1998).

[22] Keiji Murata, Hiroki Saito, and Masahito Ueda, Broken-axisymmetry phase of a spin-1 ferromagnetic Bose-Einstein condensate, Phys. Rev. A, **75**, 013607 (2007).

[23] C. K. Law, H. Pu, and N. P. Bigelow, Quantum Spins Mixing in Spinor Bose-Einstein Condensates, Phys. Rev. Lett. **81**, 5257 (1998).

[24] Masato Koashi and Masahito Ueda, Exact Eigenstates and Magnetic Response of Spin-1 and Spin-2 Vectorial Bose-Einstein Condensates, Phys. Rev. Lett. **84**, 1066 (2000).

[25] Adilet Imambekov, Mikhail Lukin, and Eugene Demler, Spin-exchange interactions of spin-one bosons in optical lattices: Singlet, nematic, and dimerized phases, Phys. Rev. A **68**, 063602 (2003).

[26] Shunji Tsuchiya, Susumu Kurihara and Takashi Kimura, Superfluid-Mott insulator transition of spin-1 bosons in an optical lattice, Phys. Rev. A **70**, 043628 (2004).

[27] Takashi Kimura, Shunji Tsuchiya, and Susumu Kurihara, Possibility of a First-Order Superfluid.Mott-Insulator Transition of Spinor Bosons in an Optical Lattice, Phys. Rev. Lett. **94**, 110403 (2005).

[28] Mateusz Łacki, Simone Paganelli, Veronica Ahufinger, Anna Sanpera, and Jakub Zakrzewski, Disordered spinor Bose-Hubbard model, Phys. Rev. A **83**, 013605 (2011).

[29] J. Jiang, L. Zhao, S.-T. Wang, Z. Chen, T. Tang, L.-M. Duan, and Y. Liu First-order superfluid-to-Mott-insulator phase transitions in spinor condensates, Phys. Rev. A **93**, 063607 (2016).

[30] K. Rodríguez, A. Argüelles, A. K. Kolezhuk, L. Santos, and T. Vekua, Field-Induced Phase Transitions of Repulsive Spin-1 Bosons in Optical Lattices, Phys. Rev. Lett **106**, 105302 (2011).

[31] Mukund Vengalattore, private communication (2015).

[32] M.-S. Chang, C. D. Hamley, M. D. Barrett, J. A. Sauer, K. M. Fortier, W. Zhang, L. You, and M. S. Chapman, Observation of Spinor Dynamics in Optically Trapped $^{87}$Rb Bose-Einstein Condensates, Phys. Rev. Lett. **92**, 140403 (2004).

[33] Ming-Shien Chang, Qishu Qin, Wenxian Zhang, Li You and Michael S. Chapman, Coherent spinor dynamics in a spin-1 Bose condensate, Nature Physics **1**, 111 (2005).

[34] C. Becker, P. Soltan-Panahi, J. Kronjäger, S. Dörscher, K. Bongs, K. Sengstock, Ultracold quantum gases in triangular optical lattices New J. Phys.**12**, (2010) 065025

[35] Patrick Windpassinger and Klaus Sengstock, Engineering novel optical lattices, Rep. Progr. Phys. **76**, 086401 (2013).

[36] Omjyoti Dutta, Mariusz Gajda, Philipp Hauke, Maciej Lewenstein, Dirk-Sören Lühmann, Boris A Malomed, Tomasz Sowiński, and Jakub Zakrzewski, Non-standard Hubbard models in optical lattices: a review, Rep. Progr. Phys. **78**, 066001 (2015).

[37] Daniel S. Rokhsar and B. G. Kotliar, Gutzwiller projection for bosons, Phys. Rev. B **44**, 10328 (1991).

[38] Werner Krauth, Michel Caffarel, and Jean-Philippe Bouchaud, Gutzwiller wave function for a model of strongly interacting bosons, Phys. Rev. B **45**, 3137 (1992).

[39] B. Capogrosso-Sansone, N. V. Prokof'ev, and B. V. Svistunov, Phase diagram and thermodynamics of the three-dimensional Bose-Hubbard model, Phys. Rev. B **75**, 134302 (2007).

[40] Barbara Capogrosso-Sansone, Şebnem Güneş Söyler, Nikolay Prokof'ev, and Boris Svistunov, Monte Carlo study of the two-dimensional Bose-Hubbard model, Phys. Rev. A **77**, 015602 (2008).

[41] L. de Forges de Parny, F. Hébert, V. G. Rousseau, and G. G. Batrouni, Interacting spin-1 bosons in a two-dimensional optical lattice, Phys. Rev. B **88**, 104509 (2013).

[42] Hosho Katsura and Hal Tasaki, Ground States of the Spin-1 Bose-Hubbard Model, Phys. Rev. Lett. **110**, 130405 (2013).

[43] Stefan S. Natu, J. H. Pixley, and S. Das Sarma, Static and dynamic properties of interacting spin-1 bosons in an optical lattice, Phys. Rev. A **91**, 043620 (2015).

[44] Dirk-Sören Lühmann, Cluster Gutzwiller method for bosonic lattice systems, Phys. Rev. A **87**, 043619 (2013).

[45] Dénes Petz, A survey of certain trace inequalities, Banach Center Publication, **30**, (1994).

[46] K. Sheshadri, H. R. Krishnamurthy, R. Pandit, and T. V. Ramakrishnan, Superfluid and Insulating Phases in an Interacting-Boson Model: Mean-Field Theory and the RPA, Europhys. Lett. **22**, 257 (1993).

[47] Ramesh V. Pai, K. Sheshadri, and Rahul Pandit, Phases and transitions in the spin-1 Bose-Hubbard model: Systematics of a mean-field theory, Phys. Rev. B **77**, 014503 (2008).

[48] D. van Oosten, P. van der Straten, and H. T. C. Stoof, Quantum phases in an optical lattice, Phys. Rev. A **63**, 053601 (2001).

[49] Andreas Wagner, Andreas Nunnenkamp, and Christoph Bruder, Mean-field analysis of spinor bosons in optical superlattices, Phys. Rev. A **86**, 023624 (2012).

[50] J. L. Roberts, N. R. Claussen, S. L. Cornish, E. A. Donley, E. A. Cornell, and C. E. Wieman, "Controlled Collapse of a Bose-Einstein Condensate" Phys. Rev. Lett. **86**, 4211 (2001).

[51] J. Guzman, G.-B. Jo, A. N. Wenz, K. W. Murch, C. K. Thomas, and D. M. Stamper-Kurn, Long-time-scale dynamics of spin textures in a degenerate $F = 1$ $^{87}$Rb spinor Bose gas, Phys. Rev. A 84, 063625 (2011).

[52] Lode Pollet, Recent developments in quantum Monte Carlo simulations with applications for cold gases, Rep. Prog. Phys. **75**, 094501 (2012).